GPM/DPR Level-2
Algorithm Theoretical Basis Document

Authors: Toshio Iguchi, Shinta Seto, Robert Meneghini,
Naofumi Yoshida, Jun Awaka, Minda Le,
V. Chandrasekar, Stacy Brodzik, Takuji Kubota and Nobuhiro Takahashi

TABLE OF CONTENTS

0. INTRODUCTION AND CAVEATS

This document describes the basic idea of DPR data processing. It was originally written for the algorithm used in the at-launch version (V03). The algorithm has been modified and improved since then. Although the basic idea of data processing remains the same, the actual flow of processing, in particular that in the solver module, has changed substantially. As a result, some part of description in section 3.1 may not be relevant any more.

DPR L2/L3 V06X products are regarded as "experimental products", not "standard products". The V06X provides early outcomes of the full-swath coverage after the DPR scan pattern change in 21st May 2018 aiming to apply dual-frequency observation for full-swath of KuPR observation by assigning KaHS rays to outer swath. Basic concept of V06X algorithm is the same as V06A, but, there were several new features of the algorithm for the V06X, due to progresses by algorithm developments. Preliminary evaluations showed that estimated precipitation in the outer swath from the dual-frequency method tended to be underestimated in V06X. Users need to be cautious about this. This underestimation was regarded as one of future tasks in V07.See full descriptions by the following link.
$https://www.eorc.jaxa.jp/GPM/doc/algorithm/DPRL2\_V06X\_algorithm\_June2020b.pdf$

Major changes in the DPR algorithm from V04 to V05

In level 1 algorithm, based on the new calibration results, the system parameters of DPR were re-examined, and the offset parameters for the transmitting powers, receiver's gains, the beam widths, and the pulse width of both KuPR and KaPR were redefined. As a result, Z_m of KuPR has increased by about +1.3 dB, and Z_m of KaPR by about +1.2 dB.

In level 2 algorithm, in addition to the changes in the DPR L1 calibration, adjustment factors were introduced in the preparation module to remove small trends in the overall system gains in KuPR and KaPR. The adjustment factors change the measured received powers only by a small fraction of dB. New flags, such `flagHeavyIcePrecip`, `flagSurfaceSnowfall`, `flagAnvil` and `snowIceCover`, are introduced in V05. A DSD database that depends on the month, region, surface type and rain type was created from the statistics of DSD parameters estimated with the dual-frequency algorithm and is applied to the single frequency (Ku-only and Ka-only) data processing. These changes are described in the relevant sections of this document.

Changes in the DPR algorithm from V05 to V06

1. A new SRT code has been modified to include calculations of Hitschfeld-Bordan PIA as well as a hybrid PIA that combines HB and SRT results. As a result of applying the new PIA in SLV module, erroneously large estimates of high precipitation over ocean (near coast) are mitigated and both DPR(MS) and Ku rain estimates in V06A agree better with Gound Validation data over USA.

2. A new classification algorithm is introduced by the University of Washington (Stacy Brodzik and Robert Houze) to reclassify the stratiform rain type. The new algorithm improved an angle-bin dependence of rain classification and SLH profiles.

Minor changes in DPR L2 algorithm:

· KaHS's sidelobe clutter is mitigated and it is used to re-calculated the data base for KuPR's sidelobe clutter.

· New variables are introduced. They are `flagScanPatten` in PRE module, `PIAhb`, `PIAhybrid`, `reliabFactorHY`, `reliabFlagHY`, `stddevEff`, `stddevHY` and `zeta` in SRT module. The meanings of these variables should be referred to the user's manual.

· The surface snow index is modified for the winter temperature inversions.

· The latest SRT data base is applied.

· A bug in flagEcho is fixed in dual frequency data processing.

There are cases of instantaneous retrieved precipitation rate classified as stratiform rain that exceed 40 mm/hr. These cases are rare, and the frequency is latitude dependent with more cases near the equator than in the extra-tropics.

Changes in the DPR algorithm from V06 to V06X

1. Implementation of a new format. The latest TKIO supports the new format including "FS" that is full swath dual-frequency product with 125 m range resolution.

2. Algorithm updates.

   PRE module

   · A sidelobe clutter reduction method after the scan pattern will be installed in the V06X algorithm because that sidelobe clutter contaminations of KaHS became more problematic in the new Ka scan pattern.

   · A sildelobe clutter filter technique for the KaHS is applied also for the Ku.

   · Clutter free detection in the Ku is improved in cases when the brightband (BB) is found near the surface.

   CSF module

   · Dual frequency technique of the classification module was improved to be applied in the FS.

   · Changed parameters will be used in the HS of the dual frequency technique.

   · New variables related to solid precipitation is implemented.

   · Reclassification by the slope method is improved.

   SRT module

   · The latest temporal reference files were applied.

   · SRT codes have been updated so that they now read temporal data over the full swath.

   · Dual-frequency SRT and Hybrid estimates are now applicable to the full swath.

   SLV module

   · We applied the same dual-frequency precipitation estimation in Solver (SLV) module of V06A for V06X.

KaHS scan pattern change

1. As of May 21, 2018, the scan pattern of KaHS beams was changed as shown in Fig. 0.1. The KaHS beams scanned in the inner swath before May 21 2018, but now they scan in the outer swath and match with KuPR's beams. Please note that the range resolution of KaHS is 500m and differs from that of the KuPR or KaMS. One scan of KuPR over the full swath consists of 49 beams which are numbered from 1 to 49 in Fig. 0.1 below. The array for one scan of KaMS data consists of 25 beams which correspond to KuPR's central beams from 13 to 37, whereas one scan of KaHS data array for 24 beams consists of two parts. The first 12 elements in the array correspond to KuPR's beams from 38 to 49, and the last 12 elements correspond to KuPR's beams from 1 to 12 of the following scan. All KaMS beams and the first 12 KaHS beams match well with KuPR's beams from 13 to 49. The magnitude of misalignment between these KuPR and KaPR beams is estimated to be less than 50 m after May 21. However, KaHS's beams from 13 to 24 are slightly shifted from the corresponding KuPR beams from 1 to 12 in the along-track direction. The magnitude of misalignment in these beams is about 400 m.

   The dual-frequency algorithm can be applied to the full swath of data after the change of scan pattern. However, because it takes time to develop a new algorithm applicable to the full swath and to adjust the necessary parameters to ensure the quality of the products, KaHS data are not processed in V06 L2 algorithm. Missing values are stored in the output variables that use KaHS data. KaHS's received power data are available only in L1 products in V05B and V06.

2. All beam directions of KuPR and KaPR were adjusted to match better with the nominal footprint locations. The difference between KuPR and KaPR's footprint centers is now about 30 m at nadir. It was about 300 m before May 21, 2018. This improvement of beam matching is not considered to make a big difference in the L2 output products except for very heavy rain cases because the mismatch was small (300 m) from the beginning.

Figure 0.1 DPR's scan pattern before May 21 2018.

(a) and after May 21 2018 (b). KaHS beams scan in the inner swath before May 21 2018, but now they scan in the outer swath and match with KuPR's beams. Numbers in color indicate angle bin numbers for KuPR (blue), KaMS (yellow), and KaHS (red).

1. OBJECTIVES

The objective of the level 2 DPR algorithms is to generate from the level 1 DPR products radar-only derived meteorological quantities on an instantaneous FOV (field of view) basis. A subset of the results will be used by the level 2 combined radar-radiometer algorithm and the level 3 combined and radar-only products.

The general idea behind the algorithms is to determine general characteristics of the precipitation, correct for attenuation and estimate profiles of the precipitation water content, rainfall rate and, when dual-wavelength data are available, information on the particle size distributions in rain and snow. It is particularly important that dual-wavelength data will provide better estimates of rainfall and snowfall rates than the TRMM PR data by using the particle size information and the capability of estimating, even in convective storms, the height at which the precipitation transitions from solid to liquid.

2. BACKGROUND INFORMATION

2.1 Historical Perspective

The Dual-Frequency Precipitation Radar (DPR) on the GPM core satellite will be the second space-borne precipitation radar, following the first such radar, the Precipitation Radar (PR), launched on the TRMM satellite in November, 1997. The TRMM PR has already revolutionized the measurement of precipitation from space by providing high resolution 3-dimensional rain echoes in the tropics and subtropics. The DPR consists of Ku-band (13.6GHz) and Ka-band (35.5GHz) channels. A major source of error in the rainfall estimates from the TRMM/PR comes from the uncertainty in the conversion of radar reflectivity into rainfall rate. This uncertainty originates in the variations of the raindrop size distribution (DSD) that changes by region, season and rain type. One of the reasons for adding the Ka-band frequency channel to the DPR is to provide information on the DSD that can be obtained from non-Rayleigh scattering effects at the higher frequency.

Another reason for the new Ka-band channel is to provide more accurate estimates of the phase-transition height in precipitating systems. This information is very important not only in increasing the accuracy of rain rate estimation by the DPR itself, but in improving rain estimation by passive microwave radiometers.

The third reason for the Ka-band channel arises from the fact that the GPM core satellite will provide coverage up to about 65 degrees latitude; by increasing the sensitivity of this channel, a larger fraction of snow events will be detected.

Since the Ku-band channel of the DPR is very similar to the TRMM PR, the principal challenge in the development of the DPR level 2 algorithms is to combine the new Ka-band data with the Ku-band data to achieve the objectives mentioned above.

2.2 Instrument Characteristics

The DPR consists of the Ku-band precipitation radar and the Ka-band precipitation radar. They are abbreviated as KuPR and KaPR, respectively. These Earth-pointing KuPR and KaPR instruments will provide rain sensing over both land and ocean, both day and night. The KuPR and KaPR design specifications, with all active phased array elements functioning, are shown in Table 2.2-1. The spacecraft orbital information is shown in Table 2.2-2.

Figure 2.2-1 shows the DPR scan pattern. KuPR's scan pattern is similar to that of the TRMM PR. It has 49 footprints in a scan and the footprint size is about 5 km in diameter. The scan swath is 245 km. The KaPR also has 49 footprints, but these are divided into two types of scan. In the first type of scan (Ka_MS), the beams are matched to the central 25 beams of KuPR, providing a swath of 120 km. In the second type of scan (Ka_HS), the KaPR is operated in the high-sensitivity mode to detect light rain and snow. In this case, its beams are interlaced within the scan pattern of the matched beams as shown in Fig. 2.2-1. The KuPR and

9

KaPR for the Ka_MS scan have the same range resolution (250 m), while the range resolution of data in Ka_HS is 500m. In both cases, radar echoes are over-sampled at twice the rate of the corresponding resolution: 125 m for the matched beams and 250 m for the Ka_HS.

Table 2.2-1 DPR Design Specification

Item	KuPR	KaPR
Swath Width	245 km	120 km
Range Resolution	250 m	250/500 m
Spatial Resolution	5.2 km (Nadir at the height of 407 km)	
Beam Width	0.71° (Center Beam)	
Transmitter	128 Solid State Amplifiers	
Peak Transmit Power[1]	1012.0 W	146.5 W
Pulse Repetition Freq.[2]	4000 to 4500 Hz	
Pulse Width	two 1.6 μs pulses	two 1.6 μs pulses (matched beams)
		two 3.2 μs pulses (interlaced scans)
Beam Number	49	49 (25 in matched beams
		and 24 in interlaced scans)
Min. measurable rain rate	0.5 mm/h	0.2 mm/h
Beam matching error	Less than 1000 m	
Observable range	19 km to Surface (to −5 km near nadir)	
Dynamic range	From −5 dB below the system noise level	
	to +5 dB above the nominal maximum surface echo level	
Receiver power accuracy	±1 dB	
Scan Angle	±17° Cross Track	±8.5° Cross Track
Frequencies	13.597 and 13.603 GHz	35.547 and 35.553 GHz
Bandwidth	14 MHz	
Max. Mass	472 kg	336 kg
Power (max)	446 W (orbit average)	344 W (orbit average)
Science Data Rate (max)	109 kbps	81 kbps
	(The Total of KuPR and KaPR is 190 kbps)	
Housekeeping Data Rate[3]	1 kbps (nominal)	

1. This parameter is for informational purposes in the ICD.
2. In nominal operation mode.
3. 1 kbps may increase up to 2 kbps during SCDP switch-overs.

Table 2.2-2 Spacecraft Orbital Information

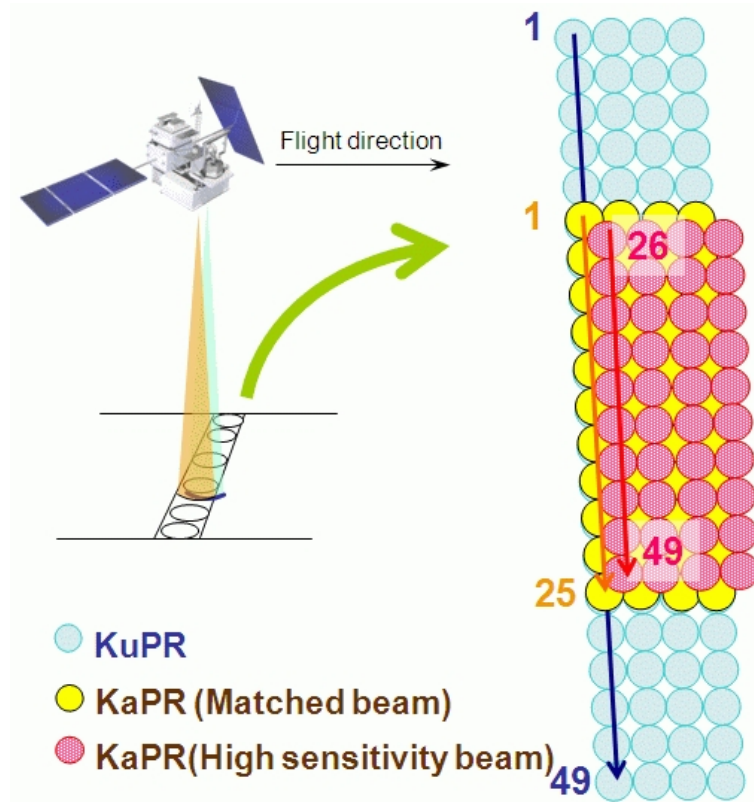| Inclination	65°
Mean semi-major axis	6776.14 km
S/C Altitude Control Box	±1 km
Orbit Eccentricity	0.00010 (0-0.0005 tolerance)
Geodetic Altitude Variation Range	397 km to 419 km

Figure 2.2-1. DPR scan pattern.

Figure 2.2-2 shows the observation range. The DPR's echo sampling is designed to cover a range that, at minimum, extends from the surface to 19 km above the sea level (or from the Ellipsoid). The pulse repetition interval is adjusted according to the satellite altitude and the angle of observation. As a result, the number of independent samples changes slightly as a function of the scan angle.
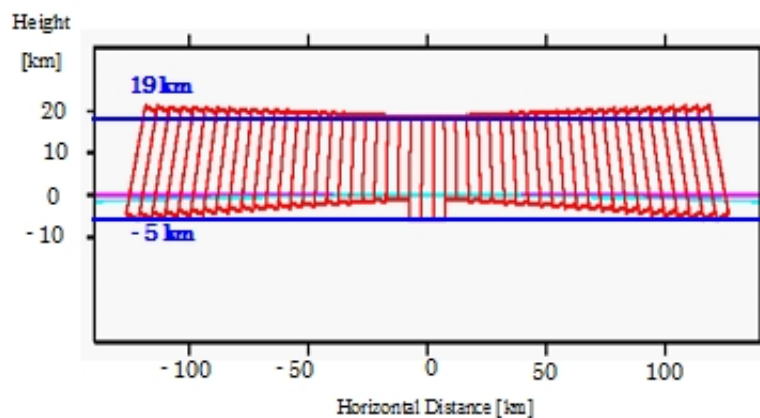

Figure 2.2-2 DPR's data sampling range

11

3. ALGORITHM DESCRIPTION

3.1. Theoretical Description

3.1.1. Physical Basis of the Algorithm

The radar transmits a pulse of radio waves and receives an echo from an object. The object in the case of precipitation radar is a distribution of rain drops in the volume defined by the antenna directivity, the pulse width and the time between the transmission and the reception of the pulse. The received power P_r from rain at range r is proportional to the apparent radar reflectivity factor $Z_{m0}(r)$.

$$P_r(r) = \frac{C|K|^2}{r^2} Z_{m0}(r) \tag{3.1-1}$$

where C is the radar constant, and K is a constant defined as a function of complex refractive index m of scattering particles by the following equation.

$$K = \frac{m^2 - 1}{m^2 + 2} \tag{3.1-2}$$

When the radar electric specifications and range r are given, Z_{m0} can be calculated from P_r. Therefore, we can assume that $Z_{m0}(r)$ can be derived from a measurement of the echo power. Z_{m0} is related to the effective radar reflectivity factor Z_e by

$$Z_{m0}(r) = A(r)Z_e(r) \tag{3.1-3}$$

where A is the attenuation factor. The effective radar reflectivity factor Z_e can be expressed in terms of the backscattering cross section $\sigma_b(D)$ of a precipitation particle of diameter D and the particle size distribution $N(D)$:

$$Z_e = \frac{\lambda^4}{\pi^5 |K|^2} \int \sigma_b(D) N(D) \, dD \tag{3.1-4}$$

Here λ is the wavelength of the electromagnetic waves, and rainfall rate R can also be expressed in terms of $N(D)$,

$$R = \int V(D) v(D) N(D) \, dD \tag{3.1-5}$$

where $V(D)$ is the volume of the precipitation particle of diameter D, $v(D)$ is its falling velocity.

If $N(D)$ is characterized by a single parameter, for example D^*, then Z_e and D^* are in one-to-one correspondence. Since R and D^* is in a one-to-one correspondence as well, once Z_e is obtained, then $N(D)$ can be specified by D^* corresponding to this Z_e, and R can be calculated. In this case, therefore, the attenuation correction used to obtain Z_e from Z_{m0} is the primary problem to be solved. This is the principle of rain estimation for a single frequency radar

such as the TRMM PR. In fact, however, variations of $N(D)$ in nature cannot be characterized sufficiently by a single parameter in many cases. As a result, rain estimates from a single frequency radar often involve errors and biases.

In contrast, variations in $N(D)$ can be well represented by two parameters as far as the conversion from Z_e to R is concerned. If rain is measured by the radar at two wavelengths and if one of the wavelengths divided by 2π is smaller than or comparable to the average raindrop size, then the corresponding backscattering cross section will deviate from that of Rayleigh scattering, and Z_e at this wavelength differs from Z_e at the longer wavelength where Rayleigh scattering generally applies. This situation enables us to estimate two parameters of the model function of $N(D)$ and results in a better estimate of rainfall rate. This is the idea of rainfall estimation with a dual-wavelength radar. In other words, if $N(D)$ is characterized by two parameters N^* and D^*, Z_e at two wavelengths Z_{e1} and Z_{e2} become functions of N^* and D^*,

$$Z_{e1}(N^*, D^*) = \frac{\lambda_1^4}{\pi^5 |K|^2} \int \sigma_{b1}(D) N(D; N^*, D^*) \, dD \tag{3.1-6}$$

$$Z_{e2}(N^*, D^*) = \frac{\lambda_2^4}{\pi^5 |K|^2} \int \sigma_{b2}(D) N(D; N^*, D^*) \, dD \tag{3.1-7}$$

Once Z_{e1} and Z_{e2} are given, we can solve (3.1-6) and (3.1-7) for N^* and D^*, and R can be calculated from $N(D; N^*, D^*)$.

As in the single-wavelength case, the attenuation corrections to obtain Z_{e1} and Z_{e2} at two frequencies from measured or apparent radar reflectivity factors Z_{m1} and Z_{m2} are crucial. Since the major attenuation comes from precipitation itself, and the DSD parameters can be estimated from Z_{e1} and Z_{e2}, we look for a profile of pairs of DSD parameters (one pair per range gate) that gives the attenuation corrected profiles of Z_{e1} and Z_{e2} that are consistent with the attenuations caused by the precipitation particles whose size distributions are characterized by these DSD parameters. This part of the algorithm is the heart of the rainfall retrieval with dual-frequency radar data. Details of the algorithm are described in section 3.2.5.

Attenuation caused by non-precipitation particles and atmospheric gases must be compensated for beforehand. Specifically, we need to take into account the attenuation caused by cloud water, water vapor and oxygen molecules. Meteorological data and storm models are used to estimate their profiles for this purpose.

3.1.1-1 Effective radar reflectivity factor Z_e, specific attenuation k and measured radar reflectivity factor

The effective radar reflectivity factor Z_e is given by (3.1-4). Similarly, the specific attenuation k is given in terms of the drop size distribution $N(D)$ and the total extinction cross section $\sigma_e(D)$ by

$$k = c_k \int \sigma_e(D) N(D) \, dD \tag{3.1-8}$$

where $c_k = 0.01/\ln(10)$ if k is expressed in [dB (km^{-1})], $\sigma_e(D)$ in [mm^2], and $N(D)$ in [mm^{-1} m^{-3}]. Let r [km] denote the distance from the radar along the range. The measured radar reflectivity factor $Z_{m0}(r)$ [mm^6 m^{-3}] involves the attenuation by precipitation particles $A_P(r)$ and by non-precipitation particles $A_{NP}(r)$ as is expressed in the following equation.

$$Z_{m0}(r) = Z_e(r)A_{NP}(r)A_P(r) = Z_e(r)A_{NP}(r)\exp\left[-0.2\ln(10)\int_0^r k(s)\,ds\right] \qquad (3.1\text{-}9)$$

where s is a dummy variable. Equation (3.1-9) can be rewritten in decibels as shown below.

$$10\log_{10}Z_{m0}(r) = 10\log_{10}Z_e(r) + 10\log_{10}A_{NP}(r) - 2\int_0^r k(s)\,ds \qquad (3.1\text{-}10)$$

After attenuation correction for non-precipitation particles, $Z_{m0}(r)$ becomes $Z_m(r)$, where $Z_m(r)$ is given by.

$$Z_m(r) = Z_{m0}(r)A_{NP}^{-1}(r) = Z_e(r)A_P(r) \qquad (3.1\text{-}11)$$

By substituting Eq. (3.1-11) into Eq. (3.1-9), the following equation is obtained.

$$10\log_{10}Z_m(r) = 10\log_{10}Z_e(r) - 2\int_0^r k(s)\,ds \qquad (3.1\text{-}12)$$

3.1.1-2 HB method

Let us assume a power-law relation between k and Z_e as shown below.

$$k(r) = \alpha(r)Z_e^\beta(r) \qquad (3.1\text{-}13)$$

where α and β are coefficients, α can be range dependent, but β should be constant along the range. With the help of Eq. (3.1-13), Eq. (3.1-12) can be solved for Z_e and written in the form of (3.1-14),

$$Z_e(r) = \frac{Z_m(r)}{\left[1 - 0.2\ln(10)\beta\int_0^r \alpha(s)Z_m^\beta(s)\,ds\right]^{1/\beta}} \qquad (3.1\text{-}14)$$

Alternatively, the equation can be solved for the attenuation factor, A_P, giving,

$$A_P(r) = \left[1 - 0.2\ln(10)\beta\int_0^r \alpha(s)Z_m^\beta(s)\,ds\right]^{1/\beta} \qquad (3.1\text{-}15)$$

14

3.1.1-3 Path integrated attenuation (PIA)

Here, Path Integrated Attenuation (PIA) is defined as integrated attenuation caused by precipitation particles from the radar to the surface. If $r = r_s$ at the surface, PIA is given as shown below.

$$\text{PIA} = -10 \log_{10} A_{\text{P}}(r_s) = 2 \int_0^{r_s} k(s) \, ds \qquad (3.1\text{-}16)$$

Eq. (3.1-12) can be rewritten as a function of the PIA.

$$10 \log_{10} Z_m(r) = 10 \log_{10} Z_e(r) - \text{PIA} + 2 \int_r^{r_s} k(s) \, ds \qquad (3.1\text{-}17)$$

By substituting Eq. (3.1-15) at $r = r_s$ into Eq. (3.1-16), the following equation is obtained.

$$\text{PIA} = -\frac{10}{\beta} \log_{10} \left[1 - 0.2 \ln(10) \beta \int_0^{r_s} \alpha(s) Z_m^\beta(s) \, ds \right] \qquad (3.1\text{-}18)$$

The PIA can be estimated by taking the difference between the surface backscattering cross sections with and without precipitation (surface reference technique).

3.1.1-4 Parameterization of drop size distribution function

From a mathematical point of view, $N(D)$ should be parameterized with at most two unknown parameters in order to characterize $N(D)$ deterministically from dual-frequency measurements. To keep the discussion fairly general, $N(D)$ is parameterized in the following way.

$$N(D) = N^* n(D; D^*), \qquad (3.1\text{-}19)$$

where N^* and D^* are unknown parameters and n is a function of D. By substituting Eq. (3.1-19) into Eq. (3.1-4) and (3.1-8), Z_e and k are given as below.

$$Z_e = N^* I_b(D^*), \quad I_b(D^*) = \frac{\lambda^4}{\pi^5 |K|^2} \int \sigma_b(D) n(D; D^*) \, dD \qquad (3.1\text{-}20)$$

$$k = N^* I_e(D^*), \quad I_e(D^*) = \frac{0.01}{\ln(10)} \int \sigma_e(D) n(D; D^*) \, dD \qquad (3.1\text{-}21)$$

which shows that Z_e and k can be decomposed into N^* and a function of D^* ($I_b(D^*)$ and $I_e(D^*)$).

3.1.1-5 Retrieval

3.1.1-5-1 Dual-frequency retrieval

If Z_m is available at two frequencies, N^* and D^* can be obtained by solving the following two equations.

$$10 \log_{10} Z_{m1}(r) = 10 \log_{10} N^*(r) + 10 \log_{10} I_{b1}(D^*(r)) - 2 \int_0^r k_1(N^*(s), D^*(s)) \, ds \qquad (3.1\text{-}22)$$

$$10 \log_{10} Z_{m2}(r) = 10 \log_{10} N^*(r) + 10 \log_{10} I_{b2}(D^*(r)) - 2 \int_0^r k_2(N^*(s), D^*(s)) \, ds \qquad (3.1\text{-}23)$$

The third term of the right hand side of Eq. (3.1-22) or (3.1-23) is equal to the 2-way attenuation from the storm top to range r, which implies that the retrieval should be performed sequentially from the top range bin to the gate of interest. This attenuation can be treated as a known quantity if the attenuation is expressed as a function of the DSD parameters derived at each gate. Since the solution progresses from the storm top downwards, the method is called the forward retrieval method. If an independent estimate of the PIA is available, in addition to Z_m,

$$10 \log_{10} Z_{m1}(r) = 10 \log_{10} N^*(r) + 10 \log_{10} I_{b1}(D^*(r)) - \text{PIA} + 2 \int_r^{r_s} k_1(N^*(s), D^*(s)) \, ds$$
$$(3.1\text{-}24)$$

$$10 \log_{10} Z_{m2}(r) = 10 \log_{10} N^*(r) + 10 \log_{10} I_{b2}(D^*(r)) - \text{PIA} + 2 \int_r^{r_s} k_2(N^*(s), D^*(s)) \, ds$$
$$(3.1\text{-}25)$$

Eqs. (3.1-24) and (3.1-25) instead of Eq. (3.1-22) and (3.1-23) can be used to calculate N^* and D^*. In this case, the fourth term of the right hand side of Eq. (3.1-24) or (3.1-25) is equal to the 2-way attenuation from the gate of interest (at range r) to the surface, implying that the retrieval should be done sequentially from the bottom range bin to the gate of interest. As in the forward method, if the attenuation is related to the DSD parameters at each range gate, the fourth terms can be treated as known. This method is called backward retrieval method. In reality, because of ground clutter, the fourth term cannot be calculated without some assumptions regarding the profile of the precipitation in the clutter region. Furthermore, because PIA estimates by the SRT have some error, equations (3.1-24) and (3.1-25) differ from (3.1-22) and (3.1-23), and the backward retrieval method yields different solutions from the forward retrieval method. However, the backward retrieval method is preferable, as it gives numerically stable and unique solutions, while the forward retrieval method usually has two solutions at each range bin.

In the backward retrieval method, we define $10 \log_{10} Z_{b1}$ and $10 \log_{10} Z_{b2}$ by moving the third and fourth term of the right hand side to the left hand side in Eqs. (3.1-24) and (3.1-25).

$$10 \log_{10} Z_{b1}(r) \equiv 10 \log_{10} Z_{m1}(r) + \text{PIA} - 2 \int_r^{r_s} k_1(N^*(s), D^*(s)) \, ds$$
$$= 10 \log_{10} N^*(r) + 10 \log_{10} I_{b1}(D^*(r)) \qquad (3.1\text{-}26)$$

$$10 \log_{10} Z_{b2}(r) \equiv 10 \log_{10} Z_{m2}(r) + \text{PIA} - 2 \int_r^{r_s} k_2(N^*(s), D^*(s)) \, ds$$
$$= 10 \log_{10} N^*(r) + 10 \log_{10} I_{b2}(D^*(r)) \qquad (3.1\text{-}27)$$

By taking the difference between Eqs. (3.1-26) and (3.1-27), we obtain:

$$10 \log_{10} Z_{b1}(r) - 10 \log_{10} Z_{b2}(r) = I_{b1}(D^*(r)) - I_{b2}(D^*(r)) \qquad (3.1\text{-}28)$$

As the left hand side of Eq. (3.1-28) is known, D^* can be derived. For liquid precipitation, the right-hand side of (3.1-28) has a maximum, and Eq. (3.1-28) has generally two solutions.

3.1.1-5-2 Single-frequency retrieval

If Z_m is available only at a single frequency, we need to characterize $N(D)$ with a single parameter. This means that we assume a relationship between N^* and D^*. Once such a relation is assumed, we can translate the N^*-D^* relation to the k-Z_e relation, and the attenuation correction can be carried out by (3.1-14). If a PIA estimate by SRT ($\mathrm{PIA_{SRT}}$) is substituted into PIA in (3.1-18), the equality is generally not satisfied. This inequality is caused either by an error in the SRT or by an error in the k-Z_e relation. If the SRT is correct, the k-Z_e relation can be modified to $k = \epsilon \alpha Z_e^\beta$ where ϵ satisfies (3.1-29). This is called the α-adjustment method.

$$\mathrm{PIA_{SRT}} = -\frac{10}{\beta} \log_{10} \left[1 - 0.2 \ln(10) \beta \epsilon \int_0^r \alpha(s) Z_m^\beta(s)\, ds \right] \tag{3.1-29}$$

Once the ϵ parameter is found from (3.1-29), the Hitschfeld-Bordan solution with the modified k-Z_e relation provides the attenuation-corrected radar reflectivities. From the above attenuation correction process, k and Z_e are obtained. Then, by taking the ratio of (3.1-20) to (3.1-21), D^* can be retrieved.

$$\frac{k}{Z_e} = \frac{I_e(D^*)}{I_b(D^*)} \tag{3.1-30}$$

Generally, the right hand side of (3.1-30) is a monotonic function of D^* so that (3.1-30) has a unique solution. Since $N(D)$ is characterized by a single parameter, there is one-to-one correspondence between Z_e and D^* or k and D^*, and we can directly calculate D^* as well.

3.1.2. Overall structure of the algorithm

3.1.2-1 Algorithms

There are three kinds of Level 2 algorithms for the DPR: DPR algorithm, Ku-only (KuPR) algorithm, and Ka-only (KaPR) algorithm. The latter two are single-frequency (SF) algorithms. The DPR algorithm is a dual-frequency (DF) algorithm. The DF algorithm employs both KuPR and KaPR L2 standard products as inputs. Pixels observed by DPR can be categorized into three types: pixels in the inner swath of normal scans (observed both by KuPR and KaPR), pixels in the outer swath of normal scans (observed only by KuPR), and pixels in the interleaved scans (observed only by KaPR in the high-sensitivity mode). The KuPR algorithm is executed for pixels in both inner and outer swaths of normal scans. The KaPR algorithm is executed for pixels in the inner swath of normal scans and in the interleaved scans. The DF algorithm is executed for pixels of all the three kinds.

In the DF algorithm, pixels in the inner swath of normal scans are categorized into the dual-beam (DB) pixels. The other pixels in the DF algorithm and all the pixels in the SF algorithms are categorized into the single-beam (SB) pixels. For a SB pixel, the DF algorithm can use data in dual-frequency observations at neighboring pixels, while the SF algorithms can use data only

in the corresponding single-frequency observations. For example, by using the characteristics of the drop size distribution estimated by dual-frequency measurements at DB pixels in the inner swath, the DF algorithm can give better estimates at SB pixels in outer swath than the KuPR algorithm. Each algorithm executes data for one orbit at a time. For an orbit, only after the two SF algorithms are properly executed, the DF algorithm will be executed. The order of execution between the KuPR algorithm and the KaPR algorithm is not fixed. The algorithms are designed in such a way that the order of execution for different orbits has no restrictions within the same calendar month, but one month of data should be executed as a unit to produce proper databases.

3.1.2-2 Input/Output Files

The input and output files of the KuPR, KaPR and DF algorithms are as follows.
KuPR algorithm

(Input) KuPR L1B standard product, Weather data file, Database file

(Output) KuPR L2 standard product, KuPR L2 temporary file, KuPR L2 environment data

KaPR algorithm

(Input) KaPR L1B standard product, Weather data file, Database file

(Output) KaPR L2 standard product, KaPR L2 temporary file, KaPR L2 environment data

Dual-frequency algorithm

(Input) KuPR L2 standard product, KaPR L2 standard product, KuPR L2 temporally file, KaPR L2 temporary file, Database file, KuPR L2 environment data, KaPR L2 environment data

(Output) DPR L2 standard product, DPR L2 environment data, DPR L2 temporary file

The temporary files include some results of the SF algorithms, which are not written in the standard products. The temporary products can be treated as research products, once the DPR L2 standard product and other outputs are properly produced by the DF algorithm.

The environmental data include the profiles of atmospheric parameters assumed in the L2 algorithm. Because of its large volume, the ancillary environmental data are output into a separate file from the standard product.

The weather data file is prepared by converting the resolution and/or variables of weather analysis/reanalysis/forecast dataset in advance to L2 algorithm. Database files are explained later.

3.1.2-3 Modules

The framework of the L2 algorithm is shown in Fig. 3.1-1. This framework is common to the KuPR, KaPR, and DF algorithms. The main module manages the overall procedure, and it employs seven sub-modules. The main module will open and close files, call sub-modules, and read/write all the input and output files and variables. It will also terminate the algorithm. Sub-modules can read/write files and variables as long as they are permitted. As a basic rule, they should process for all the pixels in the orbit, and the order of pixels processed is not fixed (can be determined by each module). Sub-modules cannot call other sub-modules. When a sub module is terminated, the processing is returned to the main module.
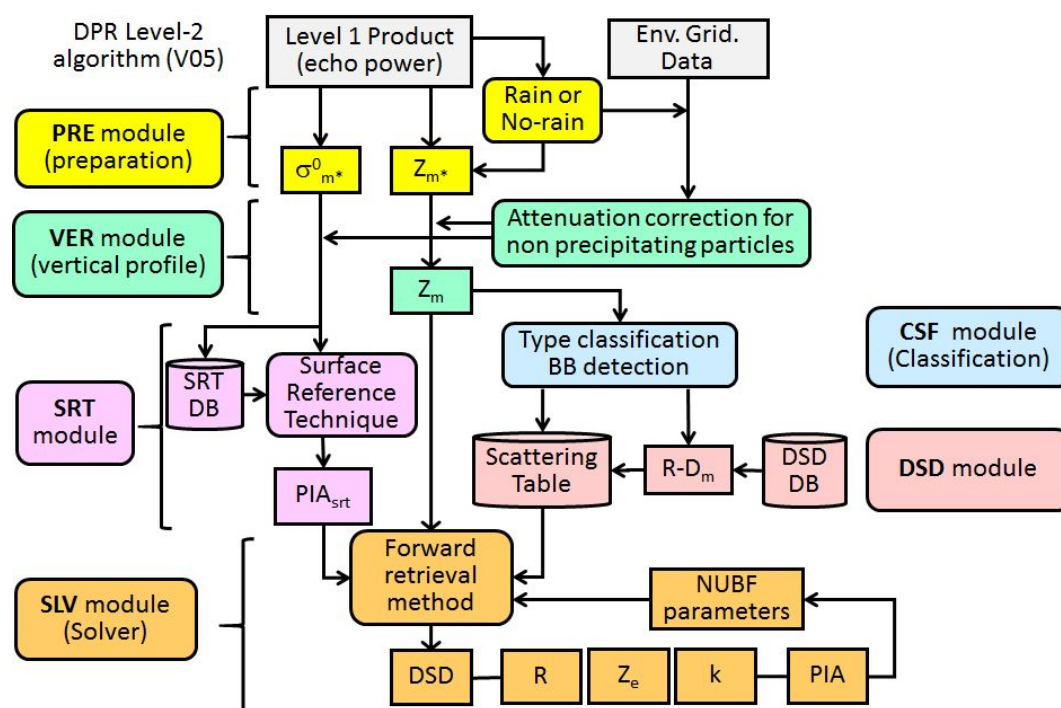

Figure 3.1-1 DPR algorithm flow

3.1.2-4 Basic roles of the modules

The L2 algorithm is to numerically solve Eq. (3.1-22) or (3.1-23) for DB pixels and Eq. (3.1-30) for SB pixels to obtain N^* and D^*. The retrieval process is carried out in the Solver module, but the preparation of equations is shared by the other six modules. The PIA in Eqs. (3.1-29), (3.1-24) and (3.1-25) can be estimated in the SRT module. The DSD module is responsible for quantifying the terms in the equations such as α, β, $n(D; D^*)$, $I_b(D^*)$, and $I_e(D^*)$ based on the physical characteristics of precipitation (precipitation types and bright band information) determined by the Classification module. Z_m is converted from Z_{m0} through attenuation correction for non-precipitation particles in the Vertical Profile module and Z_{m0} is converted from received echo power in the Preparation module.

3.1.2-5 Variables

A tentative table of variables is attached to this document. The table is used for all the three algorithms in the L2 algorithms. There are two types of variables: L1B variables and L2 variables. L1B variables are just copied from the L1B standard products. L2 variables are somehow processed in the L2 algorithms. Not all but some selected variables are written in L2 standard, temporary, or environment products. A variable with scan dependence, angle bin dependence, range bin dependence, and frequency dependence is expressed as an array in the source code. Some variables may have other dimensions than scan, angle bin, range bin, and frequency. Type (bytes) of a variable can be changed when it is written into the product to save the file size. Some variables can take different values in the SF algorithms and DF algorithm. Those variables are product dependent. Product dependence and frequency dependence are explained by examples below.

- "Location of observation" is without product dependence and without frequency dependence.
- "Measured radar reflectivity factor Z_{m0}" is without product dependence and with frequency dependence.
- "Equivalent radar reflectivity factor Z_e" is with product dependence and with frequency dependence.

In the DF algorithm, variables with product dependence should be reprocessed, but variables without product dependence can be copied from SF products. Variables without product dependence and without frequency dependence should take the same value in KuPR product and KaPR product, but there is some possibility of disagreement as the KuPR algorithm and KaPR algorithm are processed independently. In the case of disagreement, a rule (e.g., KuPR algorithm is more reliable) should be prepared to determine the value in the DF algorithm.

3.1.2-6 Databases

A database is to include useful information for the algorithm, and exists as separate files from the main body of the algorithm (source code). For example, the SRT database is used in the SRT module to increase the accuracy of the PIA estimates. The L2 algorithm can refer to and update databases. The actual updating process is done not by directly modifying the database file, but by creating an intermediate file. The intermediate files are summarized and the database file is modified off line.

3.1.2-7 Look-up tables

A look-up table has a similar role with a database, but the difference is that a look-up table will basically not be updated. Therefore, we can treat the look up tables as part of the main body of the algorithm, and do not list the look-up tables as input and output files. The L2 algorithm employs a DSD look-up table and a RTM look-up table in the DSD module and the Solver module, respectively.

3.2 Main module

The basic procedure of the main module is described in 3.2.1 below. The test version before the data release in 2014 used the basic procedure. Version 3 algorithm adopts the advanced procedure 3.2.2-1. In near future, advanced procedures described in 3.2.2-2 amd 3.2.2-3 should be tested.

3.2.1 The basic procedure

In the basic procedure, sub-modules are executed in the following order, and each module is called only once. Firstly, the Preparation module is executed. This module judges the existence of precipitation, and identifies the precipitation pixels. Secondly, the Vertical profile module is executed. The ancillary atmospheric profile data are used to correct for the attenuation caused by non-precipitation particles to obtain the surface backscattering cross sections both at precipitation and no-precipitation pixels. Thirdly, the Classification module classifies each precipitation pixel into an appropriate storm type. At no-precipitation pixels, almost no processes are taken.

Fourthly, the SRT module is executed. At no-precipitation pixels, SRT database is updated based on the measurement of surface backscattering cross sections. Note that the SRT module can be executed anytime after the Vertical profile module and before the Solver module. Finally, the Solver module is executed. At no-precipitation pixels, almost no processes are taken.

3.2.2 Advanced procedure

By executing some of the modules multiple times, improvement of results is expected. Two kinds of examples are given below.

3.2.2-1 Recursive procedure

Once the basic procedure is done, the same procedure is repeated again with the parameters estimated in the first cycle. In the second cycle, for example, we can estimate the attenuation due to cloud liquid water by referring the precipitation rate estimated in the first cycle.

3.2.2-2 Parallel procedure

In the basic procedure, the sub-modules are required to determine the values of variables in charge, but sometimes they do not have enough information to estimate the values in a deterministic way. A parallel procedure allows a sub-module to give multiple estimates and to let the following sub-modules execute with multiple estimates. For example, if the precipitation type is not determined with confidence in Classification module, then the following (DSD and Solver) modules are executed with multiple assumptions of precipitation types, and the main module checks which assumption gives the vertical profiles of Z_e and the corresponding precipitation rate R in accordance with the assumed precipitation type. Thus, the precipitation type can be determined afterwards.

3.2.2-3 Additional processes

Some important processes may be missing in the basic procedure, for example, non-uniform beam filling (NUBF) correction. They should be involved in the final version of the algorithm, but currently, it has not been determined which modules are in charge of additional processes; NUBF correction can be done inside the Solver module, or should be shared with the DSD module and/or the SRT module, or a new module (Texture module) should be introduced.

3.3 Preparation module

3.3.1. Objectives and functions of the Preparation Module (PRE)

The primary purposes of the preparation module are (1) to classify the pixels into either rain or no-rain pixels, (2) to convert the received power P_r into measured reflectivity factor Z'_m without any attenuation corrections at each range bin, and (3) to calculate apparent normalized surface cross section $\sigma_m^{0}{}'$ without any attenuation correction at each pixel.

3.3.2. Algorithm descriptions of the PRE

In this section, the preparation module of Ku-band level-2 algorithm will be described in detail. As to the preparation module of Ka-band level-2 algorithm, it is almost the same with that for the Ku-band. The DPR level-2 algorithm can use level-2 products and level-2 supplementary products of both Ku-only and Ka-only algorithms. As a result, it can provide necessary information to other modules of the DPR level-2 algorithm without re-calculations.

Reading of input data

The module reads data from a Ku-band level-1B product that includes not only the radar echoes but also other variables related to the measurements such as scan time (`ScanTime`), footprint position (`Latitude`, `Longitude`), local zenith angle (`scLocalZenith`), operational mode (`operationalMode`, elevation (`DEMHmean`), and data quality flag (`dataQuality`). In the case of the DPR level-2 algorithm, the module reads level-2 products and level-2 supplementary products of both Ku-band and Ka-band algorithms.

Status confirmation

The module refers to `dataQuality` of level-1B product and reflect `qualityData` of level-2 product scan by scan. If `dataQuality` is bad (not 0), level-2 values of the corresponding scan are overwritten by missing values.

Calculation of range distance (`rangeDist`)

The range distance (`rangeDist`) is defined by the distance from the satellite to each range bin along the radar beam. Each `rangeDist` is calculated from the range distance from the satellite to (the center of) the highest range bin (`startBinRange`), the number of range bins with normal sampling (`echoLowResBinNumber`), the number of range bins with over-sampling (`echoHighResBinNumber`) and the range bin size (`rangeBinSize`). Specifically, the range distance (`rangeDist`) for normal sampling ranges are calculated by using the following equation.

$$\texttt{rangeDist} = R_0 + (n-1) \times \Delta R, \quad (n = 1, 2, 3, \cdots, N)$$

The rangeDist for over sampling ranges are

$$\texttt{rangeDist} = R_0 + \{N + (m-1)\} \times \Delta R, \quad (m = 1, 2, 3, \cdots, M)$$

where

$$R_0 = \texttt{startBinRange} \text{ in L1B product}$$
$$N = \texttt{echoLowResBinNumber} \text{ in L1B product}$$
$$M = \texttt{echoHighResBinNumber} \text{ in L1B product}$$
$$\Delta R = \texttt{rangeBinSize} \text{ in L1B product}$$
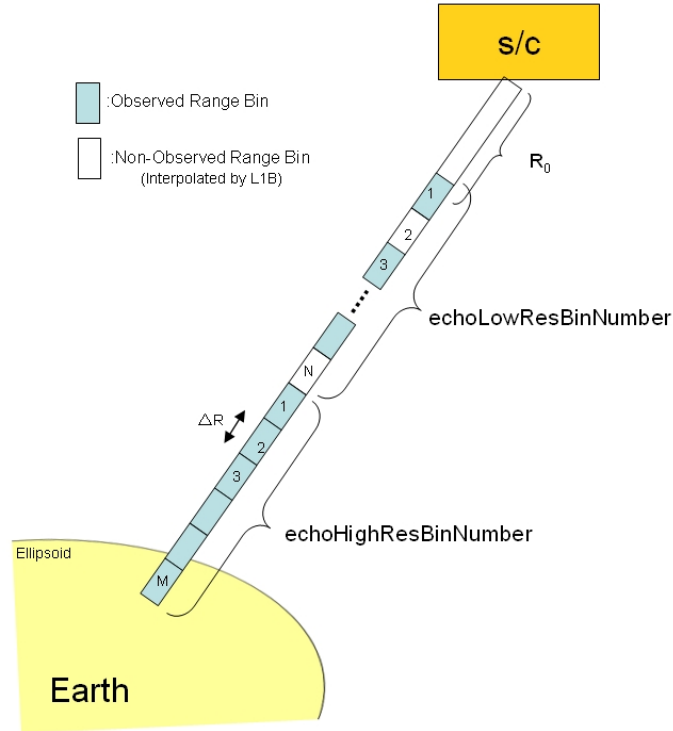
Figure 3.3-1 Definition of `rangeDist`

Calculation of height (`Height`)

The height is defined by the vertical distance from the footprint of radar beam on the Ellipsoid to the range bin in question. In order to calculate `Height`, we define `ellipsoidBinOffset` as follows.

$$\texttt{ellipsoidBinOffset} = \texttt{scRangeEllipsoid}$$
$$- \{R_0 + (\texttt{binEllipsoid} - 1) \times \texttt{rangeBinSize}\}$$

Then, `Height` of a `binRangeNo` (as shown "p" in Fig. 3.3-3) is calculated by the following equation.

$$\texttt{Height[binRangeNo]} = \{(\texttt{binEllipsoid\_2A} - \texttt{binRangeNo}) \times \texttt{rangeBinSize}$$
$$+ \texttt{ellipsoidBinOffset}\} \times \cos(\texttt{localZenithAngle})$$

25

Figure 3.3-2 Definition of `ellipsoidBinOffset`

where `binEllipsoid_2A` is the Ellipsoid range bin number in level 2. `binEllipsoid_2A` is 176 for Ku and KaMS, and 88 for KaHS. `rangeBinSize` is 125 m for Ku and KaMS, and 250 m for KaHS.
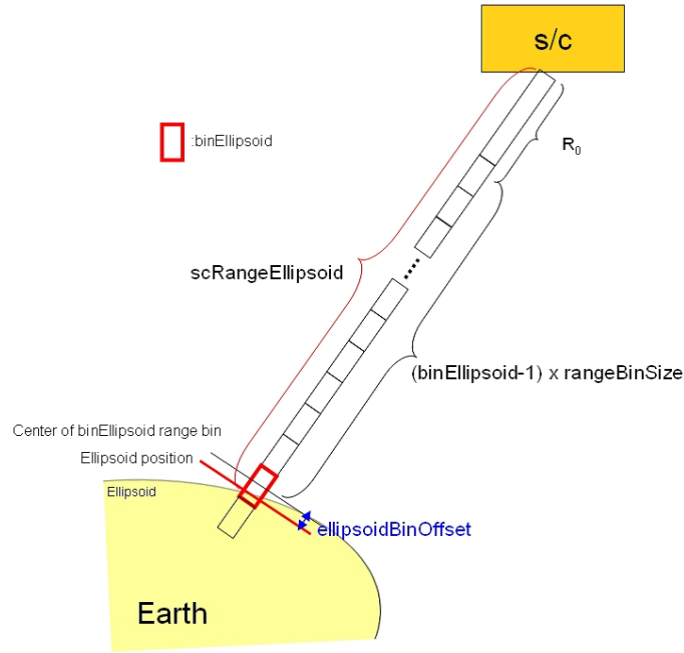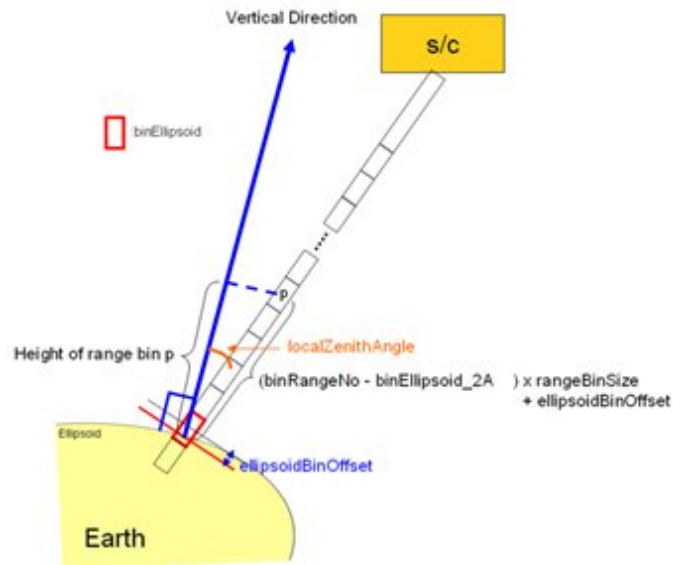

Figure 3.3-3 Definition of `Height`

Extraction of level-1B range data

`echoPower` and `echoFlag` of level-1B product are given at each range bin. The array size of

data with range-bin dependence in Ku level-1B is 260. The array sizes of data with range-bin dependence in Ka_MS and Ka_HS level-1B are 260 and 130, respectively. On the other hand, the array size of data with range-bin dependence in Ku level-2 is 176, whereas the array sizes for range bins of Ka_MS and Ka_HS level-2 are 176 and 88, respectively. The preparation module renumbers the range bins relative to the Ellipsoid position in level-2 so that the range bin number at the Ellipsoid becomes 176 in the Ku and Ka_MS level-2 products, and 88 in the Ka_HS products. Thus, at the nadir angle bin, data from 0 km to +22 km altitude relative to the Ellipsoid are extracted.

In the version 06X or later versions, 'FS' structure was introduced in all level-2 products. The FS structure in the new version of Ku level-2 product coincides NS structure in current Ku level-2 product, whereas the FS structure in the new version of Ka level-2 product (Ka_FS) stores both current Ka_MS and Ka_HS level-2 products. Note that the new version of Ka level-2 has HS structure, however, it is set to missing after the scan pattern change (See Appendix).

Figure 3.3-4 shows horizontal structure of the Ka_FS in the new version of Ka level-2 product, Ka_MS and Ka_HS in the current Ka level-2 products. As for inner swath of Ka_FS, angle bin number 1 to 25 of Ka_MS at n scan are stored at angle bin number 13 to 37 of Ka_FS at n scan. In the outer swath of Ka_FS, angle bin number 1 to 12 of Ka_HS at n scan are stored at angle bin number 38 to 49 of Ka_FS at n scan, and angle bin number 13 to 24 in Ka_HS at n scan are stored at angle bin number 1 to 12 of Ka_FS at $n+1$ scan. At the first scan of Ka_FS, invalid values are stored in angle bin number 1 to 12 because there are no corresponding angle bins of Ka_HS. Angle bin number 1 to 12 at the end of scan of Ka_FS are discarded.
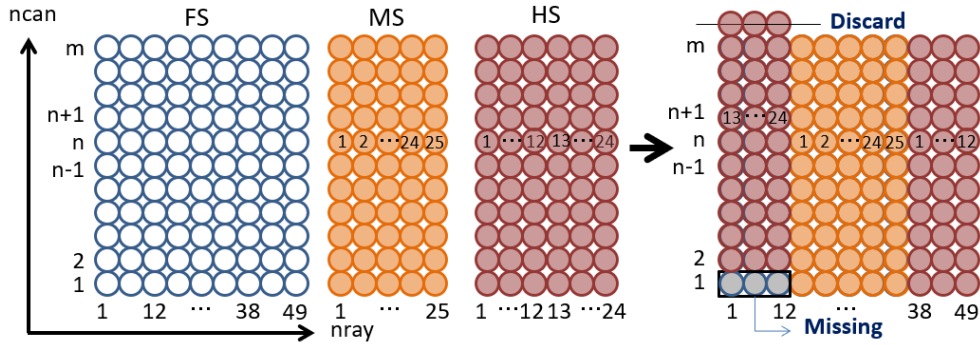
Figure 3.3-4 How to merge for horizontal structure of the Ka_MS and Ka_HS.

Vertical structure in the outer swath of the Ka_FS level-2 product differs from current Ka_HS level-2 product. Figure 3.3-5 shows the schematic image of the difference. In the current version, array size for range bins are 88, whereas the preparation module reforms the 88 range bins to 176 range bins by interpolating the `echoPower` to coincide the Ku_FS vertical resolution for the dual-frequency algorithm in the new version.

27
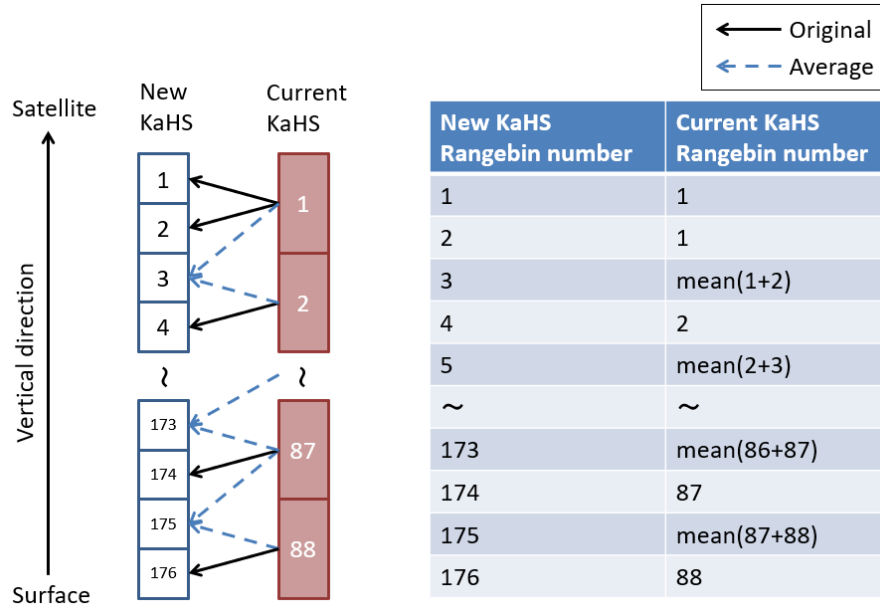
Figure 3.3-5 Interpolation for vertical structure of the Ka_HS.

Land surface type (`landSurfaceType`)

The land-and-ocean flag (`landOceanFlag`) of level-1B product gives land, ocean, inland water, and coast classification for each footprint. The preparation module adds surface type information for land and coast area, using footprint position (`Latitude` and `Longitude`) and an external data base. The surface type information is stored in `landSurfaceType`.

Snow- or Ice-covered area (`snowIceCover`)

In version 5, a new flag called `snowIceCover` is added to indicate the areas that are covered with surface snow or sea ice. This flag is used in the SRT module when it needs to separate different surface types and also when it collects surface scattering data to create the σ^0 database. The flag is based on NOAA/NESDIS autosnow.

Surface detection (`binRealSurface`)

The preparation module determines the surface range bin using the received power (`echoPower`), and DEM related data, such as `binDEM`, `scRangeDEM`, `DEMHmean`, `binDEMHtop`, and `binDEMHbottom` of level-1B product. The estimated surface position is stored in `binReal-Surface`.

Estimation of Clutter-free bottom (`binClutterFreeBottom`)

The range bin number of the clutter-free bottom is estimated using `echoPower` profiles. `binRealSurface` may be used as a reference of the search window. The clutter-free bottom range bin number is stored in `binClutterFreeBottom`.

In V5, `binclutterFreeBottom` is automatically raised up by one range bin (by adding a one

28

range bin margin to `binClutterFreeBottom`). This automatic one range bin raise-up sometimes causes the contamination of `binclutterFreeBottom` with the side lobe clutter. This problem is solved in V6 by further raising up the `binClutterFreeBottom` (by more than one range bin until the contamination disappears) when the contamination with the side lobe clutter occurs. The V5 code also has a very small bug on Ka-HS `binClutterFreeBottom`. This bug is fixed in V6.

Reduction of sidelobe clutter contamination

A routine to reduce the sidelobe clutter was installed in the KuPR-L2 algorithm. Fig. 3.3-6 shows a flowchart of the routine (Kubota et al. 2016). Sidelobe echoes are estimated from a statistical relationship between Normalized Radar Cross Section (NRCS) and sidelobe clutter obtained from observation data and then the routine subtracts sidelobe estimates from received power. In the version 06 or later versions, the routine to reduce the sidelobe clutter was installed also in the KaHS-L2. The method in the KaHS was largely similar to that in the KuPR, but it included some modifications described in Kubota et al. (2018).In V06X, a sildelobe clutter filter technique is applied for both the Ku and the KaHS. When the sidelobe estimate is subtracted at a range bin, bit 6 in the `flagEcho` is flagged by this routine.
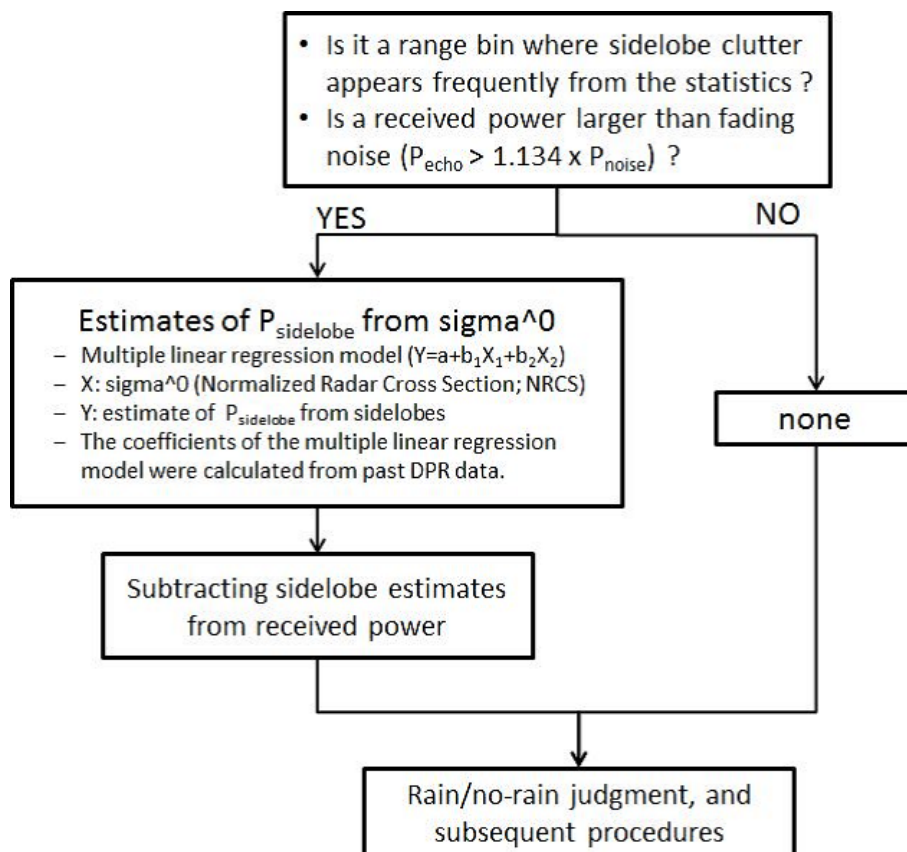

Figure 3.3-6 Flowchart of the routine to reduce sidelobe clutter installed in KuPR-L2 algorithm

Calculation of Signal power (`echoSignalPower`)

Calculations of signal power are applied to all range bin data except missing data which are flagged by `dataQuality` in L1B product.

Pecho = pow(10.0,(double) `echoPower` /10)

Pnoise = pow(10.0,(double) `noisePower` /10)

Psignal = Pecho - Pnoise

echoSignalPower = 10*log10(Psignal)

where `echoPower` and `noisePower` are stored in dB unit in L1B product. If `Psignal` values are negative, missing value is stored in `echoSignalPower`.

Rain/NoRain classification (`flagEcho`, `flagPrecip`, `binStormTop`, `heightStormTop`)

Rain/NoRain classification is carried out in two steps. At first, it is done for all range bins above the `binClutterFreeBottom` except missing data which are labeled by `dataQuality` in L1B product. If `echoSignalPower` exceeds a certain threshold, it means that rain is detected for the range bin. The results of Rain/NoRain classification for range bins are stored in `flagEcho`. Then, using the surrounding `flagEcho` results, the Rain/NoRain classification for angle bin is carried out for all angle bins except missing data. The results of Rain/NoRain classification for each angle bin are stored in `flagPrecip`. The modules in the downstream in the flow chart may use the `flagPrecip` to determine the target pixels for processing. The function also detects a highest rain position in each angle bin and provides `binStormTop` and `heightStormTop`.

In the version 06X, a function named as 'Vertical filter' was installed in the KuPR-L2 and the KaPR-L2 algorithm to compensate the routine reducing the sidelobe clutter. Figure 3.3-7 shows a flowchart of the function. The function is carried out in mainly three steps after the Rain/NoRain classification. At first, the bottom of search range bin (R_B) is determined by using the `binClutterFreeBottom` at the angle bins which is judged as rain. Then, the function evaluates whether the `flagEcho` is isolated. Search ranges and threshold of the continuity check are listed Table 3.3-1. Once the `flagEcho` is determined to be isolated, it is considered as a contamination of the sidelobe clutter and is replaced to NoRain. Finally, continuity of the `flagEcho` (i.e. 6 range bins) is re-checked in the vertical direction of both KuPR and KaPR.

Table 3.3-1. Search range and threshold of continuity check.

	KuPR	KaPR
Horizontal search range	Angle bin 1 to 20 and 30 to 49	Angle bin 1 to 12 and 38 to 49
Vertical search range	Range bin 1 to R_B	Range bin 1 to R_B
Continuous range bin	12 range bins	12 range bins
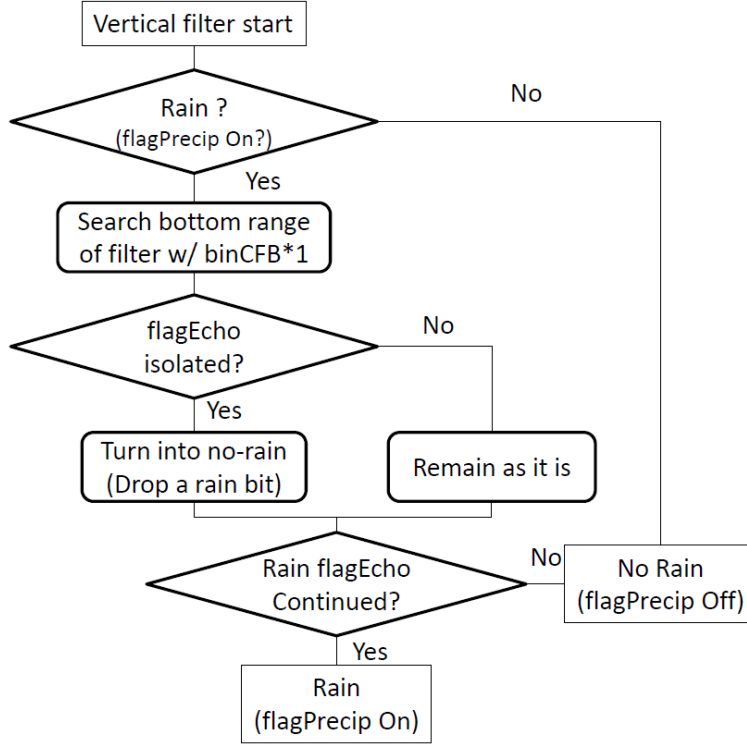
Figure 3.3-7 Flowchart of the vertical filter

Calculation of Z'_m factor (`zFactorMeasured`)

Z'_m is defined as the measured reflectivity factor without any attenuation corrections. Z'_m is calculated using a radar equation at all range bins above the `binClutterFreeBottom` except missing data which are labeled by `dataQuality` in L1B product. The result of Z'_m is stored in `zFactorMeasured`. The radar equation is as follows.

$$
\begin{aligned}
P_r &= C \cdot P \cdot L_r \cdot E \\
&= [P_t \cdot G_{\text{at}} \cdot G_{\text{ar}}] \left[\left(\frac{\lambda}{4\pi r} \right)^4 \frac{4\pi}{\lambda^2} \right] L_r \left[\frac{\pi^5}{\lambda^4} |K|^2 Z_e 10^{-18} c\tau \frac{\pi r^2 \theta_{0a}\theta_{0c}}{2^4 \ln(2)} \right] \\
&= \frac{\pi^3 c}{2^{10} 10^{18} \ln(2)} \frac{P_t G_{\text{at}} G_{\text{ar}} \theta_{0a}\theta_{0c}\tau |K|^2}{\lambda^2 r^2} L_r Z_e
\end{aligned}
$$

In the preparation module, Z'_m $(= L_r Z_e)$ is calculated by using the following equation.

$$
P_r = \frac{\pi^3 c}{2^{10} 10^{18} \ln(2)} \frac{P_t G_{\text{at}} G_{\text{ar}} \theta_{0a}\theta_{0c}\tau |K|^2}{\lambda^2 r^2} Z'_m
$$

$$
Z'_m = \frac{2^{10} 10^{18} \ln(2)}{\pi^3 c} \frac{\lambda^2 r^2 P_r}{G_{\text{at}} G_{\text{ar}} \theta_{0a}\theta_{0c}\tau |K|^2 P_t}
$$

where

r range distance (`rangeDist`)

λ wave length (`eqvWavelength` of L1B)

$|K|^2$ dielectric factor (0.9255 for KuPR and 0.8989 for KaPR)

G_t transmitter antenna gain (`txAntGain` of L1B)

G_r receiver antenna gain (`rxAntGain` of L1B)

θ_c Cross-track beam width (`crossTrackBeamWidth` of L1B)

θ_a Along-track beam width (`alongTrackBeamWidth` of L1B)

c light speed

τ transmitter pulse width (`transPulseWidth` of L1B)

P_t transmitted power (`radarTransPower` of L1B)

P_r received signal power (`echoSignalPower`)

It should be noted that $|K|$ is a constant in the preparation module. Any adjustment of $|K|$ by temperature is controlled in the solver module if necessary.

Calculation of $\sigma_m^0{}'$ (`sigmaZeroMeasured`)

$\sigma_m^0{}'$ is defined as the measured normalized surface cross section without any attenuation corrections. Calculation of $\sigma_m^0{}'$ is done for all footprints except missing data which are labeled by `dataQuality` in L1B product. The value of $\sigma_m^0{}'$ is stored in `sigmaZeroMeasured`.

$$\sigma_m^0{}'(\theta_z) = P_{rs}(r_0)\frac{512\pi^2\ln(2)}{P_t\lambda^2 G_t G_r}\frac{\text{loss}}{1}\frac{\cos(\theta_z)r_0^2}{\theta_a\theta_{bp}}$$

where

$$\theta_{bp}^{-1} = \sqrt{\theta_c^{-2}+\theta_p^{-2}}, \qquad \theta_p^{-1} = \frac{2}{c\tau}r_0\tan(\theta_z)$$

θ_c Cross-track beam width (`CrossTrackBeamWidth` of L1B)

θ_a Along-track beam width (`AlongTrackBeamWidth` of L1B)

P_t transmitted power (`radarTransPower` of L1B)

P_{rs} received signal power (`echoSignalPower`)

r_0 range distance from the satellite to the geographic surface (ref. `binRealSurface`)

θ_z zenith angle (`localZenithAngle`)

loss band path filter loss

λ wave length (`eqvWavelength` of L1B)

G_t transmitter antenna gain (`txAntGain` of L1B)

G_r receiver antenna gain (`rxAntGain` of L1B)

c light speed

τ received pulse width (`receivedPulseWidth` of L1B)

3.3.3. Interfaces to other algorithms

As to the Ku-band and Ka-band level-2 algorithms, input data for this module is Ku-band and Ka-band level-1B product, respectively. For the DPR level-2 algorithm, input data for this module are level-2 products and level-2 supplementary products of both Ku-band and Ka-band. The outputs will be used by the Solver module and other modules in the DPR algorithm.

3.3.4 Output Variables

`adjustFactor` :Adjustment factor (dB) for `zFactorMeasured` ($\mathrm{dB}Z'_m$) and `sigmaZeroMeasured` ($\mathrm{dB}\sigma\ 0'_m$). $\mathrm{dB}Z'_m = \mathrm{dB}Z_m - \mathtt{adjustFactor}, \mathrm{dB}\sigma\ 0'_m = \mathrm{dB}\sigma_m^0 - \mathtt{adjustFactor}$

`binClutterFreeBottom`: Range bin number for clutter free bottom.

`binRealSurface`: Range bin number for real surface.

`binStormTop`: Range bin number for the storm top.

`elevation`: Elevation of the measurement point.

`ellipsoidBinOffset`: Distance between the ellipsoid and a center range bin of `binEllipsoid`.

`flagPrecip`: A flag of Rain/NoRain classification.

`flagSigmaZeroSaturation`: A flag of saturation of `sigmaZeroMeasured`.

`heightStormTop`: Height of storm top.

`landSurfaceType`: Land surface type.

`localZenithAngle`: Local zenith angle of each ray.

`sigmaZeroMeasured`: Surface backscattering cross section without attenuation correction.

`snRatioAtRealSurface`: Signal/Noise ratio at real surface range bin.

`snRatioAtRealSurface` $= 10 \times \log_{10}(\mathrm{echoPowertrueV[mW]/noisePowertrueV[mW]})$

`snowIceCover`: Snow and ice cover information. It refers to the multisensor snow/ice cover maps provided by NOAA.

`zFactorMeasured`: Vertical profile of reflectivity factor without attenuation correction.

3.4 Vertical Profile Module

3.4.1 Objectives and functions of the Vertical Profile Module (VER)

The primary purposes of the VER are to read ancillary environmental data, to provide vertical profiles of the environmental parameters, to compute the path-integrated attenuation (PIA) due to non-precipitation (NP) particles, and to give radar reflectivity factors corrected for attenuation by the non-precipitation particles. The VER provides environmental information such as pressure, temperature, water vapor, and cloud liquid water at each range bin. The VER calculates the attenuation due to water vapor, molecular oxygen, and cloud liquid water.

For Ku, Ka, Ka_HS, the VER is executed using the information of the pixel lat/lon and the range bin width. For the DPR, results of the Ku, Ka, Ka_HS are introduced.

Algorithm descriptions of the VER

3.4.2 Algorithm descriptions of the VER

Basic functions of the VER were reviewed in Kubota et al. (2020). Here, they are desrcibed in terms of "Utilization of ancillary environmental data", "Calculation of attenuation by water vapor", "Calculation of attenuation by molecular oxygen", and "Calculation of attenuation by cloud liquid water (CLW)".

Utilization of ancillary environmental data

The VER inputs ancillary environmental data, objective analysis data by Japan Meteorological Agency (JMA) named as JMA Global Analysis (GANAL) product. By reading the ancillary environmental product, the VER provides pressure, temperature, water vapor, and cloud liquid water for each range bin. In addition, the VER computes the height of 0 degree centigrade and finds out the range bin corresponding to that height.

The horizontal resolutions of the GANAL data are 0.5 degree latitude/longitude, respectively. The pressure levels such as 1000, 925, 850, 700, 600, 500, 400, 300, 250, 200, 150, 100 hPa, and so on are converted to the height levels before the input of the algorithm. The temporal resolution is 6 hourly as 00, 06, 12, and 18Z. The VER inputs two 6-hourly files and computes the values of parameters at the time of measurement using linear temporal interpolation. We also use a linear horizontal and vertical interpolation to calculate the location of each range bin from the lat/lon's of the footprint and the satellite and the range bin height. Figure 3.4-1 shows how this interpoloation is carried out by finding the antenna beam direction from the lat/lon information and a local zenith angle of the spacecraft and the "height" provided by the preparation module (see Section 3.3). The VER provides pressure, temperature, water vapor, and cloud liquid water at each range bin.

$$(x_p, y_p) = (x_1, y_1) + (x_s - x_1, y_s - y_1)\frac{h}{d_{\text{ist}}}\tan\theta$$

$$d_{\text{ist}} = \sqrt{c_x^2(x_s - x_1)^2 + c_y^2(y_s - y_1)^2}$$

(x_p, y_p): (lon, lat) of target range bin
(x_s, y_s): (lon, lat) of satellite
c_x: conversion factor from longitudinal degree to m
c_y: conversion factor from latitudinal degree to m
θ: scLocalZenith (L1)
h: Height
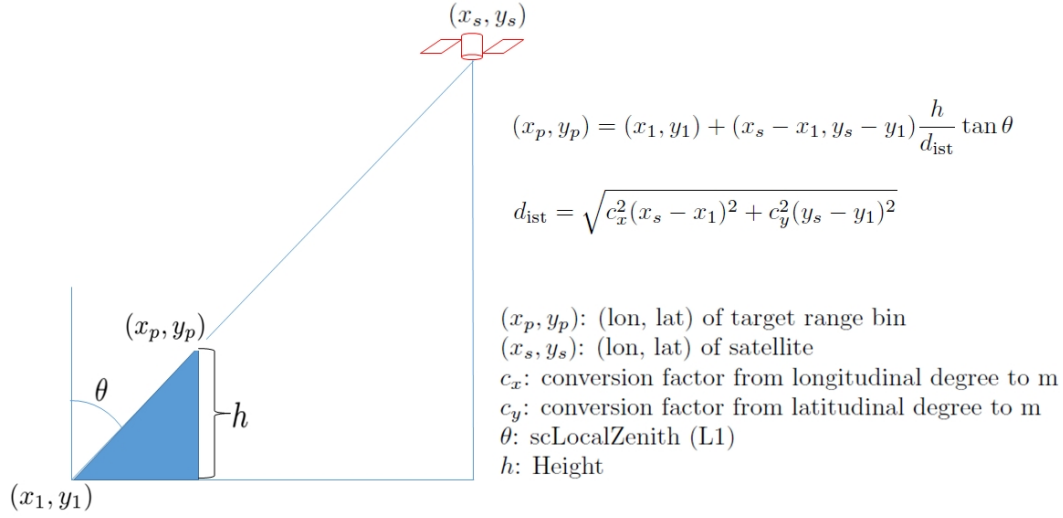
Figure 3.4-1 A concept of consideration for the antenna beam directions in the VER.

Calculation of attenuation by water vapor

At a frequency less than 100 GHz, the attenuation coefficient due to water vapor, $\kappa_{\text{H2O}}(f)$ (dB/km) is expressed as follows (Waters 1976, Ulaby et al. 1981, Meneghini and Kozu 1990),

$$\kappa_{\text{H2O}}(f) = 2f^2\rho_\nu\left(\frac{300}{T}\right)^{3/2}\gamma_l\left[\left(\frac{300}{T}\right)e^{-644/T}\frac{1}{(494.4 - f^2)^2 + 4f^2\gamma_l^2} + 1.2\times10^{-6}\right]$$

where

f: frequency (GHz)

ρ_ν: water vapor content (g/m3)

γ_l: parameter of line width (GHz)

T: temperature (K)

The line width parameter γ_l is given as

$$\gamma_l = 2.85\left(\frac{P}{1013}\right)\left(\frac{300}{T}\right)^{0.626}\left(1 + 0.018\frac{\rho_\nu T}{P}\right)$$

where P: pressure (hPa).

In precipitation pixels, the water vapor content provided by the GANAL may be problematic due to its relatively low resolution (0.5x0.5 deg. lat/lon). Therefore, a minimum threshold is used in the VER. The relative humidity is set to 90% when the GANAL gives a value less than 90% in precipitation pixels.

Calculation of attenuation by molecular oxygen

For attenuation by molecular oxygen, the following expression is valid for frequencies less than 45 GHz (Rosenkranz 1975, Ulaby et al. 1981, Meneghini and Kozu 1990).

$$\kappa_{\text{O2}}(f) = 1.1\times10^{-2}f^2\left(\frac{P}{1013}\right)\left(\frac{300}{T}\right)^2\gamma\left[\frac{1}{(f - f_0)^2 + \gamma^2} + \frac{1}{f^2 + \gamma^2}\right]$$

where

f: frequency (GHz)

f_0: 60 GHz

γ: parameter of line width (GHz)

T: temperature (K)

Line width parameter γ is given by

$$\gamma = \gamma_0 \left(\frac{P}{1013} \right) \left(\frac{300}{T} \right)^{0.85}$$

where

$$\gamma_0 = \begin{cases} 0.59, & \text{for } 333 \leq P \text{ (hPa)}; \\ 0.59[1 + 3.1 \times 10^{-3}(333 - P)], & \text{for } 25 \leq P < 333 \text{ (hPa)}; \\ 1.18, & \text{for } P < 25 \text{ (hPa)}. \end{cases}$$

Calculation of attenuation by cloud liquid water (CLW)

For attenuation by cloud liquid water κ_{CLW} over non-precipitation pixels, cloud water contents in the ancillary environmental data product are utilized. In the cloud scheme of the JMA Climate Data Assimilation System (JCDAS) product (Onogi et al. 2007), the effective radius (r_e) of cloud liquid droplets is fixed at 15 microns. In this calculation, we assume cloud particle distribution $n_c(D)$ as mono-disperse, that is,

$$n_c(D) = N_c \delta(D - 2r_e)$$

where

D: Diameter

r_e: 15 microns

N_c: Number concentration of cloud liquid particles

For cloud liquid water content Q (kg/m3), N_c is expressed as follows,

$$N_c = \frac{3Q}{4\pi r_e^3 \rho_w}$$

κ_{CLW} is computed due to the Rayleigh scattering using $n_c(D)$. The mono-disperse assumption implies the homogeneity of the cloud distribution, although clouds generally distribute with high inhomogeneity within the grid-size of the reanalysis such as 1.25-degree latitude/longitude. Therefore, the previous formula will underestimate κ_{CLW} over precipitation pixels. In the 2A25 algorithm for the TRMM/PR, κ_{CLW} over precipitation pixels is estimated based on the result of a numerical simulation of storms with a cloud-system resolving model (CRM) that was used to create the database for the TRMM/TMI 2A12 algorithm (Iguchi et al. 2009). In their method, the attenuation due to CLW is estimated as a function of surface precipitation rate, separately for

convective columns and stratiform columns. The VER adopts a method which expands Iguchi et al. (2009) and κ_{CLW} is estimated from a CLW database as a function of surface precipitation rate, precipitation type (convective or stratiform), temperature, latitude, and land surface type (Kubota et al. 2012, 2020). The CLW database was generated by 3.5 km-mesh global simulations performed using a Nonhydrostatic ICosahedral Atmospheric Model (NICAM). The NICAM is a global cloud-system resolving model (GCRM), and explicitly calculates moist convection using a cloud microphysical scheme. The NICAM data were provided by the University of Tokyo and Japan Agency for Marine-Earth Science and Technology (JAMSTEC).

3.4.3 Input Variables

Input: from MOSS or PPS

Ancillary environmental data Two 6-hourly files

  Surface: Surface pressure, Mean sea level pressure

  Pressure levels: Geopotential height, temperature, water vapor, and cloud liquid water

Input: from Preparation Module

```
Geolocation
scanTime
Elevation
landSurfaceType
localZenithAngle
flagPrecip
binRealSurface
binStormTop
heightStormTop
binClutterFreeBottom
sigmaZeroMeasured
zFactorMeasured
rangeBottom
rangeTop
Height
```

3.4.4. Definitions of Output Variables

`airTemperature[80][49]` Temperature

`rangeZeroDeg[49]` Range bin number corresponding to the level of 0 degree centigrade.

`heightZeroDeg[49]` Height of the level of 0 degree centigrade.

`airPressure[80][49]` Pressure (hPa)

`waterVapor[80][49]` Water vapor (kg/m3)

`attenuationNPwv[80][49]` Attenuation by water vapor (dB/km)

`attenuationNPoxygen[80][49]` Attenuation by molecular oxygen (dB/km)

`cloudLiquidWater[80][49]` Cloud Liquid water content (kg/m3)

`attenuationNPclw[80][49]` Attenuation by cloud Liquid water (dB/km)

`attenuationNP[80][49]` Sum of Attenuations by water vapor, molecular oxygen, and cloud liquid water

$$\text{Atten}_{\text{NP}}(r) = \kappa_{\text{WV}}(r) + \kappa_{\text{O2}}(r) + \kappa_{\text{CLW}}(r)$$

`piaNP[80][49]` PIA by the non-precipitation particles.

$$\text{PIA}_{\text{NP}}(r) = 2\int_0^r \text{Atten}_{\text{NP}}(s)\,ds = 2\int_0^r \kappa_{\text{WV}}(s) + \kappa_{\text{O2}}(s) + \kappa_{\text{CLW}}(s)\,ds$$

`zFactoNPCorrected[80][49]` Radar reflectivity corrected for attenuation by the non-precipitation particles

$$Z_m(r) = Z'_m(r)/A_{\text{NP}}(r)$$

$$A_{\text{NP}}(r) = \exp(-q\text{PIA}_{\text{NP}}(r)) \quad \text{where} \quad q = 0.1\ln(10)$$

`sigmaZeroNPCorrected[49]` σ^0 corrected for attenuation by the non-precipitation particles

$$\sigma^0 = \sigma^{0'}/A_{\text{NP}}(r)$$

$$A_{\text{NP}}(r_{\text{sfc}}) = \exp(-q\text{PIA}_{\text{NP}}(r_{\text{sfc}})) \quad \text{where} \quad q = 0.1\ln(10)$$

3.4.5. Intermediate Files

Before the input of the algorithm, the pressure levels of the ancillary environmental data are converted to the height levels. In addition, the attenuations and PIA estimates by water vapor, molecular oxygen, and cloud liquid water are computed in advance.

3.4.6. Description of the Processing Procedure

Before the input of the algorithm, the pressure levels of the ancillary environmental data will be converted to the height levels. In addition, the attenuations and PIA estimates by water vapor, molecular oxygen, and cloud liquid water will be computed in advance.

For Ku, Ka, Ka_HS, the VER is executed using the information of the pixel lat/lon and the range bin width. For the DPR, calculated results of the Ku, Ka, Ka_HS are used.

3.4.7. Interfaces to other algorithms:

Input data for this algorithm is from the Preparation Module and Ancillary environmental data; the outputs will be used by the Classification module, DSD module, Solver Module and others.

3.5 Classification Module

3.5.1 Introduction

In reliable rain rate retrieval using space-borne radars, information about the drop size distribution (DSD) is necessary. DSD varies depending on the rain type. Therefore, rain type classification plays an important role in the GPM DPR algorithm. There exist two distinctive rain types, one is stratiform and the other is convective. Stratiform rain is characterized by its weakness in intensity, wide extension in area, and in many cases accompanying a bright band (BB) in radar echo. Because of the last characteristic, detection of a BB can be used for determining stratiform rain.

The rain type classification is made on pixel basis. Hence, the rain type is the same along a radar beam. Then there arises the following ambiguous situation. Suppose that, when the radar reflectivity being examined along a given radar beam, the precipitation echo happens to exist only at altitude higher than $0°$C height. What is the rain type for this case? Is it stratiform or convective? This is a difficult question to answer. To handle such an ambiguous case, the third category of "other" type is introduced in a similar manner to the case of the TRMM PR algorithm 2A23. The third category "other" means that there exists only cloud or possibly noise when the radar echo is examined along the radar beam.

A surprise in the early TRMM PR observation was a ubiquitous shallow isolated rain system, which may be warm rain but it still remains a puzzle what it actually is. TRMM PR observation shows that shallow isolated rain is weak, which does not agree with the concept of warm rain which is thought to be very strong. There also exists shallow non-isolated rain, whose statistical properties seem to be very similar to those of shallow isolated rain. Shallow rains (both shallow isolated and shallow non-isolated rain) are marked by a shallow rain flag, `flagShallowRain`, which is independent of the rain type flag, `typePrecip`.

Main features of each CSF module, from V5 up to V6X, are as follows.

In the V5 classification (CSF) module, new items (`flagHeavyIcePrecip`, `flagAnvil`, `surfaceSnowfallIndex`, and `flagSurfaceSnowfall`) were added to the output fields and a decision on winter convective type was also made. Section 3.5.5 describes these features.

In the V6 CSF module, reclassification of precipitation type from convective to stratiform is made by using a method developed by the UW (University of Washington) (Houze and Brodzik, 2017; private communication), which examines the slope of Z profile above the $0°$C isotherm (see Section 3.5.4-1-4-5 for details).

In the V6X CSF module, the full scan (FS) Ka band single frequency data processing and the FS dual frequency data processing were made for the first time.

3.5.2 Objectives

The CSF module detects bright band (BB) and classifies rain into three major categories, which are stratiform, convective, and other.

3.5.3 Algorithm Principles

In single frequency CSF modules, i.e., in Ku-only and Ka-only modules, rain type classification is made by a V-method (Vertical profiling method) and by an H-method (Horizontal pattern method) (Awaka et al., 1998, 2009). The rain types by the V-method and H-method are unified, and the Classification (CSF) module outputs the unified rain type, which consists of three major categories; stratiform, convective, and other.

In the dual frequency algorithm of GPM DPR, however, rain type classification is made by a new method called measured dual frequency ratio (DFR_m) method (Le and Chandrasekar, 2013a, 2013b) and by using the single frequency result from the Ku-only module. The DFR_m method is a kind of vertical profiling method, and classifies rain type into stratiform, convective and transition. Though transition is a new type, it is not a major category. The rain types by the DFR_m method and those by the Ku-only module are unified (Awaka et al. 2016). Three major categories, after the unification of rain types of DFR_m method and Ku-only results, are again stratiform, convective and other.

3.5.3-1 Single frequency: V-method

In the single frequency V-method, detection of BB is made first. Detection of a BB is made by examining the vertical profile of the radar reflectivity factor (Z) to see if the vertical profile of Z satisfies certain conditions which are typical to the profile of Z when a BB exists. When a BB is detected, the rain type is stratiform if the reflectivity factor in the rain region does not exceed a special convective threshold (46 dBZ). When a BB is not detected, and the reflectivity factor exceeds a conventional convective threshold (40 dBZ), the rain type is convective. (For details of convective thresholds, see **3.5.4-1-4-1**.) When rain type is neither stratiform nor convective, the rain type is "other" in the V-method.

3.5.3-2 Single frequency: H-method

In the H-method, a horizontal pattern of a representative radar reflectivity factor is examined. Here the representative reflectivity factor means the maximum value of reflectivity factor in the rain region along the considering radar beam. Rain type is classified using a modified University-of-Washington convective/stratiform separation method (Steiner et al. 1995, Yuter and Houze 1997). In the H-method, rain type is again classified into three categories: stratiform, convective and other. In the H-method, detection of convective rain is made first. If the rain type is not convective, the rain type is stratiform unless the reflectivity factor is very small, being almost identical to noise. If rain type is neither convective nor stratiform, the rain type is other.

41

3.5.3-3 Dual frequency: DFR_m method

In the dual frequency module, in place of the V-method, the DFR_m method is used for rain type classification and for BB detection in the inner swath. The DFR_m method uses the difference between the measured Ku-band Z in dB and the measured Ka-band Z in dB. To make the BB detection reliable, BB detected by the DFR_m method and that by the Ku-only algorithm are unified in the dual frequency CSF module. Rain types by the DFR_m method are stratiform, convective and transition. In the outer swath in which only Ku-band data is available, rain type and BB are copies of those in the Ku-only module. The DFR_m method is also used for handling HS data by interpolation, which is made vertically and horizontally. In the vertical interpolation, the Ka-band data with a 125 m interval is interpolated from the 250 m interval HS data. In the horizontal interpolation, four Ku-band pixels adjacent to the HS pixel are used for the interpolation of the corresponding Ku-band data at the HS pixel.

3.5.4 Actual Algorithm (Data Processing)

3.5.4-1 Single frequency processing

In Ku-only and Ka-only algorithms, BB detection is based on a search for a typical BB peak by examining the range profile of radar reflectivity along a given antenna beam. This method is effective for the Ku-band data which show clear BB peaks. In the case of Ka-band, however, since a clear BB peak is not expected, detection of BB is not effective.

3.5.4-1-1 Selection of pixels to be processed:

- Skip the process for the pixel if no precipitation echo exists in Ku-band and Ka-band data. This judgment can be made by examining a flag from the PRE module, `flagPrecip`.
- Skip the process for the pixel if the quality flag of Ku-band and/or that of Ka-band shows that the pixel is a bad pixel or that the data is missing. This judgment can be made by examining a flag from the PRE module, `qualityData`. (It is assumed here that the information about missing data is also available from the `qualityData` flag.)

3.5.4-1-2 Determination of range where precipitation echoes exist:

- Determination of the echo top and the echo bottom, where the echo top is given by `rangeStormTop` from the PRE module and the echo bottom is given by `binClutterFree-Bottom` from the PRE module.

3.5.4-1-3 Detection of bright band (BB) by the single frequency method

- Set the BB search window using `rangeZeroDeg` from the VER module. The BB search window ranges from `rangeZeroDeg` $- 4$ to `rangeZeroDeg` $+ 8$ with a 250 m interval, where the center of the BB window is `rangeZeroDeg` $+ 2$ which is about 0.5 km below the 0 degree height. This window range is reasonable from TRMM PR experience and many other radar

observations (unfortunately, Ka-band radar data may not exhibit a clear BB peak, but the BB search window can be the same for the Ku-band and Ka-band). Experience shows that BB peak appears about 0.5 km below the 0 degree height.

Detection of BB is made using the NP-attenuation corrected radar reflectivity factors, `zFactorNPCorrected`, from the VER module, where NP-attenuation means attenuation due to non-precipitation particles.

Detection of BB can be made by a vertical method. The vertical method examines the profile of radar reflectivity factor. If the profile of the radar reflectivity satisfies certain conditions which characterize BB, it is determined that there exists BB. The above characteristic conditions are different between Ku-band and Ka-band. In the Ku-band, a sharp BB peak should be observed in the profile of radar reflectivity. In the Ka-band, however, a clear BB peak may not be observed, but there must be a detectable characteristic change in the slope in the radar reflectivity profile near the BB.

When BB is detected, the upper boundary of BB (i.e., `rangeBBTop`) and the lower boundaries of BB (i.e., `rangeBBBottom`) are determined. The lower boundary of BB is detected first. The lower boundary of BB is defined as the point where there is the largest change in the slope of Z in the region just below the BB peak. This definition is very close to that by Fabry and Zawadzki (1995). The upper boundary of BB is determined by finding the following two points A and B:

Point A: where there is the largest change in the slope of Z in the upper region of BB peak.

Point B: where Z becomes smaller than Z at the lower boundary of BB for the first time when Z is examined upward in the upper part of BB starting from the BB peak.

When points A and B are the same, the upper boundary of BB is defined as the point A (which is the same as the point B in this case). When points A and B are different, the upper boundary of BB is defined as either A or B that is closer to the BB peak. The definition of the upper boundary is the one which is somewhere in between the definition by Fabry and Zawadzki (1995) and that by Klaassen (1998).

The width of BB (`widthBB`) is computed by the following empirical formula:

$$\texttt{widthBB} = [(\texttt{rangeBBBottom} - \texttt{rangeBBTop}) \times 125 - L\sin(\theta_z)]\cos(\theta_z) \qquad [\text{m}]$$

where θ_z is the local zenith angle, and L is given below:

$$L = L_0 F / \cos^2(\theta_z)$$

Here L_0 (=5000 [m] tentatively) is the footprint size of antenna beam, and F is an empirical factor ($F = 0.5$, tentatively). When the above equation gives $\texttt{widthBB} < 250\cos(\theta_z)$ [m], the

width is set to `widthBB` $= 250 \cos(\theta_z)$ [m]. When BB is detected, the following quantities are computed or given and written to the output of the single frequency CSF module.

- `flagBB`: This flag indicates that BB is detected. (`flagBB` > 0 when BB is detected.)

- `rangeBBPeak`: Range bin number of BB peak. In the case of Ku-band, it is simple and straight forward. In the case of Ka-band, BB peak may not be clear, and the peak position may be displaced from that of Ku-band. Nevertheless, a simple peak search method is used also at Ka-band.

- `rangeBBTop`: Range bin number of BB top.

- `rangeBBbottom`: Range bin number of BB bottom.

- `heightBB`: Height [m] of BB which corresponds to `rangeBBPeak`.

- `widthBB`: Width of BB [m].

- `qualityBB`: Quality flag of BB detection. Details are still TBD. The flag `qualityBB` is meaningful when BB is detected. In V6X, `qualityBB`=1 always when BB is detected (which means that the quality of all the detected BB is good).

3.5.4-1-4 Rain type classification by the single frequency method

In each single frequency CSF module, that is, in Ku-only or Ka-only CSF module, rain type classification is made by two methods: one is a V-method and the other is an H-method. V- and H-methods classify rain into three categories; stratiform, convective and other. The rain types by these two methods are unified, and each single frequency CSF module outputs the unified rain type, which consists of three major categories; stratiform, convective and other.

Each single frequency DPR L2 algorithm adopts a loop structure in the flow of data as shown in Fig. 3.5-0. The data go through the loop only twice. In the 1-st loop, the CSF module uses the radar reflectivity factor, zFactorNPCorrected, processed by the VER module. In the 2-nd loop, the CSF module uses the updated zFactorNPCorrected for the detection of BB in the V-method and for the H-method processing and also uses the attenuation corrected radar reflectivity factor, zFactorCorrected, processed by the SLV module for the determination of convective type in the V-method.

Input
PRE (Preparation) Module
VER (Vertical Profile) Module
zFactorNPCorrected
CSF (Classification) Module
DSD Module
SRT Module
SLV (Solver) Module
zFactorCorrected
Output

(a) Ku loop

Input
PRE (Preparation) Module
VER (Vertical Profile) Module
zFactorNPCorrected
CSF (Classification) Module
DSD Module
SRT Module
SLV (Solver) Module
zFactorCorrected
Output

(b) Ka loop

Figure 3.5-0. Loop structures of L2 data flow (single frequency algorithms only)

3.5.4-1-4-1 V-method

In the V-method, stratiform rain is detected first.

- When BB is detected, the rain type is basically stratiform. There is an exception, however, that when the following two conditions are satisfied, it is convective even though BB is detected:

  (1) $Z_{\mathrm{max_below}} > $ `conv_th_BB` (=46 dBZ for both Ku- and Ka-band),

  (2) $Z_{\mathrm{max\_below}} > Z_{\mathrm{BBPeak}}$,

  where $Z_{\mathrm{max\_below}}$ is the maximum value of `zFactorCorrected` lower than or equal to the height `H_BBBottom` $-$ (about) 0.375 km in the clutter free region and Z_{BBPeak} is the maximum value of `zFactorCorrected` in the BB. `H_BBBottom` is the height of the BB bottom.

- When BB is not detected, the rain type is convective if the following condition is satisfied. Otherwise, the rain type is other.

  (a) The radar reflectivity factor, `zFactorCorrected`, in the valid range between `rangeStormTop` and `binClutterFreeBottom` exceeds a threshold, conv_th, which is 40 dBZ for both Ku-band and Ka-band.

NOTE: When BB is not detected, but if the Ku- or Ka-band storm top is very high (> 15 km, for example), then the rain type may be convective but not other. (Not implemented: a future issue.)

3.5.4-1-4-2 H-method

In the H-method, horizontal texture of the maximum value of `zFactorNPCorrected` in the rain region along each radar beam, Z_{max}, is examined. A modified University of Washington

convective/stratiform separation method is applied to the horizontal extent of $Z_{\max}$. When one of the following conditions is satisfied, the considering pixel is a convective center:

(a) $Z_{\max}$ in the pixel exceeds a convective threshold (40 dBZ for Ku and Ka) , or

(b) $Z_{\max}$ in the pixel stands out against that in the surrounding area.

Rain type of the convective center is convective, and the rain type of pixels adjacent to the convective center is convective. If the rain type is not convective, and if $Z_{\max}$ is not small enough to be considered as noise, the rain type is stratiform. If $Z_{\max}$ is very small, being almost identical to noise, the rain type is other.

3.5.4-1-4-3 Shallow rain and small cell-size rain

Detection of shallow rain is also made independently of the above mentioned methods of rain type classification. When the following condition is satisfied, it is judged as shallow rain, which will be marked by an internal flag:

$$\texttt{heightStormTop} < \texttt{heightZeroDeg} - \text{margin}$$

where margin is currently 1000 m.

Shallow rain is separated out into shallow isolated and shallow non-isolated by examining the horizontal extent of shallow rain. In the rain type unification, both shallow isolated and shallow non-isolated are classified as convective. (It should be noted that in the TRMM PR rain type classification algorithm 2A23 V7, all the shallow isolated is convective, but shallow non-isolated can be either stratiform or convective.)

Detection of rain having small cell size is also made independently. The rain having small cell size is classified as convective in the unification of rain type.

3.5.4-1-4-4 Unification of rain type by the single frequency method

Rain types by the V-method and by the H-method are unified, and the CSF module outputs the unified rain type, which consists of three major categories: stratiform, convective and other. The unified rain type is written to the flag `typePrecip`.

Unification of single frequency rain types is made in the following way.

(1) When a BB is detected by the V-method, rain type is basically stratiform (but is convective if Z close to the surface is exceptionally strong). When a BB is detected, the unified main type follows the V-method decision (and the H-method decision does not affect the unified main type).

(2) When a BB is not detected, and Z examined by the V-method is strong enough to be convective, the unified main type is convective (and the H-method decision does not affect the unified main type).

(3) If not stratiform nor convective, rain type is other by the V-method.

(4) The other type by the V-method is further classified into one of 3 main unified types by using the H-method decision.

The above (1) - (4) form the foundation of the unification of single frequency rain types. Figure 3.5-0a illustrates this foundation. The figure clearly shows that when the V-method says it is stratiform or convective, the V-method type becomes the unified type. But the V-method covers when BB is detected or Z is very strong, the occurrence of such such cases is not so frequent. The V-method is indecisive when BB is not detected or when Z is not so strong. The other type by the V-method means such indecisive cases, which consist the majority of rain events. The H-method covers such indecisive cases by the V-method.

		H-method		
		Stra.	Conv.	Other
V-method	Stra. +BB	Stra. +BB	Stra. +BB	Stra. +BB
	Conv.+BB Conv.	Conv.+BB Conv.	Conv.+BB Conv.	Conv.+BB Conv
	Other	Stra.	Conv.	Other

Figure 3.5-0a. Single frequency rain type unification (basic part).

When the type is stratiform or convective by the V-method, this result is respected by the H-method.On the other hand, the type "other" by the V-method is further classified into stratiform, convective, or other by the the H-method.

The following considerations are also added to the above mentioned basic part.

(5) In the above unification, there are exceptions as follows:
  (a) All the shallow rain is convective in the unified main type except for other.
  (b) All the small cell-size rain is convective in the unified main type except for other. (In the Ku-band processing, some small cell-size rain be reclassified as stratiform by the slope method but its possibility would be very small.)
  (c) When HIP is detected, the unified main type is convective unless a BB is detected. (If a BB is detected and the V-method type is stratiform, the unified main type is stratiform.)
(6) For Ku-band data, some (unified) convective type is reclassified to (unified) stratiform type by the slope method. Details of the slope method are given in the next subsection.

Figure 3.5-0b shows the whole structure of the Ku-band single frequency rain type unification. The structure of the Ka-band single frequency rain type classification is similar to that of Ku-band, but the Ka-band structure does not have the slope method part.
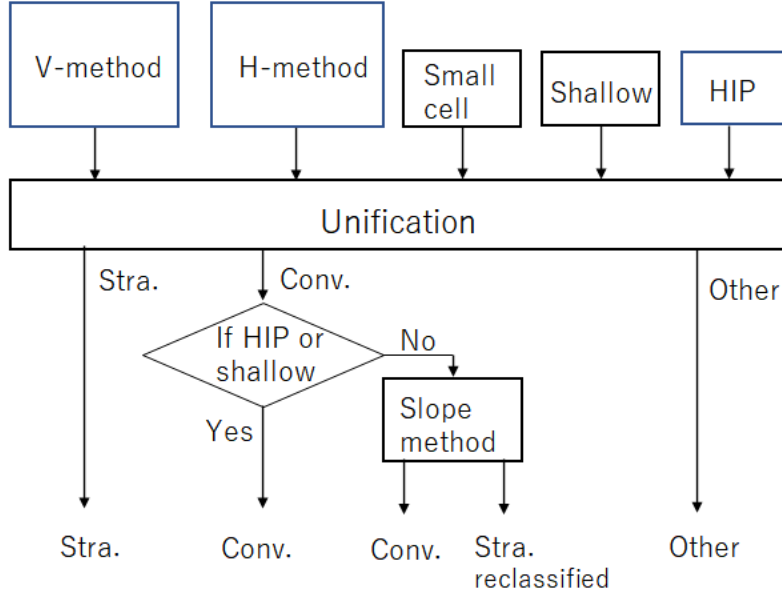
Figure 3.5-0b. Detailed flow of single frequency rain type unification.
The slope method is included in the Ku-band processing only. (When the unification result shown below the very wide narrow box is convective, there is not any further processing in the case of Ka-band.)

The unified rain type is written to the flag `typePrecip`. There are many rain type sub-categories depending on the combination of V- and H-method results. The unified rain type is expressed by eight digit numbers as follows:

$$\texttt{typePrecip} = \text{1xxxxxxx} \quad \text{for stratiform rain,}$$
$$\text{2xxxxxxx} \quad \text{for convective rain,}$$
$$\text{3xxxxxxx} \quad \text{for other rain,}$$

where xxxxxxx varies depending on sub-categories. Details are given in 3.5.9. In a computer program, the three main categories of unified rain type can be obtained easily from `typePrecip`. Let Type be the integer variable for the main category, for example, then the main category can be obtained by one of the following codes:

$$\text{Type} = \texttt{typePrecip} \ / \ 10000000 \ \text{(in Fortran)},$$
$$\text{Type} = \texttt{typePrecip} \ / \ 10000000; \ \text{(in C)}$$

3.5.4-1-4-5 Reclassification of convective type to stratiform type by the "slope method"

In 2017, after examining hundreds of cross-sections of V5 Ku-band data, R. Houze and S. Brodzik of the University of Washington (UW) recognized that many convective pixels in V5 Ku-band output were classified incorrectly. They developed a method for solving the problem by examining the slope of the Ku-band Z profile above the 0 degrees C isotherm and reclassifying the type from convective to stratiform when certain conditions were satisfied. Since the method developed by the UW examines the slope of Z, we refer to it as the "slope method" (Houze and

Brodzik, 2017). The V6 CSF module adopts the "slope method" for reclassifying some convective type to stratiform type at the end of the Ku-only rain type unification. The V6X CSF module also adopts the "slope method" in the Ku-only processing. (Since the reclassified results are handed down to the DPR CSF processing, the CSF DPR module does not carry out a duplicate (i.e., redundant) reclassification using the "slope method.")

The reclassification of convective type to stratiform type by the "slope method" is carried out by using the Z factor corrected for attenuation by the non-precipitation (NP) particles, `zFactoNPCorrected`, and the procedure is as follows:

(1) For each beam, If the unified Ku-only rain type is convective and the shallow_rain_type flag is not set, find the maximum value of Ku-band `zFactorNPCorrected` (`max_refl`) in the BB search window (from `rangeZeroDeg` -8 to `rangeZeroDeg` $+16$ with a 125 m range interval bounded by the highest BB height being 6.5km). At this stage, the V6 CSF module uses the BB search window in order to keep the consistency with the detection of BB, However, further restriction is imposed later (see (3)).

(2) Starting at the `max_refl` point, move up the ray bin by bin to the last point which satisfies this condition:

$$|(\texttt{max\_refl} - \texttt{zFactorNPCrrected})| <= \texttt{REFL\_MAX\_OFFSET} \text{ (currently defined as 2 dBZ)}$$

This is called the reference_point.

(3) If the height of the reference_point is lower than `MAX_BB_HT` (currently defined as 5km), continue. Otherwise, no reclassification will occur for this beam.

(4) Find the comparison point along the NP corrected Z profile which is 1.5 km (`DELTA_HT_FOR_SLOPE`) above the reference_point. (If `zFactorNPCorrected` at 1.5 km above the reference_point is noise, step down the ray bin by bin until a valid value of `zFactorN-PCorrected` is found. That point will become the comparison point.)

(5) Calculate the slope between the reference_point and the comparison_point (defined as $|\texttt{delta\_zFactorNPCorrected}|/|\texttt{delta\_height}|$.

(6) If the slope is greater than or equal to `SLOPE_THRESHOLD` (currently defined as 7.5 dBZ/km), then reclassify the type as stratiform.

NOTE: All parameter values for `REFL_MAX_OFFSET`, `MAX_BB_HT`, `DELTA_HT_FOR_SLOPE`, and `SLOPE_THRESHOLD` were determined empirically. While they have worked well in testing, they may need to be adjusted in the future.

3.5.4-1-4-6 Problem of V6 rain type reclassification by the slope method – Solved in V6X

Immediately after the release of V6 data, it was found that the near surface rainfall rate of the reclassified stratiform type can become very large in rare cases. For stratiform rain, a very

large rainfall rate is unacceptable. This problem has occurred mainly because the V6 "slope method" examines the Z profile aloft, but not Z close to the surface.

The V6X CSF module has solved this problem by introducing a kind of filter at the end of the "slope method" so that if the near surface rainfall rate of the reclassified stratiform type exceeds a threshold, TH_slope, then the reclassified stratiform type is put back to the convective type. In V6X, the following threshold value is used: TH_slope=20 mm/h (Awaka and Brodzik, 2019).

Though the threshold is set to be 20 mm/h, the near surface rainfall rate of the reclassified stratiform rain is found to exceed 20 mm/h in some rare cases. This occurs because the Level 2 (L2) single frequency Ku-band algorithm has a loop structure as shown in Figure 3.5-0.

Figure 3.5-0c shows the single frequency Ku-band loop in a concise form (on the left), which is the same as that shown in Figure 3.5-0, and in a detailed form (on the right). Note that the threshold is set for the 1-st loop SLV output, but the near surface rainfall rate available to the users belongs to the 2-nd loop SLV output. This is the reason why the near surface rainfall rate of the reclassified stratiform rain can exceed 20 mm/h in some rare cases; the CSF module can handle the 1-st loop SLV output but not the 2-nd loop SLV output.
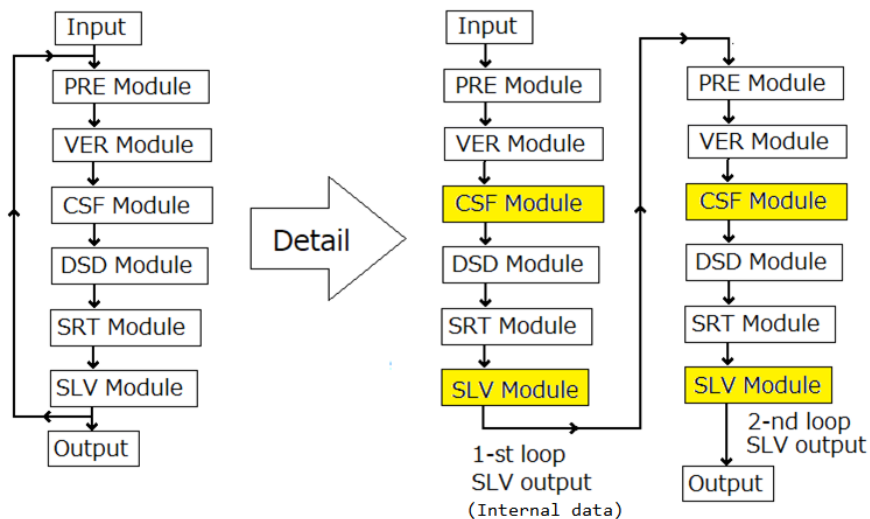
Figure 3.5-0c. Loop structure detail of the single frequency Ku-band L2 algorithm.
The CSF module can use the 1-st loop output of the SLV module, but can not use the 2-nd loop output of the SLV module. The near surface rainfall rate which is available to the users is produced by the 2-nd loop SLV module. This is the reason why, in some rare cases, the near surface rainfall rate of the reclassified stratiform rain, which is obtained by the 2-nd loop SLV module, can exceed the threshold set for the 1-st loop SLV output by the CSF module.

3.5.4-2 Dual frequency processing

In the dual frequency processing, a newly developed DFR_m method is used for the detection of melting layer (ML) and rain type classification. Details of DFR_m method is given in 3.5.4-2-3.

The concept of ML has a meaning wider than that of BB. In other words, BB which appears in the stratiform rain is a subset of ML. Since BB is a subset of ML, the DFR_m method can be used for the detection of BB. In the dual frequency processing, the DFR_m result and the Ku-only result are merged.

3.5.4-2-1 Detection of bright band (BB) by the dual frequency method

In the dual frequency method, BB detected by the Ku-only method and ML by the DFR_m method are compared. Firstly, ML detected by the DFR_m method is regarded as BB. Together with BB detected by the Ku-only method, the median of the height of BB is computed in one scan of data. When the considering height deviates from the median to a large extent, it is judged that the considering BB is not a true BB and the BB decision is rejected.

If BB is detected by both the Ku-only and the DFR_m methods at a given angle bin, it is judged that the height of BB is the height which is closer to the median of BB height.

When BB is thus detected, properties of BB such as height, width, etc., for matched beam data are then determined by using the profile of Z at Ku-band only, because Z at Ku-band shows a clear BB peak but in most cases Z at Ka-band doesn't. Because only the Ku-band Z profile is used for the determination of BB properties, NS outputs of the BB properties in the inner swath are copied to the corresponding MS outputs.

Since the concept of ML is wider than that of BB, and the upper and lower bounds of ML are different from those of BB in general, the following two items are added to the output of dual frequency CSF module (for both MS and HS data):

- `rangeDFRmMLTop`: Range bin number of ML top. (The name was `rangeDFRmBBTop` in V3.)
- `rangeDFRmMLBottom`: Range bin number of ML bottom. (The name was `rangeDFRmBBBottom` in V3.)

Names of the other BB related items are the same to those of single frequency items.

In the HS mode data processing, detection of BB is made by the DFR_m method only.

3.5.4-2-2 Rain type classification by the dual frequency method

As is shown in the next 3.5.4-2-3, the DFR_m method classifies rain into the following three types: stratiform, convective, and transition, the latter of which is a new rain type. The rain type by the DFR_m method is merged with the single frequency Ku-band rain type, and the dual frequency CSF module outputs unified rain type which consists of the following three major types: stratiform, convective and other.

Figure 3.5-0d shows the diagram for unifying rain types by the dual frequency CSF module. Rain types by the DFRm method and those of the Ku-band single frequency are unified. In V6X, the dual frequency unification is made on the full scan (FS) basis for the first time.

Some features of the unification of dual frequency rain types are as follows:
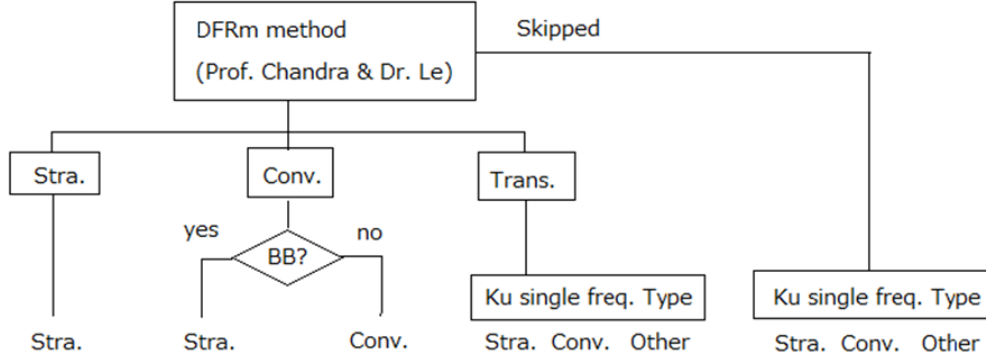
Figure 3.5-0d. Unification of rain types by the dual frequency CSF module.

(1) When the DFR_m rain type is convective or stratiform, the DFR_m decision is respected and the DFR_m rain type is the unified main type if a BB is not detected. If a BB is detected, however, the unified main type is basically stratiform.

(2) When the DFR_m rain type is transition, the single frequency Ku-band rain type is the unified main type.

(3) When the DFR_m processing is skipped, the single frequency Ku-band rain type is the unified main type.

(4) If HIP is detected, the unified main type is basically convective.

The unified rain type is expressed by eight digit numbers as follows:

    typePrecip = 1xxxxxxx for stratiform rain,
                 2xxxxxxx for convective rain,
                 3xxxxxxx for other rain,

where xxxxxxx varies depending on sub-categories. (See 3.5.9 for details.) In a computer program, the three main categories of unified rain type can be obtained easily from typePrecip. Let Rtype be the integer variable for the main category, for example, then the main category can be obtained by one of the following codes:

        Rtype = typePrecip / 10000000 (in Fortran),
        Rtype = typePrecip / 10000000; (in C)

The rain type by the DFR_m method is expressed in the 2nd digit of typePrecip. Hence the rain type by the DFR_m method, if we denote it by DFRmRtype for example, can be obtained as follows:

        DFRmRtype = MOD(typePrecip, 10000000) / 1000000 (in Fortran),
        DFRmRtype = (typePrecip % 10000000) / 1000000; (in C).

When rain exists, DFRmRtype takes one of the following values:

        1: stratiform,
        2: convective,

4: transition,

5: when stratiform is changed to convective by the extended DFR_m method explained in 3.5.5-2,

8: DFR_m method skipped at Part B in Fig. 3.5-3 (shown later in 3.5.4-3).

9: DFR_m method skipped at Part A in Fig. 3-5-3 (shown later in 3.5.4-3).

3.5.4-2-3 Detailed description of DFR_m method

Dual-frequency precipitation radar DPR offers Ku and Ka band dual-frequency observations along the vertical profile which allow us additional information to investigate the micro-physical properties using the difference between two frequency observations or so-called measured dual-frequency ratio (DFR_m) defined as

$$\text{DFR}_m = 10\log_{10}(Z_m(K_u)) - 10\log_{10}(Z_m(K_a)) \tag{3.5-1}$$

where Z_m is measured reflectivity. DFR_m profile holds rich information to assist in precipitation type classification and melting layer detection. There are two main functions of DFR_m method in classification module: (1) precipitation type classification, and (2) melting layer detection. Correspondingly, there are two models developed for dual-frequency profile classification method. Figure 3.5-1 shows typical vertical profiles of reflectivity and DFR_m for stratiform and convective rain. These profiles are observations from airborne precipitation radar.

(a)   (b)   (c)   (d)
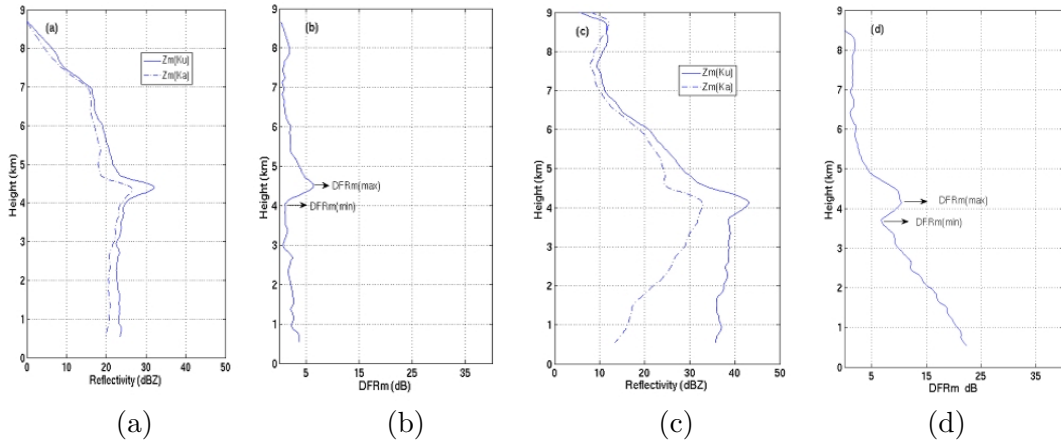
Figure 3.5-1. Typical vertical profiles for stratiform.
(a)(b) and convective (c)(d) rain. (a)(c) Measured reflectivity at Ku and Ka band; (b)(d) DFR_m. $\text{DFR}_m(\text{max})$ and $\text{DFR}_m(\text{min})$ marked on (b) and (d) are local max and min value.

3.5.4-3 Precipitation type classification model

Precipitation type classification model classifies stratiform, transition, and convective rain types. The main parameter used in the model is DFR_m and its vertical variation. In order to quantify

the features of DFR_m, a set of DFR_m indices are defined. Let $V1$ be

$$V1 = \frac{\mathrm{DFR}_{ml}(\max) - \mathrm{DFR}_{ml}(\min)}{\mathrm{DFR}_{ml}(\max) + \mathrm{DFR}_{ml}(\min)} \tag{3.5-2}$$

$\mathrm{DFR}_m(\max)$ and $\mathrm{DFR}_m(\min)$ are shown in figure 3.5-1. DFR_{ml} used in (3.5-2) means DFR_m in linear scale. Let V2 be the absolute value of the mean slope for DFR_m below the local minimum point

$$V2 = \mathrm{abs}(\mathrm{mean}(\mathrm{DFR}_m \mathrm{slope})) \tag{3.5-3}$$

Both $V1$ and $V2$ are normalized values and not dependent on the height or depth of the melting layer. $V1$ values are normally larger for stratiform rain than for convective rain and $V2$ values are larger for convective than for stratiform rain. To further enlarge the difference between stratiform and convective rain types, a third index $V3$ is defined as

$$V3 = \frac{V1}{V2} \tag{3.5-4}$$

The index $V3$ is an effective parameter and provides a separable threshold for performing precipitation type classifications. Extensive statistic studies are performed on index $V3$ using both airborne radar data and GPM real data. Cumulative density function (CDF) of index $V3$ is calculated for stratiform and convective database separated using Ku only classification algorithm. Separable thresholds of C1 and C2 can be found on index $V3$ for stratiform and convective rain types with 70% of CDF. In other words, for stratiform rain: $V3 > C2$; convective rain: $V3 < C1$; transition type: $C1 \leq V3 \leq C2$. $C1$ is smaller than $C2$. "Transition" type is neither a stratiform, nor a convective rain type, but a type transitioning from stratiform to convective rain. Figure 3.5-2 shows histogram of index $V3$ and its cumulative density function calculated using total of 73 storms data with 121859 vertical profiles. Table 3.5-1 shows the thresholds of $C1$ and $C2$ used in the current version. In the future, further adjustment of $C1$ and $C2$ is needed. Figure 3.5-3 illustrates the block diagram for precipitation type classification model that used in the current version.

Table 3.5-1. C1 and C2 thresholds used in precipitation type classification model

70% CDF	121859 vertical profiles of GPM data
C1	0.18
C2	0.20
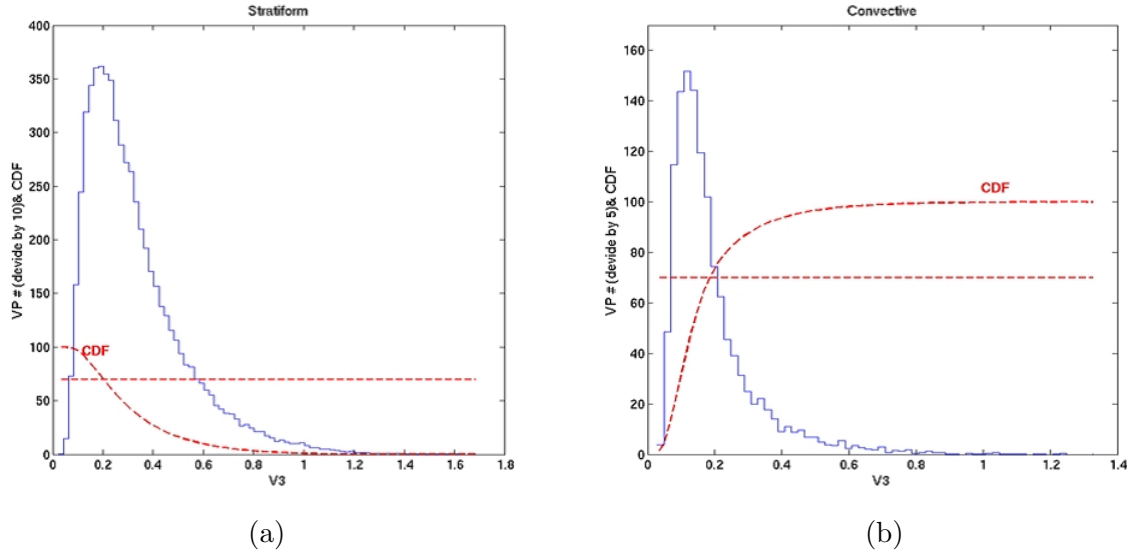
Figure 3.5-2. Histogram of DFR$_m$ index $V3$ with CDF line.
(a) stratiform rain and (b) convective rain calculated using total of 121859 vertical profiles from GPM real data.
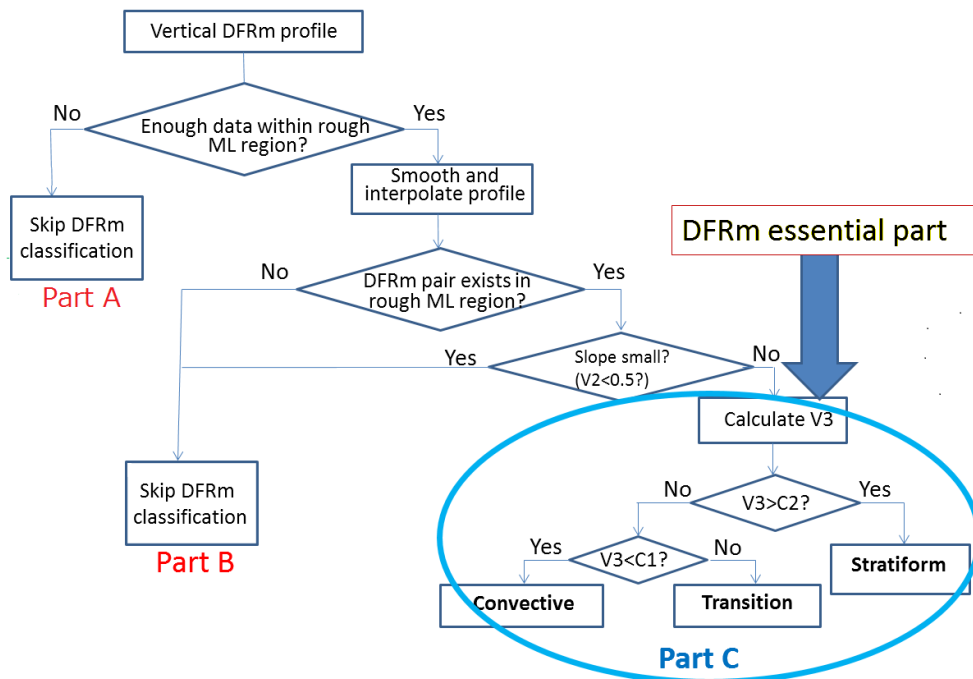
Figure 3.5-3. Block diagram of precipitation type classification model.

3.5.4-4 Melting layer detection model

Melting layer detection model detects melting layer top and bottom height for each vertical profile. The main parameter used in the model is DFR$_m$ profile and its vertical variation. When

DFR$_m$ pair as shown in Fig. 3.5-1 is detected, the melting layer top is defined as the height at which the slope of the DFR$_m$ profile hits a peak value. The melting layer bottom is defined as the height at which the DFR$_m$ profile has a local minimum value. The dashed lines in Fig. 3.5-4 show an illustration of melting layer top and bottom detected.
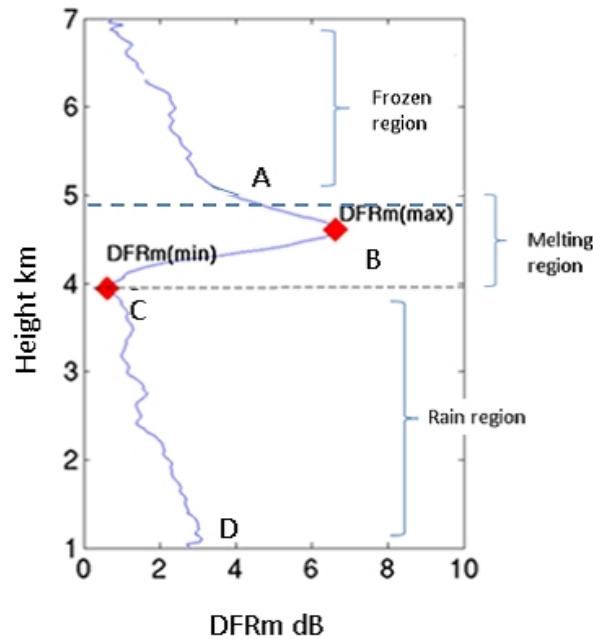
Figure 3.5-4. Schematic plot of DFR$_m$ profile with key points A, B, C, and D.
Point A: slope of DFR$_m$ has peak value. Point B: local maximum of DFR$_m$. Point C: local minimum of DFR$_m$. Point D: DFR$_m$ value near surface.

The criteria described above have been compared with other existing criteria in the literature using different radar parameters. Tilford et al. (2001) used the gradient of reflectivity (Z_m) to detect the bright band top and bottom for stratiform rain type. The linear depolarization ratio (LDR) has been pointed out by many researchers as an important signature in melting phase detection, with certain thresholds determined for different hydrometeor particles (Smyth et al., 1998; Bandera et al., 1998; Tan and Goddard, 1995; Hines, 1983). Typical vertical profiles of reflectivity as well as the corresponding velocity for stratiform and convective type were extensively studied by Fabry and Zawadzki, (1994). Baldini and Gorgucci (2006) mentioned that the rapid change of the hydrometeor fall velocity is an implication of the melting layer. The curvature of velocity was used by Zrnic et al. (1994) in characterizing the melting boundaries. Klaassen (1988) found that the melting bottom can be detected by maximum of velocity. Figure 3.5-5 shows a schematic plot of the comparisons between melting layer detection criteria in DFR$_m$ method and other existing criteria. The comparison results using airborne radar data are listed in Table 3.5-2. From the table, estimations from the DFR$_m$ method match best with velocity based criteria with normalized bias of 1.3% and 2.2% for melting layer top and bottom

respectively. The DFR_m method also compares well with the LDR criteria, with a -28 dB threshold, the bias between these two criteria is around -2.8%. Details can be found in Le and Chandrasekar (2012). Figure 3.5-6 shows a profile comparison between DFR_m method and LDR as well as velocity criteria using APR-2 observations. Figure 3.5-7 is the block diagram of melting layer detection model used in the current version of DFR_m classification method.
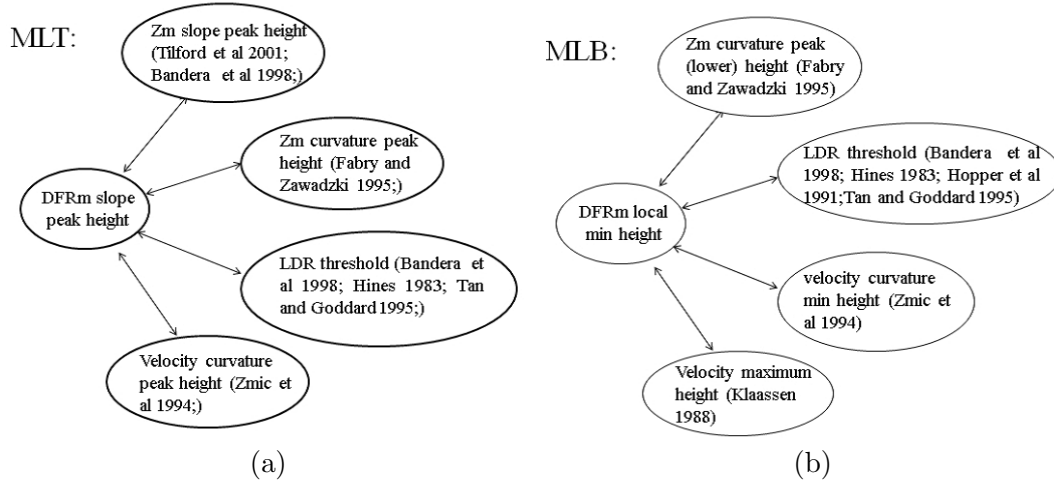
Figure 3.5-5. Schematic plots of some current criteria for melting layer boundaries detection and their possible relations with melting layer detection model used in the DFR_m method.

(a) melting layer top criteria; (b) melting layer bottom criteria.

Table 3.5-2. Comparisons of melting layer boundaries between different criteria for NAMMA, GRIP and Wakasa Bay data.

	Criteria	DFR_m slope peak (NAMMA)		DFR_m slope peak (GRIP)		DFR_m slope peak (Wakasa Bay)	
		NB	NSE	NB	NSE	NB	NSE
Melting layer top comparison	Z_m slope peak	-2.6%	3.6%	-2.5%	3.6%	-4.9%	6.6%
	Z_m curvature peak	1.6%	3.3%	1.5%	3.0%	2.8%	5.2%
	LDR	-2.8%	4.5%	-3.3%	4.2%	-6.0%	7.2%
	Velocity curvature peak	-1.3%	3.6%	-1.4%	3.7%	-1.9%	5.6%

	Criteria	DFR_m slope peak (NAMMA)		DFR_m slope peak (GRIP)		DFR_m slope peak (Wakasa Bay)	
		NB	NSE	NB	NSE	NB	NSE
Melting layer bottom comparison	Z_m curvature peak	4.3%	5.5%	3.7%	5.0%	4.3%	6.9%
	LDR	4.5%	5.9%	4.0%	5.4%	5.4%	11.2%
	Velocity curvature min	2.2%	4.9%	1.7%	4.4%	-0.08%	7.0%
	Velocity max	1.6%	5.9%	1.9%	4.3%	-2.6%	13.9%
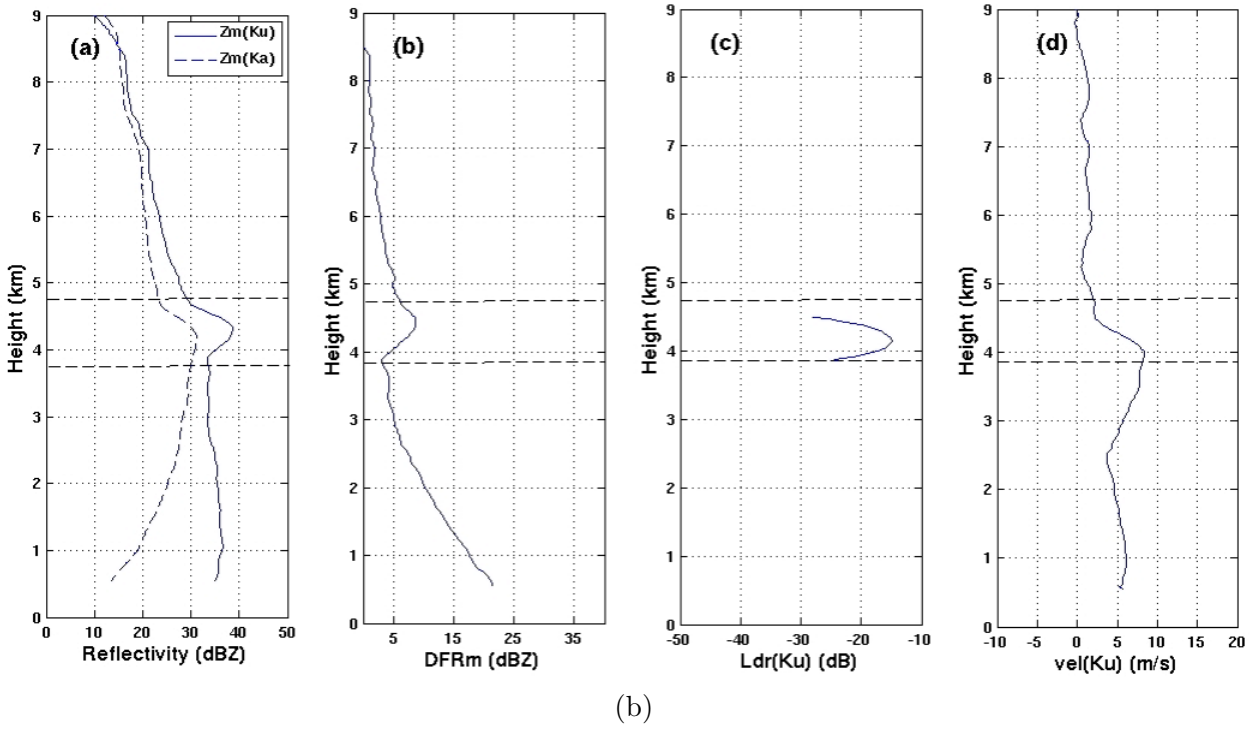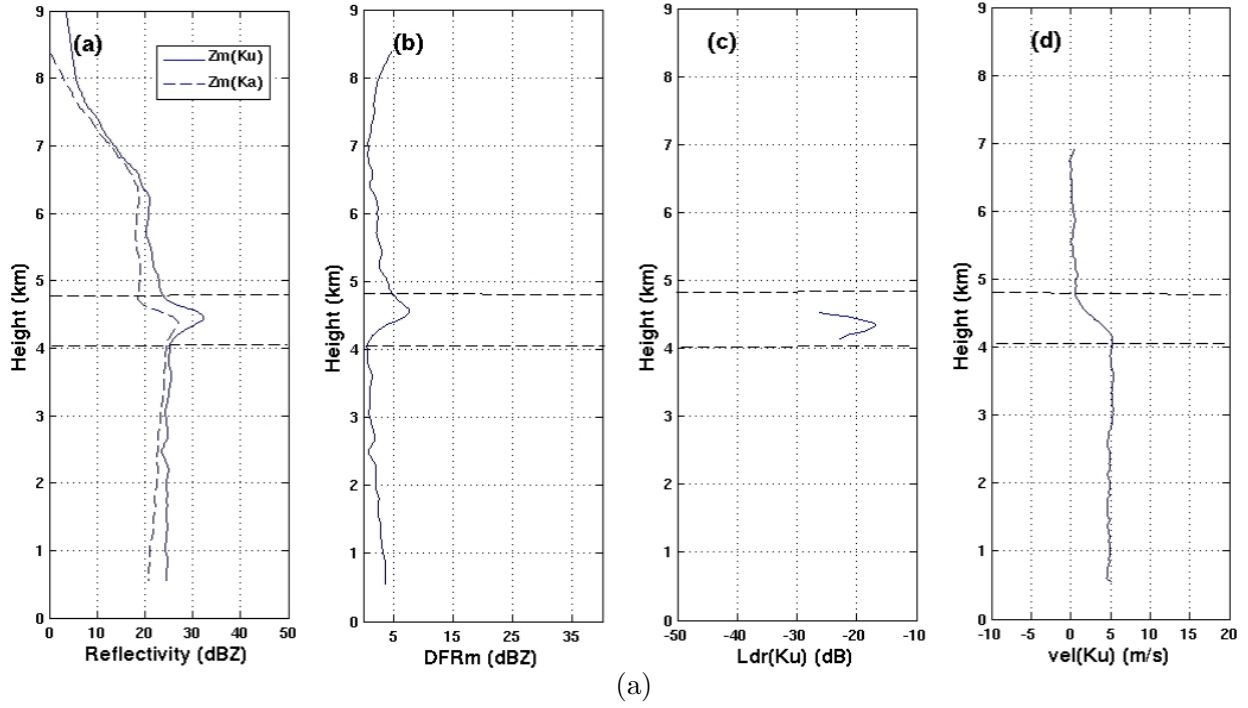
Figure 3.5-6. Sample profile from airborne radar data. Top row (stratiform rain).
(a) Z_m(Ku) and Z_m(Ka); (b) DFR_m; (c) LDR; (d) Velocity;Dashed lines are melting layer top and bottom decided by the DFR_m method. Bottom row (convective rain): (a) to (d) are the same as in top row.
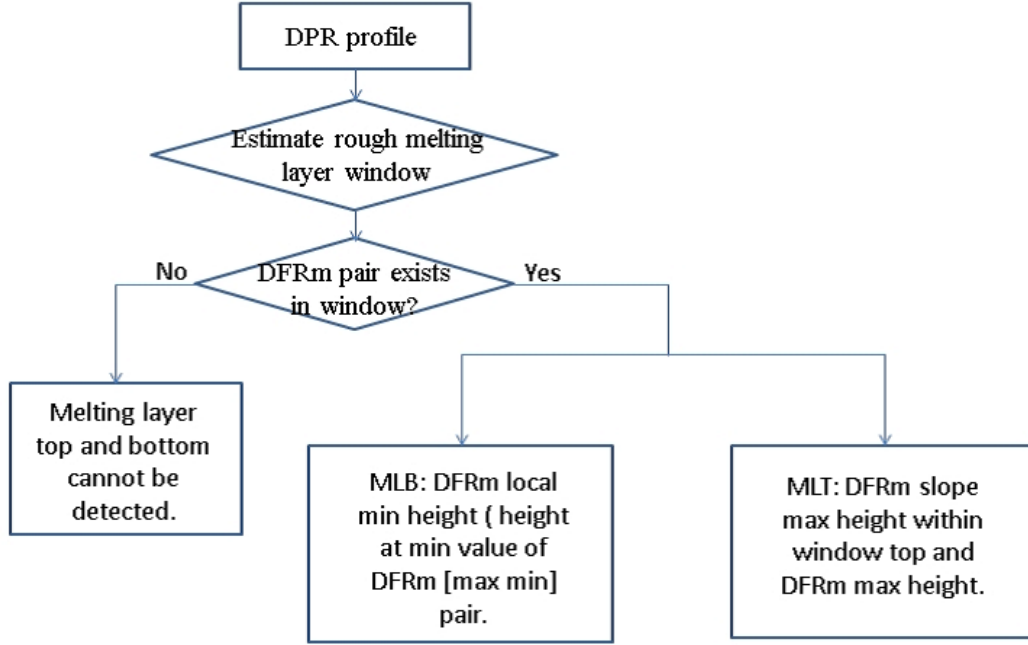
Figure 3.5-7. Block diagram of melting layer detection model for DFR_m method.

3.5.4-4b Modification on melting layer detection of dual-frequency classification model

One function of the dual-frequency classification module is to detect melting layer on a profile basis. Currently, the detection of melting layer top and bottom is done simultaneously. If either the top or bottom is not detected, both melting layer top and bottom are not available. In order to increase the detectability, we modify the current version of algorithm to separate the melting layer top and bottom detection to make it independent. This is reasonable since melting layer top is relatively easy to be detected than melting layer bottom.

In the modification, we have threshold1 and threshold2. When DFRm_diff > threshold2, melting layer top and melting layer bottom are both detected. When DFRm_diff > threshold1 and < threshold2, then only melting layer top is detected, not melting layer bottom. When DFRm_diff < threshold1 or not exist, neither melting layer top or bottom is detected. The threshold1 and threshold2 are 0.5 dB and 2 dB in the modified version. A "FlagML" info is temporarily stored at "qualityTypePrecip" for the purpose of testing the quality of melting layer detection. Independent Flag info (for both MS and HS) should be added to the output of future toolkit. Figure 3_5_3b illustrates the modified flow chart of the melting layer detection algorithm in the dual-frequency classification module.

Figure 3.5-3c shows a section (Scan range: 3032–3070) of the GPM DPR orbit #24981, where precipitation was captured over Buffalo, New York on 22 July 2018. Figure 3.5-3c (a) is Zmku at 2km, while 2 (b) is Zmka at 2 km.
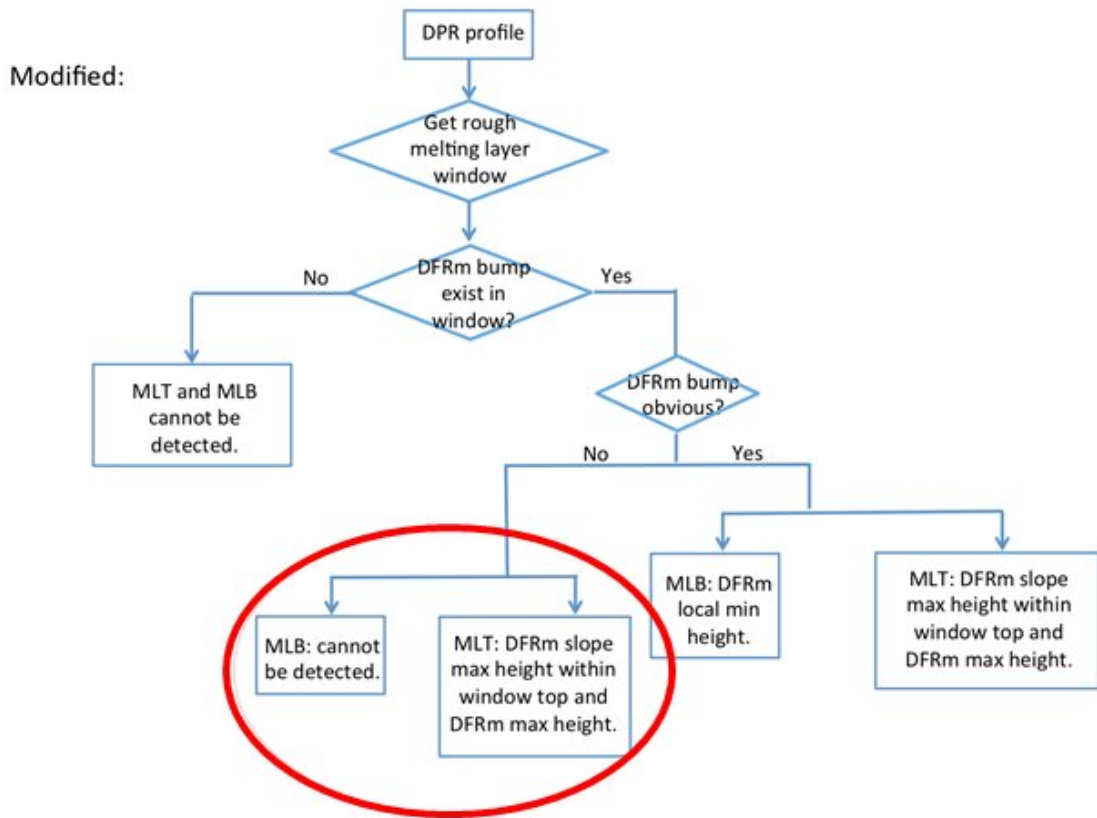
Figure 3.5-3b. Modified block diagram for melting layer top and bottom detection for dual-frequency classification algorithm.

Sample vertical cut at angle bin #18 is shown in Fig. 3.5-3c (c). Black dashed lines are melting layer top and bottom before modification. Pink dashed lines are melting layer top and bottom after modification. For both top and bottom, more detections are made after modification of the code, some of which are circled by the dotted lines. Overall, the percentage of melting layer detection in the scan range increases from 64.2% to 90.3% for top and 64.2% to 86.5% for bottom.

Table 3.5-1b illustrates the count of rain types and melting layer top detection for one day of GPM orbits on 01 August 2018. Column of "V6"indicates the results before modification and column of "new"is for after modification. Changes of stratiform /convective counts occur in the inner swath only. Those small differences between V6 and updated codes occur due to the change of threshold1 (from 2.0 to 1.5). However, melting layer top detection counts increase largely for both MS and HS condition. For MS, during one-day orbits, the count increases from 24,262 to 35,918, with increase percentage of 48%. For the HS condition, the increase percentage is around 63%. This is a big improvement on the melting layer detection part of the dual-frequency classification module. More extensive analysis will be performed in the near future.
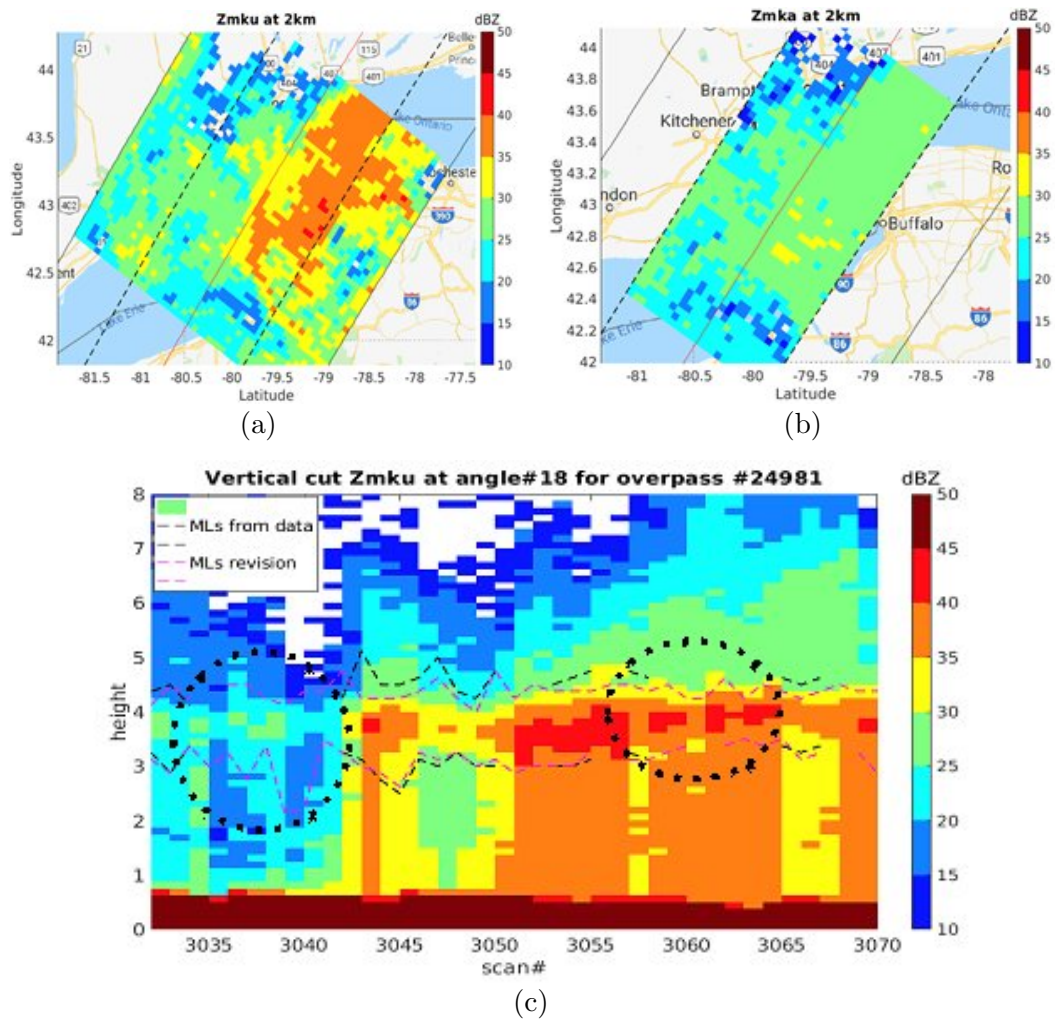
Figure 3.5-3c. GPM DPR orbit #24981 with scan range of (3032–3070).
(a) Zmku at 2km. (b) Zmka at 2 km. (3) Vertical cut at angle bin #18 of Zmku.

Table 3.5-1b. Counts of stratiform, convective rain types as well as melting layer top detection for MS and HS on one- day GPM DPR orbits of 01 August 2018.

	V6	new	
stra (MS)	132,549	132,468	
conv (MS)	33,688	33,771	
MLtop (MS)	24,262	35,918	↑
stra (HS)	120,313	120,408	
conv (HS)	17,880	18,148	
MLtop (HS)	14,020	22,938	↑

61

3.5.5 Other features in the CSF module

Most of the features described in this section arise from the advantage of dual frequency data processing.

3.5.5-1 `flagHeavyIcePrecip`

This flag indicates that a Heavy Ice Precipitation (HIP) is detected in the upper region of storm where the temperature is lower than -10 degrees in Centigrade. Here, HIP is defined as precipitation consisting of ice particles which produces a large measured Z factor (Z_m) and/or produces a large DFR_m. Detection of HIP, proposed by Dr. Iguchi, is made by examining Ku Z_m and Ka Z_m in the single frequency modules and by additionally examining DFR_m in the dual frequency module (Iguchi et al. 2018). The following values of `flagHeavyIcePrecip` are devised to distinguish by which decision HIP is detected (see Figure 3.5-8.)

Default value: `FlagHeavyIcePrecip` $= 0$ (HIP not detected, including the case of missing)

Ku-band decision (Ku FS in V6X, Ku NS in V6)

 If KuPR's $Z_m > 45$ dBZ, then `flagHeavyIcePrecip` $= 12 = $ `0x0C`

 Else if KuPR's $Z_m > 40$ dBZ, then `flagHeavyIcePrecip` $= 8 = $ `0x08`

 Else if KuPR's $Z_m > 35$ dBZ, then `flagHeavyIcePrecip` $= 4 = $ `0x04`

Ka-band decision (Ka FS in V6X, Ka MS in V6)

 If KaPR's $Z_m > 40$ dBZ, then `flagHeavyIcePrecip` $= 3 = $ `0x03`

 Else if KaPR's $Z_m > 35$ dBZ, then `flagHeavyIcePrecip` $= 2 = $ `0x02`

 Else if KaPR's $Z_m > 30$ dBZ, then `flagHeavyIcePrecip` $= 1 = $ `0x01`

DPR decision

 The addition of (A) the above Ku-band decision value, (B) the above Ka-band decision value, and (C) the following DFR_m decision value

  KuPR's $Z_m > 27$ dBZ and $\text{DFR}_m > 7$ dB, then `flagHeavyIcePrecip` $= 16 = $ `0x10`

 (therefore (A)+(B)+(C)) is assigned to the DPR `flagHeavyIcePrecip` (V6X full swath, V6 inner swath).

 Note: In V6, the flag value for the DPR outer swath is the same as that for the Ku NS outer swath.
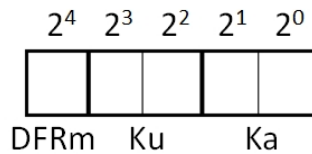
Figure 3.5-8. Bit assignment of `flagHeavyIcePrecip`

In V6X, the following new items relating to HIP are introduced in order to give some information about ranges where the HIP is detected:

(1) `binHeavyIcePrecipTop`, which shows the range bin corresponding to the top height where HIP is detected,

(2) `binHeavyIcePrecipBottom`, which shows the range bin corresponding to the bottom height where HIP is detected,

(3) `nHeavyIcePrecip`, which shows the number of range bins where HIP is detected.

In the C language, those new items are defined as follows:

In the Ku- and Ka- band single frequency standard output:

```
short binHeavyIcePrecipTop[49];
short binHeavyIcePrecipBottom[49];
unsigned char nHeavyIcePrecip[49];
```

In the DPR dual frequency standard output:

```
short binHeavyIcePrecipTop[49][3];
short binHeavyIcePrecipBottom[49][3];
unsigned char nHeavyIcePrecip[49][3];
```

with the second index showing the distinction among single frequency Ku, single frequency Ka, and dual frequency DPR quantities. For example, in the case of `binHeavyIcePrecipTop`

```
binHeavyIcePrecipTop[i][0]
```
shows the Ku decision value for the i-th angle bin,

```
binHeavyIcePrecipTop[i][1]
```
shows the Ka decision value for the i-th angle bin,

```
binHeavyIcePrecipTop[i][2]
```
shows the DPR decision value for the i-th angle bin,

where the C index i runs from 0 to 48.

3.5.5-2 Detection of winter convection

Detection of winter convection is made by examining DFR_m at the storm top and its vicinity. The basic idea is that a large DFR_m near the storm top in winter may indicate the convective nature of precipitation. Since DFR_m is examined, the method in this section can be called an 'extended DFR_m method'. It is found that the above `flagHeavyIcePrecip` plays an important role in the detection of convective precipitation in winter. When the following conditions are satisfied, it is judged that the winter convection is detected by the extended DFR_m method (See DFRmRtype in 3.5.4-2-2.).

(1) The estimated 0C height is lower than or equal to 1 km. (Winter condition.)

(2) `flagHeavyIcePrecip` > 0 is found near the considering pixel. Here, the term 'near' means the inner swath region within -3 to $+3$ scans measured from the considering pixel's scan number (see Figure 3.5-9).

(3) Examine the DFRm of 5 consecutive range bins starting from storm top towards downward direction. At three or more range bins, the following condition is satisfied:

$$\text{DFRm(at x)} > \frac{2.5 - 0.8}{5.0}x + 0.8$$

where x is the relative range bin number counted downward from the storm top.

(4) If Z_m at any of the examining range bins exceeds 35 dBZ, the process of detecting winter convection is skipped because such a large Zm near the storm top may mean the existence of BB.
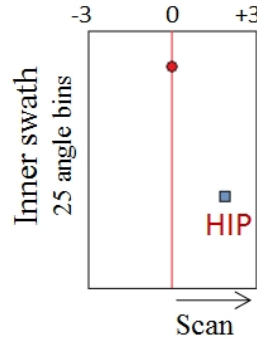
Figure 3.5-9. Nearness of the considering pixel (marked by a circle) to the pixel of `flagHeavyIcePrecip` > 0 (marked by a square)

3.5.5-3 `flagAnvil`

Since the Ku-band PR turns out to have a higher sensitivity, the Ku-band PR data can be used for the detection of 'Anvil'. For the definition of 'Anvil', we need to introduce cloud top and cloud bottom, where cloud top is identical with storm top and cloud bottom means the range bin below which no rain bins continue to some extent. (When precipitation exists, the cloud top always exists but the cloud bottom does not always exist.) As shown in Figure 3.5-10, when the cloud bottom is 500 meters higher than the estimated 0C height, it is defined that the 'Anvil' exists. If there does not exist any precipitation echoes below the 'Anvil', it is judged that the 'Anvil' type 1 is detected. If precipitation echoes exist below the 'Anvil', but if the no rain interval between the cloud bottom and the top of precipitation echoes below the 'Anvil' exceeds 1 km, it is judged that the 'Anvil' type 2 is detected (see Figure 3.5-10(b)). The V5 CSF module detects type 1 'Anvil' and type 2 'Anvil' only. The possible values of `flagAnvil` are as follows:

　　　`flagAnvil`=1: type 1 'Anvil' is detected (there is no rain echo below the 'Anvil'),

　　　　　　=2: type 2 'Anvil' is detected (there exists rain echoes below the 'Anvil'),

　　　　　　=0: 'Anvil' is not detected (including the case of data missing).

3.5.5-4 Surface snowfall

The V5 CSF module introduces a process which determines whether the precipitation at the surface is snow or rain. The process has been developed by Dr. Chandra's group. The process outputs the following two variables. (Though the decision is made in the CSF module, the two variables are available in the Experimental output fields of dual frequency MS.)
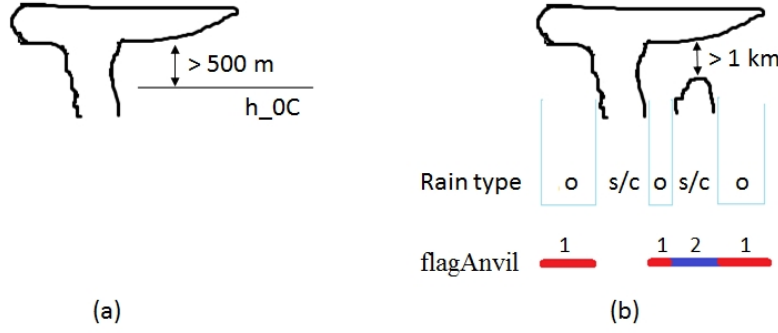
Figure 3.5-10 Definition of 'Anvil'

surfaceSnowfallIndex: If this index exceeds a predetermined threshold, it is judged
　　　that the surface precipitation is snow.

flagSurfaceSnowfall: This flag takes the following two values.

$$\texttt{flagSurfaceSnowfall} = \begin{cases} 1: & \text{The surface snowfall is possible,} \\ 0: & \text{The surface snowfall not detected.} \end{cases}$$

3.5.6 Snow and rain feature on measured dual-frequency ratio (DFR_m) profile

Figure 3.5-11 (a) shows the first snow observation caught by GPM DPR with overpass #000272. On that overpass, there are snow, stratiform and convective rain precipitation within 160 scans (around 800 km) range. In the figure, A, B and C indicates the location of snow, stratiform and convective rain. In order to study vertical profile feature for these different precipitation types, we study averaged reflectivity as well as measured dual-frequency ratio profile for snow, stratiform and convective rain. The vertical profile is calculated from linear averaging of reflectivity at corresponding heights. If data in a pixel is missing or below noise level, it is not considered in the average. Figure 3.5-11 (b) shows the averaged reflectivity profile for snow at Ku-, Ka- band and a measured dual-frequency ratio. As expected, reflectivity at Ku- band is, most of the time, below 25 dBZ. However, the difference between Ku- and Ka- band (indicated by DFR_m) is several dBs, even when reflectivity at Ku- band remains a relatively small value. DFR_m values increase obviously when it comes toward the surface mainly due to the aggregation of the snow particles. Figure 3.5-11 (c) shows an averaged vertical profile for stratiform rain. The bright band is obvious from Ku- band reflectivity. Values of DFR_m below the melting region (or the bright band) are very small indicating that attenuation at Ka- band is very small when reflectivity at Ku- band is less than around 25 dBZ in the rain region. DFR_m values are quite constant with respect to height. In contrast, DFR_m values above melting layer is several dBs and DFR_m slope is noticeable, which is similar to the snow profile in figure 3.5-11 (b). For convective rain, from figure 3.5-11 (d), the maximum of reflectivity at Ku- band is equal or larger than 35 dBZ, while DFR_m values are considerable in the rain region. Large DFR_m

65

values in rain are contributed from both attenuation difference and the non-Rayleigh scattering effect, while the former factor plays a more important role. DFR_mslope for convective rain is large mainly due to large attenuation different change when it comes toward the surface.

One of the features for a convection storm is that it is normally formed at a higher altitude in the atmosphere (except for some warm rain or orographic rain) compared to stratiform and snow precipitation.

Based on analysis above, three ingredients of DFR_m, maximum value of reflectivity at Ku-band, as well as storm top height become important, then are used in the development of the algorithm to identify surface snowfall. To avoid calibration issues, we use the slope of DFR_m instead of DFR_m itself.

3.5.7 Algorithm description

Snow index (SI) is carefully chosen from the features discussed in section 3.5.6. The definition of SI is

$$\text{SI} = \frac{\text{mean}(|\text{DFRm}_{\text{slope}}|)}{\text{Zmku}_{\text{max}} \times \texttt{Storm\_top\_height}} (1)$$

DFR_m slope (in dB/km) is used instead of DFR_m value due to its immunity to calibration change. Zmku_{max} (in dBZ) represents maximum of reflectivity at Ku-band along the profile. Storm_top_height represents altitude of storm top in km. In general, absolute value of DFR_m slope in the numerator of (1) is larger for snow than for stratiform rain. Zmku_{max} value in the denominator is larger for convective rain than for snow, while storm top height in the denominator is lower for snow and stratiform rain than for convective rain. Therefore, SI is expected to be a larger value for snow profile than for rain. In the algorithm, we use the normalized value of Zmku_{max} and Storm_top_height. A statistics study of snow index is performed on large scale of GPM DPR vertical profiles. A total of 353166 rain profiles and 4935 snow profiles are used in this study. Rain profiles are chosen from tropical regions during the summer season and snow profiles are chosen from northern Europe and the northern US in the winter season. Information of 0 degree isotherm is used in profile selection. Figure 3.5.12 shows the histogram of snow index (SI) defined in (1) for snow and rain profiles respectively. In general, as expected, snow index is larger for snow profiles. The cumulative density function (CDF) is calculated for rain, and illustrated as a blue dashed curve in figure 3.5-12, while red dashed curve represents 1- CDF for snow profiles. At around 97% of CDF (or 1-CDF), SI index can separate snow and rain profiles. In other word, 97% of snow profiles have SI > 17, while 97% of rain profiles have SI <= 17. The statistics study considers calibration changes that will be applied to version 5 of the GPM DPR level 2 algorithm.

Figure 3.5-13 shows the flow chart of the surface snowfall identification algorithm that uses snow index. Besides snow index, other auxiliary information such as 0 degree isotherm and clutter free height are used in the algorithm. Although 0 degree isotherm (or surface
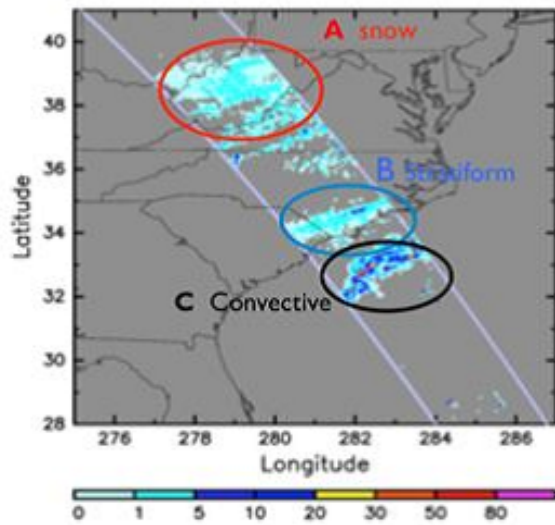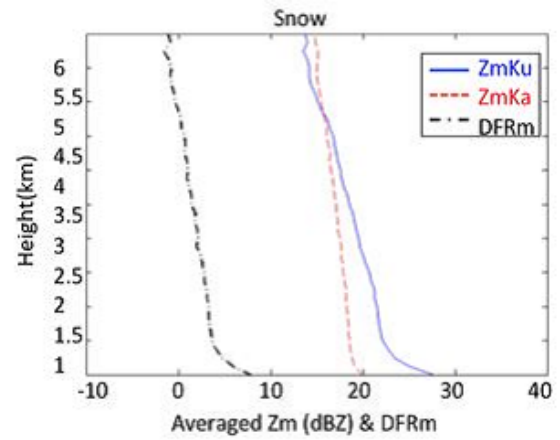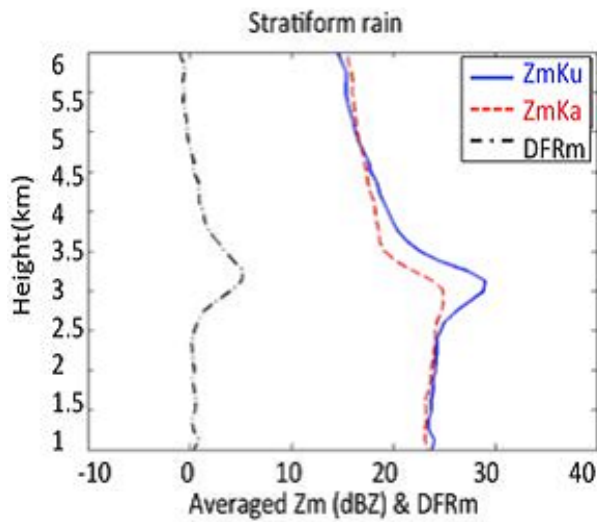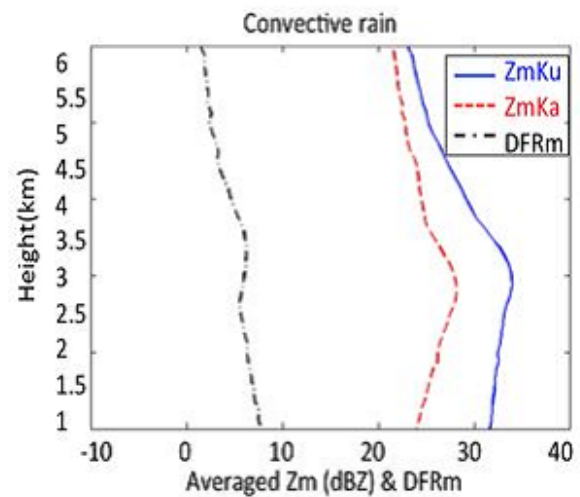
Figure 3.5-11. GPM DPR overpass of rainfall rate on March 17, 2014 (#000272). Circled A, B and C represents snow, stratiform rain, and convective rain. (b) Averaged reflectivity profiles as well as dual-frequency ratio profile for snow. (c) Same as (b) for stratiform rain. (d) Same as (b) for convective rain.

temperature) plays an important role in snowfall detection, its accuracy is a challenge for space-borne weather radars such as GPM. Therefore, in this algorithm, 0 degree isotherm is not the dominant parameter but rather a constraint parameter. Snow index is calculated for profiles with 0 degree isotherm heights not higher than 10 range bins ($\sim$ 1.25 km) above clutter free height. This serves more like a sanity check to filter out nonsense profiles.

67
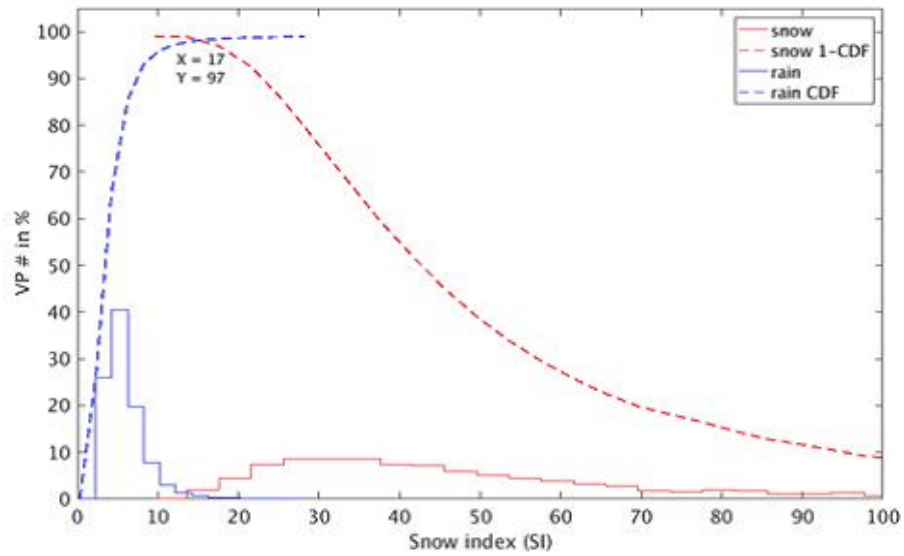
Figure 3.5-12. Large scale study of snow index using GPM DPR profiles.

Histogram of snow index for rain (blue) and snow (red). Blue dashed curve is the cumulative density function (CDF) for rain. Red dashed curve is 1- CDF for snow.
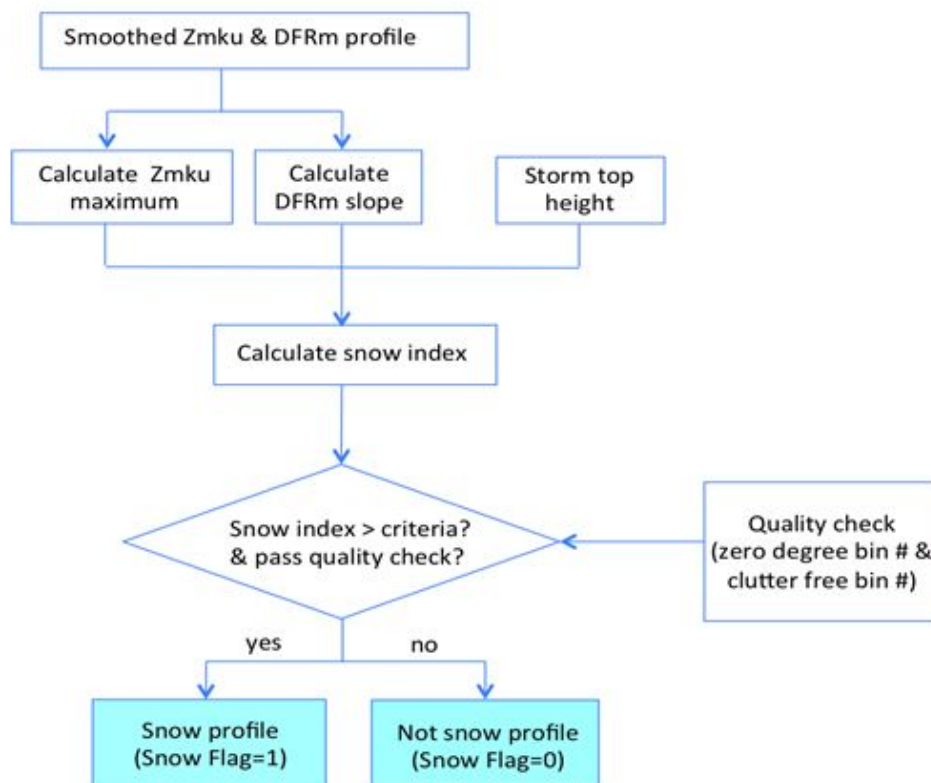
Figure 3.5-13. Flowchart to perform surface snowfall identification in profile classification module of GPM DPR level 2 algorithm.

68

3.5.8 Enhancement of GPM DPR level 2 dual-frequency classification module

In the current DPR level 2 classification module, the vertical profile is classified as either stratiform, convective or other type following the TRMM legacy. However, GPM orbits cover both cold and tropical regions. It is reasonable to add snow flag to vertical profiles that indicate whether there is snow on the surface or not. The surface snowfall identification algorithm takes advantage of dual-frequency measurements from GPM DPR, thus it provides a new approach to detect snow other than the method using surface temperature or surface echo. The algorithm outputs `flagSurfaceSnowfall` and `surfaceSnowfallIndex` to each vertical profile in the DPR inner swath. This snow flag provides useful information for microphysics retrieval for other modules such as the solver module. Therefore, this algorithm enhances the current dual-frequency classification module in GPM DPR level 2 algorithm and has been implemented as an experiment version.

3.5.9 Eight digit rain type number

As mentioned in 3.5.4-1-4-4 and 3.5.4-2-2, the unified rain types for Ku-only, Ka-only, and DPR are expressed by eight digit numbers. Figure 3.5-14 illustrates the eight digit rain type number, which has a common structure for Ku-only, Ka-only, and DPR.
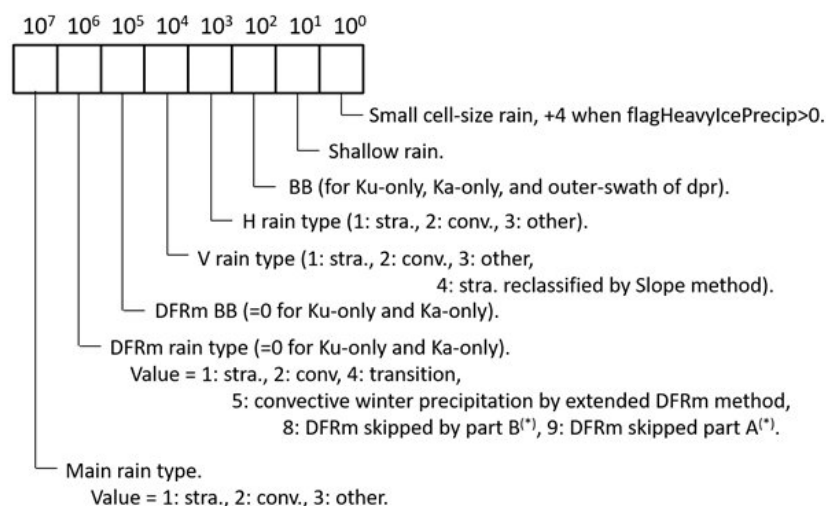
Figure 3.5-14. A summary of eight digit rain type number.
(*): For part A and part B, see Figure 3.5-3.

3.5.10 New EXPERIMENTAL items related to the CSF module

In V6X, the following two new items are obtained by the dual frequency CSF module, and added to the EXPERIMENTAL group of the dual frequency output.

(a) flagGraupelHail

(b) MixedPhaseTop

Descriptions of these are given in the following subsections.

3.5.10(a) flagGraupelHail

3.5.10(a)-1 Graupel and Hail identification for DPR

Similar to the product of "flagSurfaceSnowfall" (Le and Chandrasekar, 2019), the precipitation type index (PTI) with different threshold has been proven to be able to effectively identify graupel and hail profiles (Le and Chandrasekar, 2018). The product of "flagGraupelHail" (or "GH flag") has been implemented in the Experimental structure. Figure 3.5-15 illustrates a cartoon plot for the geometry of GPM product "flagGraupelHail". The output is a Binary value for each DPR matched footprint. 1 represents "graupel and hail exists" and 0 means "graupel and hail not exists". This is for along the vertical profile, not for surface.
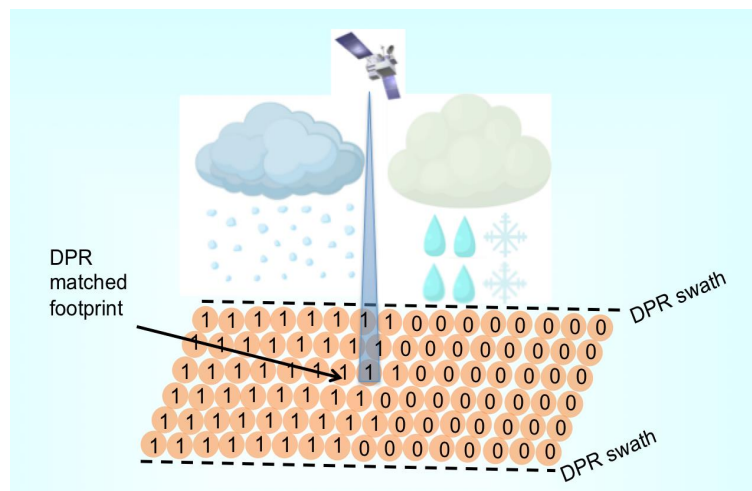
Figure 3.5-15. Cartoon illustration of GPM product "flagGraupelHail".

Three ingredients in calculating PTI are DFRm slope, Zm maximum value and storm top height. We collect more than 1000 DPR profiles with graupel and hail identified using WSR-88D radar network. Features of these vertical profiles are studied. Good separation can be observed which forms the fundamental of the algorithm. Figure 3.5-16 is the flowchart of the graupel and hail identification algorithm.

3.5.10(a)-2 Ground Validation of the Graupel and Hail Identification Algorithm

Between 2018 May to September, intense weather events are chosen from the United States for ground validation. These precipitation events are simultaneously captured by GPM-DPR and WSR-88D radars. Hydrometeor identification algorithm is performed on WSR-88D radars first. Chosen cases are all detected with Graupel or Hail. Graupel and Hail identification algorithm for GPM is applied and the product of "flagGraupelHail" is compared with ground radar results. More than 10 validation cases were chosen and validated showing excellent comparisons. The performance for a sample case is shown in figure 3.5-17. In figure 3.5-17, a strong precipitation
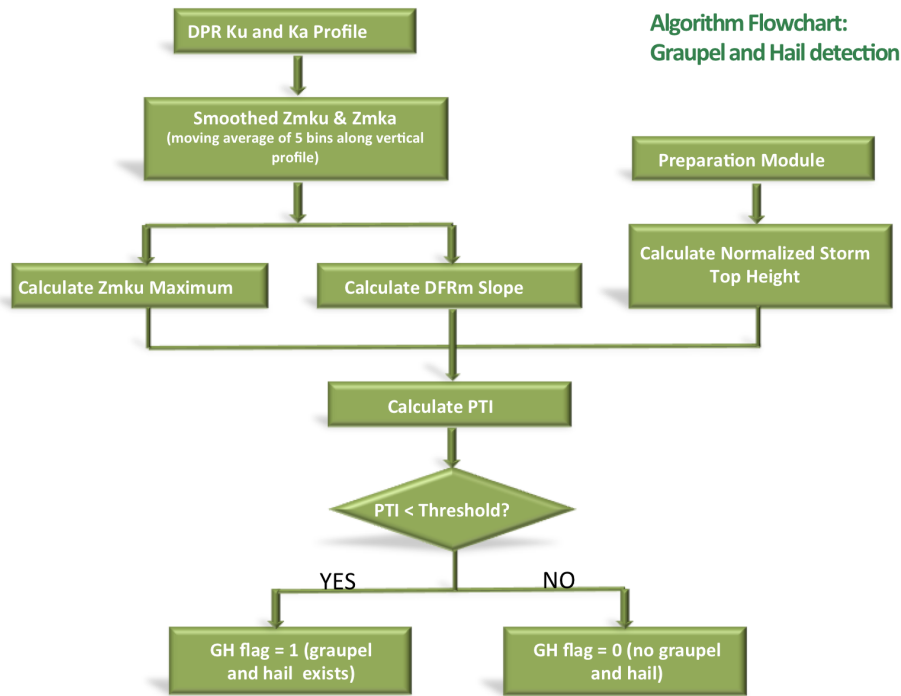
Figure 3.5-16. The flowchart of graupel and hail identification algorithm for GPM DPR.

event on Aug 24th, 2018 is simultaneously captured by GPM DPR orbit # 25489, UTC 02:42:57 together with the WSR-88D radar KABR located at Aberdeen, SD. Figure 3 (a) shows the map of the overpass and the location of KABR radar. In figure 3 (b) and (c), two PPI scans illustrate S band reflectivity of KABR at elevation of 2.42 and 6.41 degree respectively. High reflectivity value above 45 dBZ can be observed at east side as well as southwest side to the radar. "GR" and "HA" represents graupel and hail in the algorithm. Not surprisingly, we find graupel at east and southwest to the KABR rdar. The orange ovals indicate the locations. Figure 3.5-17 (f) is the plot of DPR Ku band reflectivity at 2km. dashed and solid black lines are DPR inner and outer swath. The circle is 100 km range of KABR. The result of "flagGraupelHail" is shown in (g), with dark green color representing Graupel and Hail exists. Comparing (d), (e) and (g), we find good agreements between two algorithms. It needs to be noticed that, in the validation cases, only inner swath data is taken for right now. The graupel and hail identification algorithm is applied to GPM DPR matched footprint for whole year 2018. Figure 3.5-18 illustrates the global distribution of "flagGraupelHail" count mapping to the 2° x 2° Latitude / Longitude box for year 2018. From the plot, we spot peaks of graupel and hail occurrence are at e.g., equatorial Africa, the equatorial and subtropical Americas, the Pampas of Argentina, the Himalayan Forelands, Indonesia etc. It shows great association with the World Lightening Map generated by NASA's Lightning Imaging Sensor on the Tropical Rainfall Measuring Mission satellite between 1995 and 2002, which demonstrates that "flagGraupelHail" is producing very reasonable results on a global scale. More validation details can be found in Le and Chandrasekar (2020).

(a)

(b)

(c)

(d)

(e)

(f)

(g)
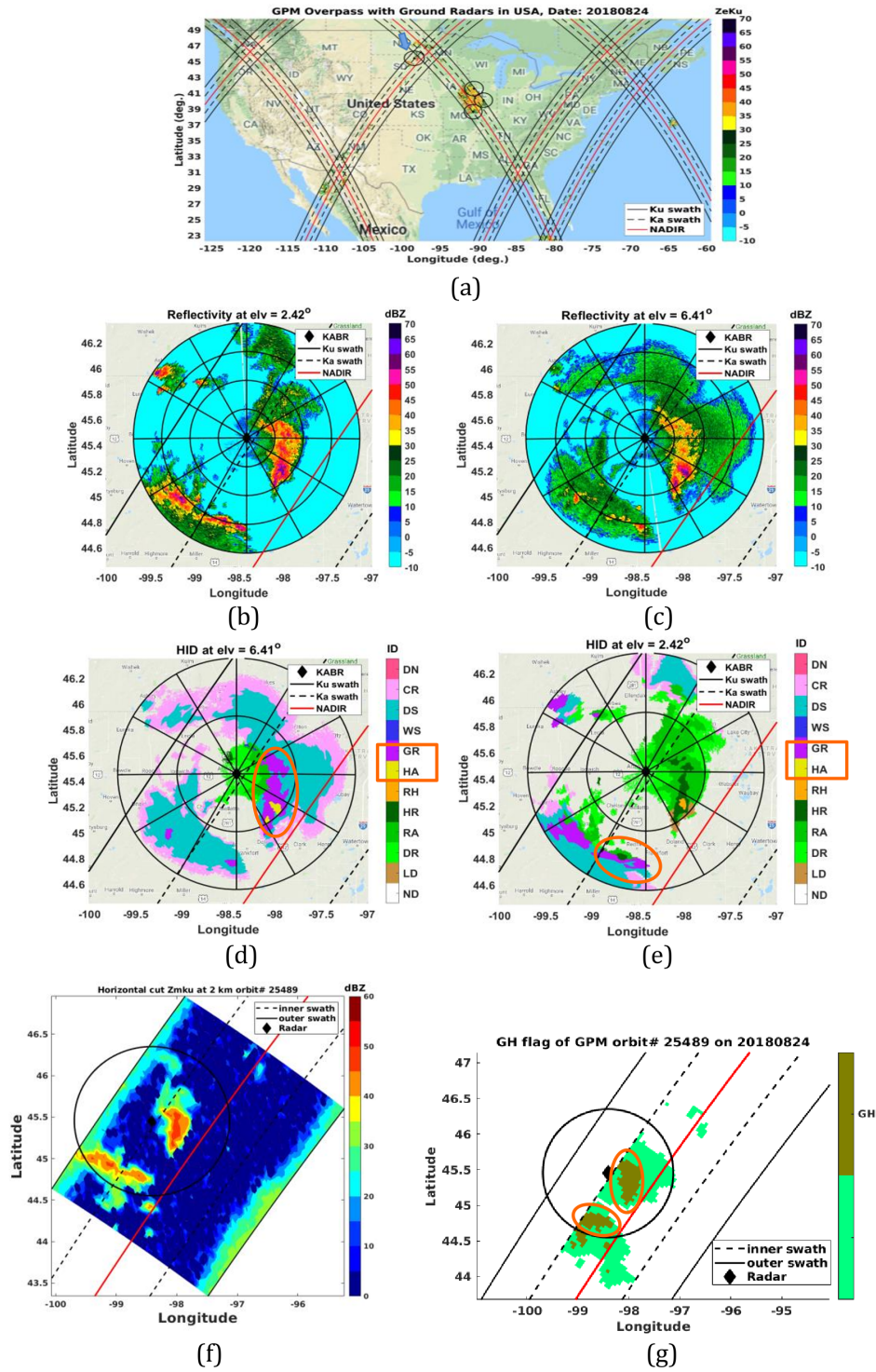
Figure 3.5-17 Validation case on 2018-08-24.

Precipitation event is observed by GPM DPR orbit # 25489, UTC 02:42:57 together with WSR-88D radar KABR located at Aberdeen, SD with UTC 02:42:02. (a) Map of overpass and location of KABR radar. (b) Reflectivity of KABR at elevation of 2.42 degree. (c) Same as (b) for elevation of 6.41 degree. (d) HID of KABR at elevation of 2.42 degree. (e) Same as (d) for elevation of 6.41 degree. (f) DPR reflectivity Zmku at 2km. (g) "flagGraupelHail" for precipitation in (f). Dark green means Graupel and Hail exists.
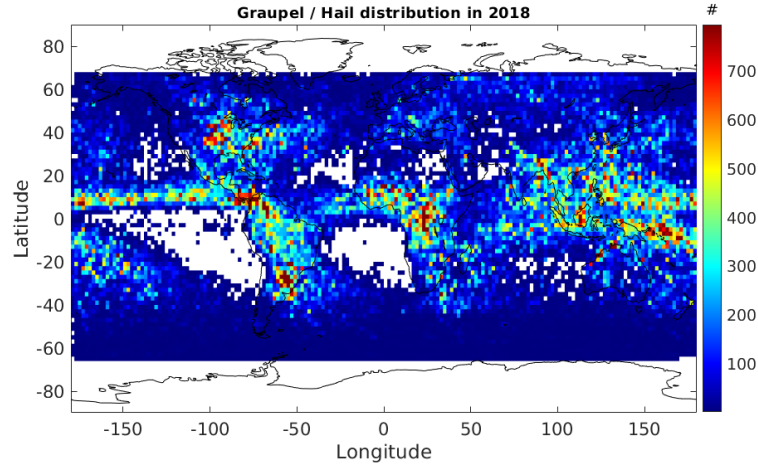
Figure 3.5-18 Global distribution of " flagGraupelHail " count mapping to the 2° x 2° Lat / Lon box for year 2018.

3.5.10(b) MixedPhaseTop

3.5.10(b)-1 Introduction

The experimental flag `MixedPhaseTop` is included in V06X to identify the location where the phase of precipitation particles turns from solid (ice) to liquid (water). The flag is set at nearly all pixels in which precipitation is detected even when no bright band is detected.

When a bright band is detected, the range at which this `MixedPhaseTop` flag is set is generally very close to the bright-band top or the melting-layer top in the classification module.

The flag is set based on an empirical fact that the dual-frequency ratio (DFR) changes substantially when particles change their phase state. This method works well in stratiform rain in which ice particles melt into water droplets as they descend. In particular, when a bright band is formed, the average particle size increases as snow flakes form aggregates in it and the DFR increases rapidly before it decreases to a low value that corresponds to small melted water droplets.

In convective rain, however, the drop size does not change much and the method does not work well in many cases. In a convective system, a coalescence process is supposed to be happening as liquid particles are lifted into a below-freezing temperature region by updraft. In this process, the diameters of particles, which are a decisive factor in determining DFR, do not change much. As a result, the change in DFR is mainly caused by the change in the dielectric constant of particles from water to ice when they are carried to a higher elevation. This change should be considered to be detectable. In reality, however, the change of phase state of particles does not seem to occur at a single well defined height, but it depends on the size of particles. Small particles may remain unfrozen to a relatively high altitude because of their high surface tension that requires an ambient air temperature well below 0 degree C to freeze. They can be

73

frozen by riming to other solid particle by collisions. As a result, the phase transition height may not be well defined in a convective storm. Since liquid particles contribute to the attenuation of radar echoes that also increases the apparent DFR, detection of the phase transition by measured DFR in convective precipitation is very complicated and difficult.

The current algorithm that is implemented in V06X still assigns a flag in convective storms using the same criteria even though the flag position may not be trustworthy, simply because this is an experimental flag.

A simplified flow of the algorithm is as follows (not exactly the same as the actual flow).

1. DFR is estimated from DFR_m (measured apparent DFR) with small attenuation corrections.
2. Calculate the second derivative of DFR with respect to range r.
3. Find the maximum of its absolute value within the pre-defined interval around $0°C$, and identify that height as the mixed-phase top height.

The advantage of this algorithm is its simplicity. It does not depend on the calibration of radar. It has higher detectability than the bright band detection algorithm implemented in the standard product. Disadvantages are that it is susceptible to noise so that we need to smooth the data before processing and that the solution depends on the estimated $0°C$ height in some cases.

3.5.10(b)-2 Idea behind the algorithm

Both effective radar reflectivity factor Z_e and specific attenuation k are functions of N_w, D_m and f_m, where N_w is a parameter proportional to the number density of the particle size distribution, D_m is the volume-weighted mean diameter (or any mean diameter), and f_m is the melting fraction of particles. (Note that D_m here is the actual diameter without melting if the particles are not totally liquid. It is not an equivalent melted mean diameter.) They are all functions of range r.

$$Z_e(r) = Z_e(N_w(r), D_m(r), f_m(r))$$

$$k(r) = k(N_w(r), D_m(r), f_m(r))$$

Measured radar reflectivity factor Z_m is related to Z_e and k through

$$Z_m(r) = Z_e(r) \exp(-2q \int_0^r k(s)\, ds) \tag{1}$$

where $q = \log_e(10)/10$.

In this section, we use notations dBZ_e and dBZ_m defined by the following equations.

$$\text{dBZ}_e \overset{\text{def}}{=} 10 \log_{10}(Z_e), \qquad \text{dBZ}_m \overset{\text{def}}{=} 10 \log_{10}(Z_m)$$

With these symbols, equation (1) becomes

$$\text{dBZ}_m(r) = \text{dBZ}_e(r) - 2 \int_0^r k(s)\, ds.$$

74

We are concerned with radar echoes at two different frequencies. Radar variables at these two frequencies are distinguished by subscript 1 and 2. Subscript 1 is used for the lower frequency (Ku band) and 2 for the higher frequency (Ka band). No subscript is attached if the statement is applicable to both frequencies.

The dual-frequency ratio (DFR) is defined by

$$\mathrm{DFR} \overset{\mathrm{def}}{=} \mathrm{dBZ}_{e1} - \mathrm{dBZ}_{e2}$$

Similarly, we define an apparent measured dual-frequency ratio (DFR_m) by

$$\mathrm{DFR}_\mathrm{m} \overset{\mathrm{def}}{=} \mathrm{dBZ}_{m1} - \mathrm{dBZ}_{m2} = \mathrm{DFR} - 2\int_0^r (k_1(s) - k_2(s))\, ds$$

Note that

$$\frac{\partial \mathrm{DFR}}{\partial N_w} = 0,$$

because both Z_{e1} and Z_{e2} are linearly proportional to N_w, and that

$$\frac{\partial \mathrm{DFR}}{\partial D_m} > 0 \quad \text{(for ice)} \quad \text{and} \quad \frac{\partial \mathrm{DFR}}{\partial D_m} \begin{cases} > 0 & \text{for} \quad D_m > D_p \\ = 0 & \text{for} \quad D_m = D_p \\ < 0 & \text{for} \quad D_m < D_p \end{cases} \quad \text{(for water)}$$

where D_p is about 1 mm if the two frequency bands are Ku and Ka bands. If particles change their phase state from solid to liquid without changing their dimensions, DFR decreases, i.e.,

$$\frac{\partial \mathrm{DFR}}{\partial f_m} < 0$$

(Note that this inequality does not necessarily hold if the freezing ratio depends on the particle size.)

Therefore, for $D_m > D_p$, DFR changes with N_w, D_m and f_m as follows.

$$\frac{\partial \mathrm{DFR}}{\partial N_w} = 0, \quad \frac{\partial \mathrm{DFR}}{\partial D_m} > 0, \quad \text{and} \quad \frac{\partial \mathrm{DFR}}{\partial f_m} < 0$$

On the other hand, Z_e's dependence on N_w, D_m and f_m is different.

$$\frac{\partial \mathrm{dBZ}_e}{\partial N_w} > 0, \quad \frac{\partial \mathrm{dBZ}_e}{\partial D_m} > 0, \quad \text{and} \quad \frac{\partial \mathrm{dBZ}_e}{\partial f_m} > 0$$

In this algorithm, we look at the changes in DFR (or DFR_m) and in dBZ_e. Their derivatives with respect to r are

$$\frac{d\mathrm{DFR}}{dr} = \frac{\partial \mathrm{DFR}}{\partial N_w}\frac{dN_w}{dr} + \frac{\partial \mathrm{DFR}}{\partial D_m}\frac{dD_m}{dr} + \frac{\partial \mathrm{DFR}}{\partial f_m}\frac{df_m}{dr} = \frac{\partial \mathrm{DFR}}{\partial D_m}\frac{dD_m}{dr} + \frac{\partial \mathrm{DFR}}{\partial f_m}\frac{df_m}{dr}$$

$$\frac{d\mathrm{dBZ}_e}{dr} = \frac{\partial \mathrm{dBZ}_e}{\partial N_w}\frac{dN_w}{dr} + \frac{\partial \mathrm{dBZ}_e}{\partial D_m}\frac{dD_m}{dr} + \frac{\partial \mathrm{dBZ}_e}{\partial f_m}\frac{df_m}{dr}$$

In the case of space-borne radar, r increases downward. In most cases, therefore, we can safely assume that

$$\frac{df_m}{dr} \geq 0,$$

i.e., the phase of particles changes from ice to water downward. (There is a possibility that wet hail stones exist above dry hail stones in different locations within a footprint of radar. We exclude such possibilities in this algorithm.)

The signs of $\frac{d\text{DFR}}{dr}$ and $\frac{d\text{dBZ}_e}{dr}$ indicate which among N_w, D_m and f_m causes the major changes in DFR and dBZ_e. There are four possible cases.

1. $\dfrac{d\text{dBZ}_e}{dr} \geq 0$ and $\dfrac{d\text{DFR}}{dr} < 0,$

2. $\dfrac{d\text{dBZ}_e}{dr} < 0$ and $\dfrac{d\text{DFR}}{dr} \geq 0,$

3. $\dfrac{d\text{dBZ}_e}{dr} < 0$ and $\dfrac{d\text{DFR}}{dr} < 0,$

4. $\dfrac{d\text{dBZ}_e}{dr} \geq 0$ and $\dfrac{d\text{DFR}}{dr} \geq 0,$

In case 1, it is most likely that $\frac{df_m}{dr} \geq 0$ in that range. In other words, the condition that $\frac{d\text{dBZ}_e}{dr} \geq 0$ and $\frac{d\text{DFR}}{dr} < 0$ can be used to detect the interval of transition from solid to liquid phase in the vertical profile of radar echo.

If this condition is satisfied without any phase transition (i.e., $\frac{df_m}{dr} = 0$), the only other possibility is that $\frac{dD_m}{dr} < 0$ and $\frac{dN_w}{dr} > 0$ in such a way that the positive effect from $\frac{\partial \text{dBZ}_e}{\partial N_w}\frac{dN_w}{dr}$ dominates the negative effect from $\frac{\partial \text{dBZ}_e}{\partial D_m}\frac{dD_m}{dr}$. Such a situation may happen in a developing stage of a convective storm, but it is rather unlikely in a horizontally uniform precipitation system. However, if there are two convective towers in the footprint and their heights are different, there is a possibility that N_w suddenly increases downward at the top of the shorter convection and that the effective D_m decreases there. (In a melting layer of stratiform rain, D_m decreases downward as particles melt, but the number density that is proportional to N_w does not increase as much to compensate for the effect of decrease in D_m.)

Note that if we assume a Gamma distribution of DSD and that the total precipitation water amount is constant (N_w changes with D_m in this case), then $\frac{\partial \text{dBZ}_e}{\partial N_w}\frac{dN_w}{dr} + \frac{\partial \text{dBZ}_e}{\partial D_m}\frac{dD_m}{dr}$ has the same sign as $\frac{\partial \text{dBZ}_e}{\partial D_m}\frac{dD_m}{dr}$. In other words, the effect of D_m is larger than that of N_w.

In case 2, the increasing trend of DFR is caused by the increase of D_m with r (under the assumption that $\frac{df_m}{dr} \geq 0$). Therefore, if $\frac{d\text{DFR}}{dr} \geq 0$ and $\frac{d\text{dBZ}_e}{dr} < 0$, then $\frac{\partial \text{dBZ}_e}{\partial N_w}\frac{dN_w}{dr} < 0$ and N_w decreases substantially with range. In case 3, it is likely that $\frac{dD_m}{dr} < 0$. In case 4, it is likely that $\frac{dD_m}{dr} > 0$.

In the latter three cases (cases 2, 3, and 4), it is impossible to identify the effect of $\frac{df_m}{dr}$ only from the signs of $\frac{d\text{dBZ}_e}{dr}$ and $\frac{d\text{DFR}}{dr}$.

3.5.10(b)-3 Algorithm

This algorithm is based on the idea described above. It tries to find the range at which $d\text{DFR}/dr$ changes most rapidly in case 1 above. To find its minimum, the second derivative of DFR i.e., $d^2\text{DFR}/dr^2$ is sought and its range is identified as the mixed phase top.

Since neither DFR nor dBZ_e is actually a measurable variable, we need to estimate them from measurable quantities, i.e., DFR_m and dBZ_m. Derivatives of DFR_m and dBZ_e are related to those of DFR and dBZ_e through

$$\frac{d\text{DFR}_\text{m}}{dr} = \frac{d\text{DFR}}{dr} - 2(k_1 - k_2), \quad \text{and}$$
$$\frac{d\text{dBZ}_m}{dr} = \frac{d\text{dBZ}_e}{dr} - 2k$$

Note that $k_2 \geq k_1 \geq 0$ so that

$$\frac{d\text{DFR}_\text{m}}{dr} \geq \frac{d\text{DFR}}{dr} \quad \text{and} \quad \frac{d\text{dBZ}_m}{dr} \leq \frac{d\text{dBZ}_e}{dr}$$

These inequalities imply that if

$$\frac{d\text{DFR}_\text{m}}{dr} < 0 \quad \text{and} \quad \frac{d\text{dBZ}_m}{dr} > 0,$$

then we can conclude that

$$\frac{d\text{DFR}}{dr} < 0 \quad \text{and} \quad \frac{d\text{dBZ}_e}{dr} > 0$$

and that

$$\frac{df_m}{dr} > 0.$$

In other words, we can use DFR_m and dBZ_m instead of DFR and dBZ_e for the detection of the region where the condition $\frac{df_m}{dr} > 0$ is most likely satisfied. In fact, if we use radar reflectivity factor at Ku band, Z_{e1}, for Z_e, the attenuation can be generally neglected because it is very small for ice particles. Since we are dealing with only the radar echoes down to the mixed phase region, errors associated with attenuation correction in rain region is not critical.

Nevertheless, in order to minimize the error associated with attenuation, the following formulas are used to calculate the first derivatives of DFR and dBZ_e from those of DFR_m and dBZ_m.

$$\frac{d\text{DFR}}{dr} = \frac{d\text{DFR}_\text{m}}{dr} + 2(k_1 - k_2) \quad \text{and} \quad \frac{d\text{dBZ}_{e1}}{dr} = \frac{d\text{dBZ}_{m1}}{dr} + 2k_1$$

Both k_1 and k_2 are estimated approximately from Z_{m1} (Ku band Z_m) by using a power-law $k\text{-}Z_{e1}$ relationships with Z_{e1} replaced by Z_{m1}.

$$k_1 = \alpha_1 Z_{m1}^{\beta_1} = \alpha_1 \exp(q\beta_1 \text{dBZ}_{m1}), \quad \text{and} \quad k_2 = \alpha_2 Z_{m1}^{\beta_2} = \alpha_2 \exp(q\beta_2 \text{dBZ}_{m1}).$$

We assume that Z_{m1} is nearly equal to Z_{e1} because Z_{e1} suffers from attenuation only slightly down to the range where melting starts. In the case of stratiform precipitation systems, both k_1 and k_2 are small and the corrections themselves are negligibly small.

Since DFR statistically changes with Z_{e1} (and Z_{e2}) to some extent, an additional term that is proportional to $dd\mathrm{BZ}_e/dr$ is subtracted from $d\mathrm{DFR}/dr$ to minimize the effect of variation in D_m to $d\mathrm{DFR}/dr$. In other words, we try to find the range at which the following quantity changes its trend the most.

$$\frac{d\mathrm{DFR}_c}{dr} = \frac{d\mathrm{DFR_m}}{dr} + 2(k_1 - k_2) - c\frac{dd\mathrm{BZ}_{m1}}{dr}$$

where c is a proportional coefficient of $d\mathrm{DFR}/dd\mathrm{BZ}_{e1}$ at a typical value of $d\mathrm{BZ}_{e1}$ (The actual value of c used in the algorithm is $c = 1/7$.) To find such a point, the range at which the second derivative of DFR_c becomes minimum is sought. The search window for the solution is between $0°\mathrm{C}\pm1$ km.

3.5.10(b)-4 Caveats

This algorithm tries to find the minimum point of $\frac{d^2\mathrm{DFR}_c}{dr^2}$. Since derivatives are susceptible to noise, it is necessary to smooth the observed profiles of $d\mathrm{BZ}_{m1}$ and $d\mathrm{BZ}_{m2}$ substantially. A Savitzky-Golay filter [Savitzky and Golay, 1964; Press et al. 1992] is adopted to achieve this purpose. This filter has a nice property that it can preserve peaks of signal without much reduction up to a certain wavenumber (defined by the order of the filter) and that derivatives of the smoothed profiles can be obtained fast and easily. To suppress noise, 9 points (current point + 5 points on either side) around the point in question are used for smooting. The number of points usable for smooting reduces near the lower end of the valid echo profile because we cannot use data below the `binClutterFreeBottom`. As a result, the performance of detection decreases when the mixed phase top is close to the `binClutterFreeBottom`.

In an updraft in a convective storm, freezing of particles may not occur at the same height for different sizes of particles. As a result, some assumptions such as $\frac{\partial \mathrm{DFR}}{\partial f_m} < 0$ are considered to be not valid in some cases. In such cases, this algorithm may fail to identify the melting phase top height.

3.5.11 Input and Output Variables

Input Variables

From Preparation (PRE) module:

`lat`

`lon`

ScanTime information (`Year`, `Month`, `DayOfMonth`, `Hour`, `Minute`, `Second`, `Millisecond`, `DayOfYear`, `SecondOfDay`)

```
        elevation
        landSurfaceType
        localZenithAngle
        flagPrecip
        binRealSurface
        binStormTop
        heightStormTop
        binClutterFreeBottom
        sigmaZeroMeasured
        rangeBottom
        rangeTop
        Height
        echoSignalPower
        zFactorMeasured
    From Vertical (VER) module:
        airTemperature
        binZeroDeg
        zFactorNPCorrected
        heightZeroDeg
        flagEcho (R/W) (This flag marks possible sidelobe clutter positions.)
        qualityData (R/W)
    From Solver (SLV) module:
        zFactorNPCorrected (For convective decision by the V-method in the
        single frequency Ku- or Ka-loop)
Output Variables
        flagBB [4 byte integer]
        binBBPeak [2 byte integer]
        binBBTop [2 byte integer]
        binBBBottom [2 byte integer]
        heightBB [4 byte real]
        widthBB [4 byte real]
        qualityBB [4 byte integer]
        typePrecip [4 byte integer]
        qualityTypePrecip [4 byte integer]
        flagShallowRain [4 byte integer]
        binDFRmMLTop [4 byte integer] (dual frequency output only)
        binDFRmMLBottom [4 byte integer] (dual frequency output only)
```

`binHeavyIcePrecipTop` [2 byte integer] – Introduced in V6X

`binHeavyIcePrecipBottom` [2 byte integer] – Introduced in V6X

`nHeavyIcePrecip` [1 byte integer (unsigned)] – Introduced in V6X

`flagMLquality` [1 byte integer (unsined)] – Introduced in V6X

`flagHeavyIcePrecip` [1 byte integer]

`flagAnvil` [1 byte integer] (single frequency Ku FS and dual frequency FS only)

`flagSurfaceSnowfall` [1 byte integer] (Experimental output of dual frequency FS)

`surfaceSnowfallIndex` [4 byte real] (Experimental output of dual frequency FS)

`flagGraupelHail` [1 byte integer (unsigned)] – Intoduced in V6X

`binMixedPhaseTop` [2 byte integer] – Introduced in V6X

3.5.12 Relation to other modules

The Classification (CSF) module uses data from the Preparation (PRE) module and the vertical (VER) module. Each single frequency CSF module uses data from the corresponding Solver (SLV) module in the 2-nd part of (a kind of iteration) loop for convective decision by the V-method. The output data from the CSF module is used by the Solver (SLV) module.

3.5.13 Bug fix

This section describes bug fixes made in the V6X, V6, and V5 CSF modules.

(A) Bugs fixed in the V6X CSF module

1) The V6 CSF module reclassifies stratiform rain by the UW "slope method." The "slope method" is applied to the Ku-band processing only. But `NearSurfacePrecipitationRate` (R_{NS}) of the reclassified stratiform rain sometimes becomes very large though the occurrence of such is rare. (R_{NS} of stratiform rain must not be very large.) The V6X CSF module fixes this problem by introducing a kind of output filter.

2) In rare cases, some BB peaks are misjudged as surface peaks in V5 by a bug in the PRE module. The effect of bug becomes appreciable in the following two cases:
   a) High BB case: When BB peaks are misjudged as the surface echo over high mountain areas, the clutter free bottom becomes dangerously too high.
   b) Low BB case: In winter, a large number of low height BB are missed.

The V6X algorithms fix this problem to some extent. Further improvement will be made in V7. (Though the bug fix is made in the PRE module, the bug affects the detection of BB in the CSF module; therefore it is mentioned here.)

(B) Bugs fixed in the V6 CSF module

The following bugs in V5 are fixed in V6.

1) Some side-lobe peaks being misjudged as HIP in V5 are fixed in V6. (The fix is applied to the Ku outer swath only.)

2) When `flagHeavyIcePrecip` > 0, rain type is expected to be convective, but the DPR rain type for this case is sometimes stratiform in V5 because of a bug. This bug is fixed in V6.

(C) Bugs fixed in the V5 CSF module

The V4 CSF codes for the detection of BB contain a large number of bugs, which are fixed in V5.

Because of the bugs, almost all V4 `widthBB`s were wrong, some V4 `heightBB`s are incorrect, and in some rare cases `binBBPeak`, `binBBTop`, and `binBBBottom` are not set properly in V4.

3.5.14 Issues

Besides the parameter tunings, the following improvements are needed in the next update.

- Improvement of BB detection, in particular the detection of low BB in winter and also the detection of BB in the outer swath.
- It is found that the reclassification of the type from convective to stratiform by the "slope method"has a problem when there exist winter time temperature inversions. This problem is solved by an ad hoc fix in the V6 CSF module. (The fix remains ad hoc in V6X.) However, the winter time temperature inversion problem should be handled in more fundamental ways in the next update.
- Improvement of CSF related EXPERINENTAL codes (including validation of their results.)

Last but not least, development of the V7 CSF module is the most important issue.

3.6 DSD module

3.6.1 Objective

The objective of DSD module is to set the physical variables of precipitation particles (especially, density, dielectric constants, and falling velocity), to parameterize $N(D)$ (in other words, to set $n(D; D^*)$), and to set the R-D_m relationship.

3.6.2 Processes

The following processes are common to single- and dual-frequency algorithms.

3.6.2-1 Target pixels and range bins

Pixels with precipitation are processed. Range bins from the storm top range bin to the land surface range bin (including those without precipitation and those with ground clutter) are processed. In dual-frequency algorithm, range bins from the higher storm top range bin of the two frequencies to the lower land surface range bin of the two frequencies are processed.

3.6.2-2 Nodes and the physical temperature and phase of the particles

Five range bins are selected as nodal bins and designated as nodes A through E. Simultaneously, the physical temperature of particles (particle temperature) and the phase of particles are set. Particle temperature is related to the dielectric constants and it is not necessarily the same with air temperature. The dielectric constant is dependent on the precipitation types and the detection of bright band.

3.6.2-2-1 Stratiform precipitation with bright band

The range bin that corresponds to the upper edge of bright band is node B, the range bin at the peak of bright band is node C, and the range bin at the lower edge of bright band is node D. Between node B and node D, particle temperature is set to 0°C. Above node B, the particle temperature is basically the same with ambient air temperature, but is 0°C if the air temperature is higher than 0°C. Below node D, the particle temperature is basically set to the same with the air temperature, but 0°C if the air temperature is lower than 0°C. The range bin with particle temperature closest to −20°C corresponds to node A, and that closest to 20°C is node E. At and above node A, the phase of precipitation is *Solid*. At and below node D, the phase of precipitation is *Liquid*. At other range bins, below node A and above node D, the phase of precipitation is *Mixed* (Solid and Liquid).

3.6.2-2-2 Stratiform precipitation without bright band

The process is the same as 3.6.2-2-1, but the nodes B, C, and D are at the range bin corresponding to 0°C.

3.6.2-2-3 Convective precipitation or other-type precipitation

The process is the same as 3.6.2-2-2.

3.6.2-3 Assumption of precipitation particles

A precipitation particle is modeled as a spherical particle composed of liquid water, solid water, and air. Its diameter (or drop size) is designated as D_b [mm], and its density as ρ_b [g/cm^3]. The volume ratios of liquid water, solid water, and air to the particle are P_w, P_i, and P_a, respectively. The following equation always holds.

$$P_w + P_i + P_a = 1 \tag{3.6-1}$$

The densities of liquid water, solid water, and air are ρ_w, ρ_i, ρ_a, respectively. Then, the density of the particle can be given as below.

$$\rho_b = P_w \rho_w + P_i \rho_i + P_a \rho_a \tag{3.6-2}$$

Generally, we can assume $\rho_w = 1.0$ (g/cm^3). ρ_i is also constant (for example, $\rho_i = 0.92$). Moreover, ρ_a can be regarded to be 0 (g/cm^3) for simplicity. With these constant values, Eq. (3.6-2) can be simplified to (3.6-3).

$$\rho_b = P_w + 0.92 P_i \tag{3.6-3}$$

3.6.2-4 Setting of volume ratio and density

3.6.2-4-1 Liquid phase particle

Obviously, $P_w = 1$, $P_i = P_a = 0$, $\rho_b = 1.0$ (g/cm^3).

3.6.2-4-2 Mixed phase particle

First, P_w is set based on Awaka's model or TRMM/PR's experience. Then, ρ_b can be calculated by the following empirical equation.

$$\rho_b = \sqrt{P_w} \tag{3.6-4}$$

Then, P_i can be calculated by Eq. (3.6-2) with $\rho_a = 0$.

$$P_i = \frac{\rho_b - P_w \rho_w}{\rho_i} \tag{3.6-5}$$

3.6.2-4-3 Solid phase particle

First, ρ_b is set, for example, $\rho_b = 0.10$ (g/cm^3). As $P_w = 0$, P_i can be calculated by Eq. (3.6-5).

3.6.2-5 Dielectric constants

ε_b is calculated by mixing rule, for example, given in Eq. (3.6-6).

$$\frac{\varepsilon_b - 1}{\varepsilon_b + U} = P_w \frac{\varepsilon_w - 1}{\varepsilon_w + U} + P_i \frac{\varepsilon_i - 1}{\varepsilon_i + U} + P_a \frac{\varepsilon_a - 1}{\varepsilon_a + U} \tag{3.6-6}$$

where U is given as below,

$$U = \begin{cases} 2.0 & \text{if } \rho_b \leq 0.09 \text{ g/cm}^3, \\ 2.0 e^{13.0(\rho_b - 0.09)} & \text{if } \rho_b > 0.09 \text{ g/cm}^3. \end{cases} \tag{3.6-7}$$

ε_w and ε_i are dielectric constants of water and ice and are functions of particle temperature, and ε_a is dielectric constants of air. As ε_a is approximated to 1, Eq. (3.6-6) can be simplified to Eq. (3.6-8).

$$\frac{\varepsilon_b - 1}{\varepsilon_b + U} = P_w \frac{\varepsilon_w - 1}{\varepsilon_w + U} + P_i \frac{\varepsilon_i - 1}{\varepsilon_i + U} \tag{3.6-8}$$

3.6.2-6 Falling velocity

Falling velocity V_b of the particle can be given as below.

$$V_b = 3.3 \times [\rho_b - \rho_a]^{1/2} \qquad \text{if } \rho_b \leq 0.05 \text{ g/cm}^3; \tag{3.6-9a}$$

$$V_b = 8.8 \times [0.1 D_b (\rho_b - \rho_a)]^{1/2} \qquad \text{if } 0.05 \text{ g/cm}^3 < \rho_b \leq 0.3 \text{ g/cm}^3; \tag{3.6-9b}$$

$$V_b = \frac{\rho_b^{1/3} - 0.3^{1/3}}{1.0 - 0.3^{1/3}} (V_R - V_{b0.3}) + V_{b0.3} \quad \text{if } 0.3 \text{ g/cm}^3 < \rho_b \leq 1.0 \text{ g/cm}^3. \tag{3.6-9c}$$

In Eq. (3.6-9c), V_R is the fall velocity of rain drops, and $V_{b0.3}$ is the falling velocity calculated in Eq. (3.6-9b) with $\rho_b = 0.3$ g/cm³. The relationship between D_b and the diameter after melting D_{melt} is as follows.

$$D_b = D_{\text{melt}} \rho_b^{-1/3} \tag{3.6-11}$$

3.6.2-7 Drop size distribution function

3.6.2-7-1 Liquid phase

Gamma distribution function may be most commonly used for the drop size distribution function in liquid phase. The function is given as below.

$$N(D) = N_m D^\mu \exp\left[-\frac{(4 + \mu)D}{D_m}\right], \tag{3.6-12}$$

where D_m is the volume weighted diameter (or often called the mass weighted diameter) defined as

$$D_m = \frac{\int D^4 N(D)\, dD}{\int D^3 N(D)\, dD}.$$

N_m is the corresponding scale factor. The shape factor μ is assumed to be known and constant. N^* in (3.1-19) corresponds to N_m, D^* to D_m, and n is given as Eq. (3.6-13).

$$n(D; D_m) = D^\mu \exp\left[-\frac{(4 + \mu)D}{D_m}\right], \tag{3.6-13}$$

84

3.6.2-7-2 Mixed phase and solid phase

It is assumed that when all the particles are melted to liquid particles, the drop size distribution obeys Eq. (3.6-12). With Eq. (3.6-11), Eq. (3.6-12) can be expressed by D_b and ρ_b.

$$N(D_b)\,dD_b = N_m \rho_b^{(\mu+1)/3} D_b^{\mu} \exp\left[-\frac{(4+\mu)D_b \rho_b^{1/3}}{D_m}\right] dD_b \qquad (3.6\text{-}14)$$

Eq. (3.6-14) can be modified to Eq. (3.6-15), if we consider the difference of number density caused by the difference of falling velocity as Non-break up and Non-coalescence model (N/N model) assumes.

$$N(D_b)\,dD_b = N_m \rho_b^{(\mu+1)/3} D_b^{\mu} \frac{V_R(D_{\text{melt}})}{V_b(D_b)} \exp\left[-\frac{(4+\mu)D_b \rho_b^{1/3}}{D_m}\right] dD_b \qquad (3.6\text{-}15)$$

3.6.2-8 R-D_m relation

R-D_m relations are assumed for stratiform and convective rain separately to calculate k and Z_e for a given R at both Ka and Ku bands. In version 3 algorithm, default k-Z_e relations were given as the basic relations to constrain the DSD parameters. However, since these relations were derived from the R-Λ relation (Kozu et al. 2009) by assuming a power law between k and Z_e, the resultant k-Z_e relations did not reproduce the original R-Λ relations exactly. The discrepancy was apparent espcially in heavy rainfall cases for KaPR and solid particles, and caused a serious error in the algorithm. Since the R-D_m relation is directly derived from the R-Λ relation without approximation, we have consistent DSD parametes to relate k, Z_e at both freqencies and R.

The actual R-D_m realtions adopted are $R = 0.401\epsilon^{4.649} D_m^{6.131}$ for stratiform precipitation and $R = 1.370\epsilon^{4.258} D_m^{5.420}$ for convective precipitation, where ϵ is an adjustment factor and is the same with ϵ used in version 03 and in the TRMM/PR algorithm. The same equations are used for all range bins irrespective of its "phase", while D_m is defined for particle size when melted.

3.6.3 Phase

An index called "phase" is introduced. "phase" is an integer-type variable. If "phase" is equal to or greater than 200, particles are in liquid phase, and the difference between the value of "phase" and 200, i.e., (phase$-$200), indicates the particle temperature in unit of degrees C. For example, if "phase" is 210, the particle temperature is 10 degrees C. If "phase" is between 100 and 200, particles are in a bright band. 100 is for the top of bright band, 150 is for the peak of bright band, and 200 is for the bottom of bright band, where all particles are melted in liquid phase. 125 and 175 are used for intermediate positions, but other numbers between 100 and 200 are not used. If "phase" is smaller than 100, particle is partly or fully frozen, and the difference between "phase" and 100 means particle temperature in unit of degrees C. For example, if "phase" is 80, particle temperature is -20 degrees C.

3.6.4 DSD database

ϵ used in the R-D_m relations was assumed to follow the log-normal distribution. In the version 04, the average (μ) and the standard deviation (σ) of $\log_{10} \epsilon$ is set at 0 and 0.1, respectively. In the version 05, the statistics of ϵ is calculated based on the outputs of ϵ at dual-frequency pixels by the dual-frequency algorithm. The average and the standard deviation of $\log_{10} \epsilon$ are calculated for each precipitation type (stratiform, convective), for each land surface type (land, ocean, all), each 5 by 5 degree grid box, and each month. Not only grid values but global values are prepared. The purpose of the DSD database is to make estimates by KuPR algorithm be closer to those by the dual-frequency algorithm. DSD database is applied only to single-frequency pixels (all pixels of the single-frequency algorithms and pixels in outer swath or in interleaved scan of the dual-frequency algorithm). In the dual-frequency pixels of the dual-frequency algorithm, μ and σ is set 0 and 0.1 same as in the version 04.

3.7 Surface Reference Technique for DPR

3.7.1. Objective of the algorithm

The primary purpose of the surface reference technique (SRT) is to compute the path-integrated attenuation (PIA), or simply path attenuation, using the radar return from the surface. The SRT rests on the assumption that the difference between the measurements of the normalized radar surface cross section, σ^0 or NRCS, in dB, within and outside the rain provides an estimate of the PIA.

For the dual-frequency Precipitation Radar (DPR), the method is to be applied to the Ku-band as well as the Ka-band and Ka-band high sensitivity (KaHS) data. The basic set of output products for each of the channels (Ku, Ka and KaHS) consist of the path attenuation estimate (when rain is present) and an associated reliability. As in the TRMM algorithm 2a21, version 7, the primary output for each channel will be an effective or 'best' PIA estimate. In addition, however, path attenuation estimates corresponding to specific types of surface reference data are also generated. These are described below. The standard PIA estimates will be produced by processing the data from the 3 channels (Ku, Ka, Ka_HS) independently. However, to take advantage of the correlation in the NRCS at the two frequencies, dual-frequency-derived path attenuations at Ku- and Ka-band will also be generated in the inner swath. These are referred to as the DPR-Ku and DPR-Ka estimates.

For each 'channel' (Ku, Ka, KaHS, DPR-Ku, DPR-Ka), a spatially or temporally-averaged estimate of the rain-free normalized radar surface cross section (σ^0 or NRCS) is used as a reference value for computing the PIA. For the DPR channel, the rain-free reference data is obtained from a difference between the Ka- and Ku-band σ^0 data. The algorithm computes up to six estimates of path attenuation, corresponding to six different σ^0 reference estimates for each of the five channels. An effective PIA is obtained by weighting the individual estimates by a factor that is inversely proportional to the variance of the estimate. The reference estimates are described below:

Along-track Spatial Average: The along-track spatial average is obtained from an average of the N_s most recent rain-free σ^0 measurements at same angle bin and with the same surface type (nominally, $N_s = 8$) as the rain pixel of interest.

Hybrid or Cross-Track: The hybrid reference data set is generated from a quadratic fit of the along-track spatial average data over the angle bins within the cross-track swath. This is explained below in more detail. For the Ku-band, separate fits are done for the inner ($\theta \leq \theta_0$) and outer swath ($\theta > \theta_0$) where $\theta_0 \approx 9°$.

Temporal Average: The temporally averaged data, which are given in the form of look-up tables, presently consists of statistics (sample mean, sample mean square and number of data points) of rain-free σ^0 data at $0.5° \times 0.5°$ latitude-longitude cells, separated into incidence angle.

The look-up tables have been derived from the Ku, Ka, KaHS and differential (σ^0(Ku)- σ^0(Ka)) data categorized into 25, 13, 12, and 13 angle bins, respectively. Each of these files are further subdivided into 5 surface-dependent look-up tables that correspond to ocean, land, coast, snow-over-land, and sea-ice surface types for a total of 20 look-up tables for each 3-month period (DJF, MAM, JJA, SON). Product version 3 and earlier do not use the temporal reference data; version 4 and later versions will use the standard temporal reference file but not the 'light-rain' temporal reference file. For version 5 and above, the original 3 surface types (ocean, land, coast) were expanded into 5 surface types, with the additional categories of snow-over-land and sea-ice. Further details can be found in Section 3.7.3.

For versions V6X and higher, the number of angle bins for Ku, Ka and differential (σ^0(Ku)-σ^0(Ka)) are all equal to 25, corresponding to incidence angles from 0 to 180 with angle bin interval of 0.750. For times after May 2018, the KaHS reference data are set to missing.

Forward-Backward Processing

Different estimates for along-track and cross-track (or hybrid) methods are obtained from forward and backward processing. This provides up to six estimates - *Forward Along-track, Forward Cross-track, Backward Along-track, Backward Cross-track, and two types of Temporal reference files* - for each rain observation. Note that the hybrid/cross-track estimates are only available over ocean since the fitting procedure does not work well over land. (Cross-track fitting over land might be effective for the difference field, σ^0_{NR}(Ku) $- \sigma^0_{NR}$(Ka). Whether such an estimate is to be used is to be determined.) Note also that only the first of the temporal files have been implemented. The 'light rain' temporal reference file is not defined up to and including version 4 of the code. The different reference estimates are filtered according to various criteria. For example, an along-track estimate isn't used if the location of the reference data is too far from the observed rain point. A temporal estimate is considered invalid if the number of rain-free observations at a particular angle for the reference cell is too few. The surviving estimates are weighted by the inverse of their associated variance. The weighted estimates are combined to yield an effective PIA for each of the channels, (pathAtten_Ku, pathAtten_Ka, pathAtten_KaHS). The individual estimates, (PIAalt_Ku, PIAalt_Ka, PIAalt_KaHS), and their weights, (PIAweight_Ku, PIAweight_Ka, PIAweight_KaHS) are included in the output product. A discussion of the weights and the effective PIA, variance, and reliability factor is given in section 3.7.5.

In the spatial (along-track) surface reference data set, the mean and standard deviation of the NRCS are calculated over a running window of N_s fields of view before rain is encountered (currently, $N_s = 8$). These operations are performed separately for each of the 49 incidence angles for the Ku-band data, corresponding to the cross-track scan from $-18°$ to $+18°$ with respect to nadir. The Ka and DPR and KaHS channels are treated in the same way. Prior to

88

May 2018, the KaMS, DPR and KaHS consisted of 25, 25 and 24 angle bins, respectively. After May 2018, the KaFS and DPRFS consist of 49 angle bins, matched to those of the KuFS. Note that for the DPR or differential channel, the same procedure is used except that the reference data are formed from the $\sigma_{NR}^0(\mathrm{Ku}) - \sigma_{NR}^0(\mathrm{Ka})$ data. Prior to May 2018, the data consisted of the 25 angle bins of the inner swath; after May 2018, data became available over the full swath of 49 angle bins.

Basic Processing

When rain is encountered, at incidence angle θ_i, the means and standard deviations of the reference σ^0 values are retrieved from the along-track spatial (forward or backward), the hybrid (forward or backward) and the temporal surface reference data sets. If a valid surface reference data set exists for one of the above estimates, then, denoting this by the jth estimate, the 2-way path attenuation (PIA) is computed from the equation:

$$\mathrm{PIA}_j(\theta_i) = \langle \sigma_{NR}^0(\theta_i) \rangle_j - \sigma^0(\theta_i)$$

where $\langle \sigma_{NR}^0(\theta_i) \rangle_j$ is the mean of the jth rain-free reference estimate and $\sigma^0(\theta_i)$ is the value of the apparent normalized radar surface cross section at the raining field of view of interest.

To obtain information as to the reliability of the jth PIA estimate we consider the ratio of the PIA, as derived in the above equation, to the standard deviation associated with the jth rain-free reference data set. Labeling this standard deviation by σ_j, the reliability factor of the jth PIA estimate is defined as:

$$\mathtt{reliabFactor}_j = \frac{\mathrm{PIA}_j}{\sigma_j}$$

which is equal to the inverse of the coefficient of variation of the estimate.

The effective PIA, $\mathrm{PIA}_\mathrm{eff}$, and the corresponding reliability factor, $\mathrm{Rel}_\mathrm{eff}$, can be expressed in similar ways. From section 3.7.5, we have:

$$\mathrm{PIA}_\mathrm{eff} = \frac{\sum u_j \mathrm{PIA}_j}{\sum u_j}$$

$$\mathrm{Ref}_\mathrm{eff} = \frac{\sum u_j \mathrm{PIA}_j}{\sqrt{\sum u_j}}$$

Where u_j is the inverse of the variance, σ_j^2, associated with the jth reference data set:

$$u_j = \frac{1}{\sigma_j^2}$$

Note that the summations are assumed to range over all valid reference data sets, even if the PIA's are negative. Over land, there can be a maximum of 4 valid reference data sets (forward

and backward along-track and two temporal files) while over ocean there can be as many as six since the forward/backward cross-track reference data sets are defined over ocean but not land.

A generalized form of the above equations can be defined, where the various quantities are replaced by the difference between the Ka and Ku-band σ^0 values. Letting $\delta X = X(\text{Ka}) - X(\text{Ku})$, then for the differential PIA, the above equation becomes

$$\delta\text{PIA}_j(\theta_i) = \langle \delta\sigma^0_{NR}(\theta_i) \rangle_j - \delta\sigma^0(\theta_i)$$

The individual and effective dual-frequency estimates at Ku- and Ka-band are then derived from δPIA_j from

$$\text{PIA}_j(\text{Ku}, \theta_i) = \frac{\delta\text{PIA}_j(\theta_i)}{p - 1}$$

$$\text{PIA}_j(\text{Ka}, \theta_i) = \frac{p\ \delta\text{PIA}_j(\theta_i)}{p - 1}$$

where p is the ratio of the path attenuation at Ka-band to that at Ku-band and is nominally set to 6.

Updates for Version 6

A number of new variables have been introduced in version 6. The primary set of variables is associated with a hybrid estimate of the path attenuation that consists of a weighted sum of the SRT, Hitschfeld-Bordan (HB), and the standard dual-wavelength method (DW). For the single-frequency Ku-band and Ka-band estimates, only the SRT and HB results are used since the DW method is inapplicable.

The basic idea follows closely that used for the SRT itself: if n independent estimates of a quantity A are available and if the estimate is written in the form

$$\hat{A} = \sum_{j=1}^{n} w_j A_j$$

then the minimum variance estimate of A is obtained by choosing the weighting factors, w_j, to be inversely proportional to the variance of A_j:

$$w_j = \frac{\tau_j}{\sum_{j=1}^{n} \tau_j}; \qquad \tau_j = \text{var}(A_j)$$

It can also be shown that the variance of A is given by

$$\text{var}(\hat{A}) = \frac{1}{\sum_{j=1}^{n} \tau_j}$$

We can write explicitly the expression for the differential hybrid path attenuation as the weighted sum of the differential estimates from the SRT, HB and DW

$$\delta A_{\text{HY}} = w_{\text{SRT}}\delta A_{\text{SRT}} + w_{\text{HB}}\delta A_{\text{HB}} + w_{\text{DW}}\delta A_{\text{DW}}$$

90

As in the SRT case, the differential PIA is converted into Ku- and Ka-band results by assuming the ratio of Ka/Ku path attenuation is 6 so that, for the DPR results, $A_{\mathrm{HY}}(\mathrm{Ku}) = 0.2 \times \delta A_{\mathrm{HY}}$ and $A_{\mathrm{HY}}(\mathrm{Ka}) = 1.2 \times \delta A_{\mathrm{HY}}$.

For the single-frequency case, the hybrid path attenuation is given by

$$A_{\mathrm{HY}} = w_{\mathrm{SRT}} A_{\mathrm{SRT}} + w_{\mathrm{HB}} A_{\mathrm{HB}}$$

Note that the SRT estimates in the above equations should be interpreted as the effective PIA estimate described earlier, which itself is a weighted sum of the SRT estimates using different rain-free reference NRCS estimates. Since the procedures used to derive the SRT and hybrid estimates are the same, the formula for the reliability factor, the ratio of the mean of A_{HY} to the standard deviation, can be written in the same form:

$$\mathrm{Rel}_{\mathrm{eff}} = \frac{\sum \tau_j A_j}{\sqrt{\sum \tau_j}}$$

where

$$A_1 = A_{\mathrm{SRT}}; \qquad \tau_1 = \frac{1}{\mathrm{var}(A_{\mathrm{SRT}})}, \quad \mathrm{etc.}$$

The A_{HB} is given by the following formula:

$$A_{\mathrm{HB}} = -\frac{10}{\beta} \log_{10}[1 - \zeta(r)]^{1/\beta}$$

$$\zeta(r) = 0.2\beta \ln 10 \int_0^r \alpha(s) Z_m^{\beta}(s) \, ds; \quad k = \alpha Z_e^{\beta}$$

where the range, r, is taken to be the last clutter-free range bin above the surface and Z_m is the measured radar reflectivity factor. The expression for δA_{HY} is obtained simply by taking the difference between A_{HB} at Ka-band and at Ku-band. The only difference between these is in the values that are taken for α and β as shown in the Table.3.7-1.

Table 3.7-1. Coefficients in the k-Z relationship

	Snow	Mixed Phase	Rain
$\alpha(\mathrm{Ku})$	5.97×10^{-5}	1.39×10^{-3}	7.60×10^{-4}
$\alpha(\mathrm{Ka})$	1.2×10^{-3}	9.51×10^{-3}	5.47×10^{-3}
$\beta(\mathrm{Ku})$	0.661	0.661	0.661
$\beta(\mathrm{Ka})$	0.691	0.691	0.691

An expression for the standard dual-wavelength PIA estimate, DW, can be obtained by noting that the differential path attenuation is equal to the difference between the measured and actual dual-frequency ratio, DFR

$$\delta A_{\mathrm{DW}}(r) = \mathrm{DFRm}(r) - \mathrm{DFR}(r)$$

The first term is the difference of the measured reflectivity factors at Ku- and Ka-band and is a measured quantity. The second term in the above equation, the true DFR, is not known but we approximate it by using the measured dBZm(Ku) so that

$$\delta A_{\mathrm{DW}}(r) = [\mathrm{dB}Z_m(\mathrm{Ku}, r) - \mathrm{dB}Z_m(\mathrm{Ka}, r)] - \mathrm{DFR}(\mathrm{dB}Z_m(\mathrm{Ku}, r))$$

As in the HB method, the range is evaluated at the clutter-free gate nearest the surface.

To implement the hybrid method, it is necessary to approximate the variances for the SRT, HB and DW. Expressions for the variance of the SRT are given above and in section 3.7.5; for the HB and DW, measured drop size distributions are used to estimate the errors.

Updates for V6X

On May 21, 2018, the 24 beams of the KaHS interleaved swath were redirected to the outer swath of the KaMS swath so that, for data products since then (V6X and later), the 49 beams of the Ku and Ka-band are approximately aligned in space and time. The angle bin dimension of all Ka-band products was changed from 25 to 49 and the interleaved KaHS data are set to missing. For the temporal look-up tables, the number of angle bins for the Ka-band was increased from 13 to 25. The KaHS database exists only for months before May 2018.

3.7.2. Input Variables

sigmaZeroMeasured [real*4]: Normalized backscattering radar cross section of the surface (dB) (NRCS) at Ku-band, Ka-band or KaHS for the angle bins in the radar scan (unitless), from the Preparation Module.

flagPrecip [integer*2]: rain/no-rain flag from Preparation Module.

localZenithAngle [real*4]: incidence angle from Preparation Module.

landSurfaceType [integer*2]: surface type from Preparation Module. These are modified so that only 5 surface classes are defined: ocean, land, coast, snow-over-land and sea-ice.

lat, lon [real*4]: latitude, longitude of the center of the FOV from Preparation Module.

zFactorMeasured(176/88) [real*4]: range profile of the measured radar reflectivity factor in dB from the Preparation Module. For the KuNS and KaMS the range resolution is 0.125 km with 176 gates while for the KaHS the range sampling is 0.25 km with 88 gates.

binStormTop [integer*2]: range bin number corresponding to the first gate at which precipitation is detected, from the Preparation Module.

snowIceCover [integer*2]: an indicator flag for the presence of snow-over-land or sea-ice, from the Preparation Module.

`snRatioAtRealSurface` [real*4]: signal-to-noise ratio at the surface range gate, from the Preparation Module.

`binNode`(5) [integer*2] provides the range bins corresponding to storm height, top, center and bottom of melting layer and lowest bin of the precipitation, from the DSD module

`binBBTop, binBBBottom` [integer*2]: bin numbers corresponding to the top and bottom of the bright-band, from the Classification Module.

3.7.3. Output Variables

Five sets of path-integrated attenuation and associated quantities are produced. These consist of: single- and dual-frequency derived Ku-band attenuation, single- and dual-frequency derived Ka-band attenuation and a single-frequency derived KaHS-band attenuation. The single-frequency Ku-band attenuation and associated products are stored in the 49 angle bins (full swath) of the Ku-NS structure.

Prior to version V6X, the single-frequency KaMS/ KaHS products were stored in the KaMS/KaHS structures and were available for the 25 angle bins of the inner swath/ 24 angle bins of the interleaved swath. The dual-frequency PIA products for Ku- and Ka-band are stored in the DPR-NS and DPR-MS structures, respectively, and are produced for the 25 angle bins comprising the inner swath. (For the DPR-NS structure, the dual-frequency derived Ku-band path attenuations are contained in angle bins 13 through 37.) Note that for versions prior to V6X, the single-frequency Ku-band results are used in the outer swath of the DPR-NS structure, covering the angle bins from 1 to 12 and from 38 to 49.

For versions V6X and later, the products are stored in the KuFS, KaFS, DPRFS (FS=full scan) structures consisting of 49 angle bins. For products generated after May 2018, all angle bins are filled. For V7 and for times before May 2018 only the central angle bins (13-37) will contain data and the remainder will be filled with missing values. The Ka-band interleaved data will be retained in the KaHS structure for data taken before May 2018. After May 2018, the variables will be filled with missing values.

The output variables for each of these channels are defined below.

`pathAtten` [real*4]: The estimated effective 2-way path-attenuation in dB where

$$\texttt{pathAten} = 2 \int_0^r k(s)\, ds$$

where $k(s)$ is the attenuation coefficient in dB/km where the integral is taken from the storm top to the surface. The path attenuation is often designated as the PIA, the path-integrated attenuation. In the notation used above and in section 3.7.5:

$$\text{pathAtten} = \text{PIA}_{\text{eff}} = \frac{\sum u_j \text{PIA}_j}{\sum u_j}$$

93

Where u_j is equal to the inverse of the variance associated with the jth reference data point:

$$u_j = 1/\sigma_j^2$$

`PIAalt(6)` [real*4]: The path-integrated attenuation (dB) from the jth estimate, (PIA_j in the notation above), where

`PIAalt` (1)= PIA derived from the forward along-track spatial reference data

`PIAalt` (2)= PIA derived from the backward along-track spatial reference data

`PIAalt` (3)= PIA derived from the forward hybrid/cross-track reference data

`PIAalt` (4)= PIA derived from the backward hybrid/cross-track reference data

`PIAalt` (5)= PIA derived from standard temporal reference data

`PIAalt` (6)= PIA derived from the light-rain temporal reference data

Note that for product versions 1 through 3, the standard temporal path-attenuation estimate, `PIAalt`(5), is set to missing but is defined for versions 4 and higher. For product versions 1 through 6, the light-rain temporal estimate, `PIAalt`(6), is set to missing. Note also that the forward/backward hybrid/cross-track path attenuations are defined only over ocean and are set to missing over land.

`PIAweight(6)` [real*4]: The weights, w, of the individual PIA estimates used in deriving the effective PIA. The weight for a particular PIA estimate is proportional to the inverse of the error variance associated with the method. The sum of the weights should equal one. As with `PIAalt`(6), `PIAweight`(6) is set to missing.

$$w_j = \frac{1}{\sigma_j^2} \frac{1}{\sum \frac{1}{\sigma_j^2}} \equiv \frac{u_j}{\sum u_j}$$

where

$$u_j = 1/\sigma_j^2$$
$$\sum w_i = 1$$

`reliabFlag` [integer*2]: Reliability Flag for the PIA_{eff} estimate,

$= 1$ if $\text{Rel}_{\text{eff}} > 3$; PIA_{eff} estimate is considered reliable

$= 2$ if $3 \geq \text{Rel}_{\text{eff}} > 1$; PIA_{eff} estimate is considered marginally reliable

$= 3$ if $\text{Rel}_{\text{eff}} \leq 1$; PIA_{eff} is unreliable

$= 4$ if $\text{SNR}_{\text{at surface}} < 2$ dB; provides a lower bound to the path-attenuation

$= 9$ (no-rain case)

`reliabFactor` [real*4]: Reliability Factor for the effective PIA estimate, `pathAtten`. This is defined as:

$$\texttt{reliabFactor} = \text{Rel}_{\text{eff}} = \left(\sum u_j\right)^{-1/2} \sum u_j \text{PIA}_j$$

`reliabFactorAlt(6)` [real*4]: The reliability factors associated with the individual PIA estimates in `PIAalt`. As with `PIAalt`(6), `reliabFactorAlt`(6) is set to missing.

$$\texttt{reliabFactorAlt}_j = \text{Rel}_j = \text{PIA}_j/\sigma_j; \qquad j = 1, \dots, 6$$

`refScanID(2,2)` [integer*2]: `refScanID` gives the number of scan lines between the current scan and the beginning (or end) of the along-track reference data at each angle bin. The values are computed by the equation: Current Scan Number $-$ Reference Scan Number. The values are positive for the Forward estimates and negative for the Backward estimates. The Fortran indices are:

    1,1 - Forward - Near reference

    2,1 - Forward - Far reference

    1,2 - Backward - Near reference

    2,2 - Backward - Far reference

To illustrate, consider the following example. At a certain incidence angle assume that rain is present at scan numbers from 100 to 105 and from 110 to 120. At scan number 112, refScanID(1,1)=3, refScanID(2,1)=16; i.e., the eight rain-free NRCS data points, used to estimate the mean and standard deviation of the rain-free NRCS, begin at scan 112-16 = 96 and end at scan 112-3=109. These numbers provide information on the distance (in terms of the numbers of scans where 1 scan $\sim$ 5 km) of the rain-free reference data from the rain pixel of interest. See section 3.7.6 for further details.

`PIAhybrid` [real*4] (V6): For the dual-frequency output, PIAhybrid (dB) is a weighted sum of the path attenuations from the SRT, HB, and DW methods. For the single-frequency outputs, PIAhybrid is a weighted sum of the SRT and HB methods.

`reliabFlagHY` [integer*2] (V6): `reliabFlagHY` is the reliability flag for the PIAhybrid and is defined in the same way as reliabFlag where PIAeff is replaced by PIAhybrid.

`reliabFactorHY` [real*4] (V6): `reliabFactorHY` is the reliability factor associated with the PIAhybrid estimate and is defined as the mean over the standard deviation of the estimate.

`stddevHY` [real*4] (V6): `stddevHY` is the standard deviation (dB) of the hybrid estimate of path attenuation.

`PIAhb` [real*4] (V6): `PIAhb` (dB) is the path attenuation estimate derived from the Hitschfeld-Bordan equation.

`zeta` [real*4] (V6): `zeta` (unitless) is a parameter in the Hitschfeld-Bordan equation.

`stddevEff(3)` [real*4] (V6):

stddevEff(1) contains the standard deviation of the PIAeff (i.e., the composite or effective SRT or hybrid path attenuation estimate). It is given by $\sigma_1 = \left(\sum 1/\sigma_e, j^2 \right)^{-1/2} = \left(\sum u_j \right)^{-1/2}$. It is important to note that in the definition of the reliability factor, it is this standard deviation that is used. In other words, with the notation in section 3.7.5, we have $\sigma_1 = \sigma_{\text{eff}}$

stddevEff(2) is a weighted root mean square error and provides a measured of the error of the individual PIA estimates from the effective PIA estimate. It is given by $\sigma_2 = \left(\sum w_j (A_{\text{eff}} - A_j)^2 \right)^{1/2}$.

stddevEff(3) is given by $\sigma_3 = [\sigma_1^2 + \sigma_2^2]^{1/2}$

PIAdw [real*4] (V6X): PIAdw(dB) is the path-integrated attenuation as estimated from the standard dual-wavelength technique.

PIAHYweight(3) [real*4] (V6X): PIAHYweight contains the weights of the SRT, HB, and DF methods in the calculation of the hybrid PIA. For single-frequency results, since the DF method is inapplicable and PIAHYweight(3)=0.

3.7.4. Temporal Reference Files

Temporal reference files or look-up tables (LUT) are needed to estimate the path attenuation using temporal reference data. The temporal reference data are simply the mean and standard deviations of previously measured rain-free σ^0 data that have been categorized with respect to incidence angle and location. In particular, the LUTs contain the rain-free sample mean and standard deviation of the σ^0 data at each (lat, lon, incidence angle) bin, where the incidence angles, with respect to the radar, consist of nadir, $\pm 0.71°$, $\pm 1.42°$, $\cdots$ up to the maximum angle. Also stored is the number of σ^0 data points acquired at the particular bin in question and used in computing the statistics.

For version 4 of the algorithm, a $0.5° \times 0.5°$ grid is used which covers the GPM-DPR latitude range of 67°S–67°N so that 268 latitude bins and 720 longitude bins are needed. Four LUTs are derived from DJF (December-January-February), MAM, JJA, SON input data. For each of these, five LUTs are prepared corresponding to ocean, land, coast, snow-over-land and sea-ice background type. Note that separate tables are produced for σ^0(Ku), σ^0(Ka), σ^0(KaHS), and the difference field, $[\sigma^0(\text{Ka}) - \sigma^0(\text{Ku})]$ so that a total of 20 LUT's are generated for each three-month season.

As noted earlier, two types of temporal reference files have been defined: the standard temporal reference files as described above and a light-rain reference file which, as of version 6 of the code, is undefined. The results derived from the standard temporal reference file can be found in the fifth entry in the variables PIAalt, PIAweight, reliabFactorAlt. The sixth entry for these variables, corresponding to the 'light-rain' temporal reference file, is set to missing.

3.7.5. Definitions of the Effective PIA, Variance and Reliability Factor

As noted above, multiple estimates of PIA can be generated for each channel corresponding to different surface reference estimates. Specifically, we have the following situation

$$\mathrm{PIA}_j = \langle \sigma^0_{NR} \rangle_j - \sigma^0_R \tag{3.7-1}$$

where the first term on the right-hand side is the jth surface reference value and the second term is the apparent NRCS in rain. Associated with the jth reference data set is a variance, σ^2_j:

$$\mathrm{var}(\mathrm{PIA}_j) = \mathrm{var}[\langle \sigma^0_j \rangle] + \mathrm{var}(\sigma^0_R) \equiv \sigma^2_j + \sigma^2_s \tag{3.7-2}$$

Note that the second term in (3.7-2) corresponds to the variance due to sampling error in the measurement of σ^0 in rain. With a logarithmic receiver, it is equal to $5.57^2/\mathrm{N}$ where N is the number of independent samples used to estimate this quantity. For the DPR, N depends on the incidence angle and varies between 100 and 109. It should be noted that the sampling error was neglected versions up to V6X but is included in V7.

From these PIA estimates we want to obtain an effective or 'best' PIA. We assume it can be written in the form:

$$\mathrm{PIA}_{\mathrm{eff}} = \sum w_j \mathrm{PIA}_j \tag{3.7-3}$$

Where the weights, w_j, are such that

$$\sum w_j = 1 \tag{3.7-4}$$

We assume that the individual PIA estimates are statistically independent so that the variance of $\mathrm{PIA}_{\mathrm{eff}}$ is:

$$\mathrm{var}(\mathrm{PIA}_{\mathrm{eff}}) = \sum w_j [\sigma^2_j + \sigma^2_s] \tag{3.7-5}$$

To simplify the equations below, we define an effective variance, $\sigma^2_{e,j}$

$$\sigma^2_{e,j} = \sigma^2_j + \sigma^2_s \tag{3.7-6}$$

To minimize (3.7-5), subject to the side condition given by (3.7-4), we use the method of Lagrange multipliers where the expression

$$\sum w^2_j \sigma^2_j + \lambda \left(\sum w_j - 1 \right) \tag{3.7-7}$$

is minimized with respect to the weights, w_j. Taking the partial derivatives of (3.7-7) with respect to w_i, then

$$2w_i\sigma_i^2 + \lambda = 0 \quad \Rightarrow \quad w_i = -\lambda/2\sigma_{e,j}^2 \tag{3.7-8}$$

Also, using (3.7-4) gives

$$\sum w_j = -(\lambda/2)\sum(1/\sigma_{e,j}^2) \quad \Rightarrow \lambda = -2/\sum(1/\sigma_{e,j}^2) \tag{3.7-9}$$

Substituting (3.7-9) into (3.7-8) gives an expression for the weights:

$$w_j = u_j/\sum u_j \tag{3.7-10}$$

Where

$$u_j = 1/\sigma_{e,j}^2 \tag{3.7-11}$$

The effective PIA is then

$$\text{PIA}_{\text{eff}} = \left(\sum u_j\right)^{-1}\sum u_j\text{PIA}_j \tag{3.7-12}$$

If we define the reliability factor, Rel, as the ratio of the PIA to the standard deviation of the reference estimate, then for the jth reference estimate, we can write:

$$\text{Rel}_j = \text{PIA}_j/\sigma_{e,j} \tag{3.7-13}$$

To apply this definition to the present situation, we define Rel_{eff} by the equation:

$$\text{PIA}_{\text{eff}} = \left(\sum u_j\right)^{-1}\sum u_j\text{PIA}_j \equiv \sigma_{\text{eff}}\text{Rel}_{\text{eff}} \tag{3.7-14}$$

Computing Rel_{eff} requires a value for the standard deviation of the effective PIA. This can be found by substituting (3.7-9) into (3.7-5) and by noting that $\sigma_{\text{eff}}^2 = \text{var}(\text{PIA}_{\text{eff}})$. This gives

$$1/\sigma_{\text{eff}}^2 = \sum(1/\sigma_{e,j}^2) \quad \Rightarrow \quad \sigma_{\text{eff}}^2 = [\sum(1/\sigma_{e,j}^2)]^{-1} = \left(\sum u_j\right)^{-1} \tag{3.7-15}$$

Using (3.7-15) in (3.7-14) gives

$$\text{Rel}_{\text{eff}} = \left(\sum u_j\right)^{-1/2}\sum u_j\text{PIA}_j \tag{3.7-16}$$

Equations (3.7-10), (3.7-12) and (3.7-16) define, respectively, the weights, effective PIA, and effective reliability factor that are computed in the algorithm. In addition to the σ_{eff} error defined above in (3.7-15), a kind of RMS error can be defined by the following equation:

$$\text{RMS}_{\text{eff}}^2 = \sum_j w_j[\text{PIA}_{\text{eff}} - \text{PIA}_j]^2 \tag{3.7-16}$$

where the summation runs over the j estimates of PIA. Note that when the weighting factors are all the same then this reduces to the usual definition of RMS error.

There are several issues related to these equations. For example, what should be done if none of the reference data sets exist? This situation can occur for measurements over small islands or small bodies of water or at coastal fields of view. For example, over a small island, there may be an insufficient number of non-raining fields of view adjacent to the rain area to form a valid spatial reference. In most cases, the temporal reference data set would be used and the other reference estimates would be discarded. However, in some cases, there may be an insufficient number of data points in the temporal file to provide a valid estimate. In this case, a flag is set indicating that no valid reference data are available and all the output variables are set to -9999.9

A somewhat different situation occurs if some of the reference data sets exist but all yield a negative PIA. For these cases, the individual variances will exist so that Rel_{eff}, PIA_{eff} and the effective variance should all exist. Note that for these cases Rel_{eff}, PIA_{eff} will be negative but the effective variance will be positive, as it should be.

A third type of situation occurs if one or more of the PIA estimates are positive and one or more of the PIA estimates are negative. In this case, the negative PIAs will be included in the definition of PIA_{eff}. In general, as long as the reference data is considered to be valid, the PIA will be used even if the value is negative.

According to these scenarios, there will be only one type of raining situation where the output variables will need to be set to some default value and this occurs when none of the reference data sets exist or are valid. This is expected to be a small fraction relative to the total number of rain cases.

3.7.6. Excluding Spatial Reference Data based on the `refScanID` Variable

This section relates to determining the circumstances under which we assume a spatial reference estimate to be valid. For the forward-going spatial reference, reference data will almost always exist. An exception is if rain is encountered at the beginning of the orbit before $N_s(=8)$ rain-free fields of view have been measured at a particular incidence angle. A similar exception occurs for the backward spatial methods: this occurs, however, at the end of the orbit rather than the beginning. In all other cases, forward and backward spatial reference data should exist. The question is how should we exclude spatial reference estimates if the data are taken at locations far from the raining area. To make this definite we implement the following rules in the algorithm.

See definition of `refScanID`(2,2) in section 3.7.3.

The forward along-track spatial reference at angle bin j will be assumed to be invalid if:

$$|\texttt{refScanID}(2,1,j)| > 50.$$

Similarly, the backward along-track spatial reference at angle bin j will be assumed to be invalid if:

$$|\texttt{refScanID}(2,2,j)| > 50.$$

The above conditions are equivalent to stating that, for a particular incidence angle, all the spatial reference data must be taken within 50 scans of the scan at which rain is encountered. The criteria for the hybrid cross-track are more complicated because two quadratic fits are used for the inner and outer portion of the swath. Nominally, we will assume that if there are 15 or more angle bins in the inner portion of the swath for which:

$$|\texttt{refScanID}(2,1,j)| \leq 50$$

then the forward hybrid cross-track method will be applied. Similarly in the outer portion of the swath, if there are 15 or more angle bins in this portion of the swath for which:

$$|\texttt{refScanID}(2,1,j)| \leq 50$$

then the forward hybrid cross-track method will be applied. Application of the backward hybrid cross-track will follow the same rule, based on $\texttt{refScanID}(2,2,j)$.

3.7.7. Additional Comments and Version-dependent Variables

The presence of sea-ice is a source of error in the method since its scattering properties differ significantly from those of ocean. (Most occurrences of sea-ice are presently categorized as ocean surface type.) If sea-ice information becomes available, under both rain and rain-free conditions, an additional surface category will be defined so that the reference data are matched to the surface type encountered during rain.

Because the Ku-band has greater sensitivity than the matched-swath Ka-band, there are a number of cases for which rain is detected at Ku-band but not at Ka-band. As dual-frequency derived estimates at Ku- and Ka-band are produced when either or both channels detect rain, a number of dual-frequency derived Ka-band estimates of path attenuation will be produced without corresponding single-frequency estimates.

Versions 1 through 3 of the SRT products do not contain path attenuations based on the temporal reference data. Versions 4 and higher will include such results and which can be found in $\texttt{PIAalt}(5)$. The light-rain/wet soil temporal reference data set has yet to be derived so this product will be unavailable up to and including version 4. As a consequence $\texttt{PIAalt}(6)$ will be set to 'missing' (-9999.9). As already noted, the hybrid/cross-track reference data are derived only over ocean so that over land, $\texttt{PIAalt}(3)$ and $\texttt{PIAalt}(4)$ are set to 'missing'.

3.8 Solver module

3.8.1 Objective

The primary objective of the Solver module is to retrieve the drop size distribution and calculate some physical variables.

3.8.2 Algorithm Overview

The solver module employs an R-D_m plane, where the vertical axis is the precipitation rate (R) and the horizontal axis is the mass weighted mean diameter (D_m). Once an R-D_m relation (as $R = \epsilon^r p D_m^q$) is assumed, the retrieval process goes from the top to the bottom range bin. At a "precipitating"range bin, a combination of R and D_m which satisfies both the R-D_m relation and the given Z_f is usually selected. Z_f is the radar reflectivity factor corrected for attenuation caused at the higher range bins but not for attenuation caused at the current range bin. For drawing the contour of Z_f on the R-D_m plane, scattering tables are used. After R and D_m are calculated at all "precipitating"range bins, the path integrated attenuation (PIA) is calculated. When the surface reference technique (SRT) gives a reliable PIA estimate, the calculated PIA and SRT's PIA estimate can be compared.

The R-D_m relation is linked to ϵ, which is originally an adjustment factor for the k-Z_e realtion. The retrieval is done multiple times for different ϵ or different R-D_m relations corresponding ϵ ranging from 0.2 to 5.0. The best ϵ or the best R-D_m relation is selected by checking the likelihood of ϵ and the difference between the calculated PIA and SRT's PIA.

3.8.3 Retrieval processes

The major input data to the Solver module are radar reflectivity factor corrected for attenuation by non-precipitating particles (here it is denoted by Z_m), μ and σ of $\log_{10} \epsilon$, SRT's PIA estimates PIA_SRT, its reliability, precipitation type and the information of "phase". The retrieval algorithm first defines range bins to be processed: It mainly processes the data between the storm top and the actual surface.

From the storm top to the clutter free bottom, Z_m is usually available for the retrieval. By correcting the attenuation caused by higher range bins, Z_m is converted to Z_f. Then, the contour of the given Z_f is drawn on the R-D_m plane by reference to the scattering tables. If there is only one crossing point between the contour of Z_f and the curve for the assumed R-D_m relation, R and D_m can be determined easily. If there are multiple crossing points, a set of R and D_m which has smaller R and D_m, is preferred. Unfortunately if there are no crossing points, the point that is on the curve of R-D_m relation and gives the closest Z_f to the given value is selected. In this case, given Z_f (Z_{f1}) and the finally determined Z_f (Z_{f2}) are different.

In the main-lobe clutter region (below the clutter free bottom), Z_m is not useful for the retrieval. Here, the vertical profile of Z_e is assumed to be constant, or the same value of Z_e

at the clutter free bottom is used in the clutter region. The same method is also applied for range bins in which Z_m's are smaller than the noise level if such small Z_m's are caused by large attenuation due to heavy rain above them. Specifically, if Z_m's above the point in question are reliable at 8 (4 for HS) or more liquid-phase range bins in the same pixel, Z_e is extrapolated.

In the dual-frequency algorithm, the following preference is set.

(1) Z_f of KuPR

(2) Z_f of KaPR

(3) extrapolated Z_e of KuPR

(4) extrapolated Z_e of KaPR

3.8.3-1 Determination of ϵ and use of SRT

Different R-D_m relations are tested by changing ϵ from 0.2 to 5.0. Using the following conditions, the best R-D_m relation is selected. Generally, the three conditions a) to c) are checked for the single-frequency algorithms and the four conditions a) to d) are checked for the dual-frequency algorithm.

a) A priori probability of ϵ; $(\log(\epsilon) - \mu)^2$ is minimized, where μ is given by the DSD database or $\mu = 0$ if DSD database is not applied.

b) The difference of PIA calculated by the retrieval (PIA_SLV) and PIA estimated by SRT (PIA_SRT); $(\text{PIA\_SLV} - \text{PIA\_SRT})^2$ is minimized. When PIA_SRT is saturated, $(\min(\text{PIA\_SLV} - \text{PIA\_SRT}, 0))^2$ is minimized.

c) The difference of Z_{f1} and Z_{f2}; The sum of $(Z_{f1} - Z_{f2})^2$ is minimized.

d) If Z_m of KuPR is used for the retrieval and Z_m of KaPR is normal, estimated DSD should be also agreed with KaPR; $(\max(Z_{f2} \text{ of KaPR} - Z_{f1} \text{ of KaPR}, 0))^2 + (\min(Z_{f2} \text{ of KaPR} - Z_m \text{ of KaPR}, 0))^2$ should be minimized. If Z_{f2} of KaPR is between Z_m of KaPR and Z_{f1} of KaPR, the vaule is zero.

The following preference is set to select the use of PIA.

(1) δPIA_SRT=KaPR's PIA_SRT$-$KuPR's PIA_SRT (if both are reliable and not saturated)

(2) KaPR's PIA_SRT (if it is reliable and not saturated)

(3) KuPR's PIA_SRT (if it is reliable and not saturated)

(4) KaPR's PIA_SRT (if it is reliable and saturated)

(5) KuPR's PIA_SRT (if it is reliable and saturated)

If none of PIA_SRT is available, or if selected PIA_SRT is saturated, abnormally high precipitation rates may be resulted. To avoid them, condition e) is used.

e) R estimated from Z_m (not extrapolated Z_e) at liquid-phase range bins should be vertically constant; the variance of R is minimized.

PIA_SRT is set to be not "reliable" if the standard deviation of sampled surface backscattering cross section is larger than 10 dB. PIA_SRT is set to be "saturated"if the signal-to-noise ratio of measured surface backscattering cross section is smaller than 2.

From Version 06, the following condition is added. PIA_SRT is set to be not "reliable" if PIA_SRT is more than 10 times as large as PIA_HB, where PIA_HB is PIA calculated with $\epsilon = 1$.

3.8.3-2 NUBF correction

Two NUBF parameters (`p_area` and `rainvar`) are set in the algorithm, but `p_area` (the ratio of rain part in an FOV) is fixed to 1.0 for the version 04 and version 05. `rainvar` (the square of coefficient of variation of R) is estimated by a fractal approach. In the single-frequency algorithms, NUBF correction is not applied in the first main loop. In the second (final) main loop, the NUBF parameter is estimated from `piaFinal` of the first main loop. In the dual-frequency algorithm, the NUBF parameter is estimated from `piaFinal` of the single-frequency algorithms. KuPR's `piaFinal` is preferred to KaPR's `piaFinal`. For the details, please refer to Seto et al. (2015).

4. VALIDATION (TEST AND VERIFICATION)

4.1 Pre-launch of the GPM core satellite

Before the launch of the GPM core satellite, we will test the algorithm test and physically validate it as much as possible with collaboration of the GPM GV team. In the algorithm test, algorithm mechanics and robustness will be checked. More than one type of test data will be needed. We will generate synthetic Ka-band data in the central swath from actual TRMM PR data (Ku-band) by assuming a relationship among the DSD parameters and the attenuation by clouds and water vapor (Kubota et al. 2014). Airborne data (PR-2, APR-2) will provide realistic dual-frequency radar data although with many unknown parameters (e.g., clouds). Ground-based dual-frequency radars including NASA's dual-frequency and dual-polarized Doppler radar (D3R) and JAXA's dual Ka-band radar system will also provide realistic dual-frequency radar data. Synthetic data created by using a numerical model have an advantage that all parameters are known so that we can test the performance of the algorithm by checking whether the algorithm can retrieve the parameters correctly. Note that many parameters needed to reproduce radar echoes accurately are not handled well in most of the current numerical models. They include melting or partially frozen particles. Nevertheless, synthetic data created with simple assumptions are very helpful for sanity check of the algorithm. In the physical validation, various parameters of the DPR algorithm will be tested with collaboration of the GPM GV team. The physical validation will validate the parameters in the physical model of the precipitation system assumed in the algorithm. They include the DSD parameters, density and shape of snow and melting particles, width and structure of the melting layer, supercooled droplets, attenuation by the water vapor and cloud, inhomogeneity of rain distribution and so on.

4.2 Post-launch of the GPM core satellite

After the launch of the GPM core satellite, product validation will be performed, in addition to the physical validation. Data taken nearly simultaneously by the GPM/DPR and the TRMM/PR enable us to make a direct comparison. Statistics such as averages and histograms of radar echoes taken by the DPR can be compared with the corresponding statistics of the TRMM/PR data. Ground instruments such as a dense rain gauge network and ground-radar including NASA's D3R and JAXA's dual Ka-band radar system can be used to validate the DPR products. Validations by using airborne data are desirable.

4. INTERFACE TO OTHER ALGORITHMS

The combined DPR-GMI algorithm requires outputs from the preparation module (PRE), the vertical profile module (VER), the surface reference technique module (SRT), and the classification module (CSF), in addition to the DPR radar reflectivity profiles. Precipitation detection from the PRE, pressure, temperature and humidity profiles from the VER, the PIA from the SRT, and bright band detection, altitude of the bright band (if it exists), and classification as convective or stratiform precipitation from the CSF will be used in the DPR-GMI combined algorithm.

The DPR products will be utilized also in the GPM Passive Microwave-Radar Enhanced Algorithm of an Optimal Estimation approach that uses the DPR/GMI data as the a-priori constraint.

5. REFERENCES

Awaka, J., T. Iguchi, H. Kumagai, and K. Okamoto, 1997: Rain type classification algorithm for TRMM precipitation radar, *Proc. IEEE IGARSS*, 317–319.

Awaka, J., T. Iguchi, and K. Okamoto, 1998: Early results on rain type classification by the Tropical Rainfall Measuring Mission (TRMM) precipitation radar, *Proc. 8th URSI Commission F Open Symp.*, Aveiro, Portugal, 143–146.

Awaka, J., T. Iguchi, and K. Okamoto, 2009: TRMM PR standard algorithm 2A23 and its performance on bright band detection, *J. Meteor. Soc. Japan*, **87A**, 31–52.

Awaka, J., M. Le, V. Chandrasekar, N. Yoshida, T. Higashiuwatoko, T. Kubota, and T. Iguchi, 2016: Rain Type Classification Algorithm Module for GPM Dual-Frequency Precipitation Radar, *J. Atmos. Oceanic Technol.*, **33**, 1887–1898.

Awaka, J. and S. Brodzik, 2019: Improvements of GPM DPR rain type classification algorithm, *IGARSS 2019*, 4470–4472, doi: 10.1109/IGARSS.2019.8898365

Baldini, L. and E. Gorgucci, 2006: Identification of the melting layer through dual-polarization radar measurements at vertical incidence, *J. Atmos. Ocean. Technol.*, **23**, 829–839.

Bandera, J., A. D. Papatsoris, P. A. Watson, and J. W. Goddard, 1998: Method for detecting the extent of the melting layer, *Electron. Lett.*, **34(22)**, 2104–2105.

Caylor I.J., G.M. Heymsfield, R. Meneghini, and L.S. Miller, 1997: Correction of sampling errors in ocean surface cross-sectional estimates from nadir-looking weather radar. *J. Atmos. Oceanic Technol.*, **14**, 203–210.

Durden, S.L., L. Li, E. Im and S.H. Yueh, 2003: A surface reference technique for airborne Doppler radar measurements in hurricanes, *J. Atmos. Oceanic Technol.*, **20**, 269–275, 2003.

Durden, S.L., S. Tanelli, and G. Dobrowalski, 2010: CloudSat W-band radar measurements of surface backscatter, *IEEE Geosci. Remote Sens. Lett.*, **7**, 401–405, doi: 10.1109/LGRS.2010.2079314.

Durden S.L., S. Tanelli, and R. Meneghini, 2012: Using surface classification to improve surface reference technique over land, *Indian J. Radio & Space Physics*, **41**, 403–410.

Durden, S.L., 2018: Estimating attenuation from GPM radar reflectivity profiles without using surface reference, *IEEE Geosci. Remote Sens.*

Fabry, F. and I. Zawadzki, 1995, Long-term radar observations of the melting layer of precipitation and their interpretation, *J. Atmos. Sci.*, **52**, 838–851.

Hines, E. L., 1983: Image processing techniques for the detection of the radar bright band, Ph.D. dissertation, Univ. Bradford, Bradford, U.K.

Hitschfeld, W. and J. Bordan, 1954: Errors inherent in the radar measurement of rainfall at attenuating wavelengths. *J. Meteor.*, **11**, 58-67.

Iguchi, T. and R. Meneghini, 1994: Intercomparisons of single-frequency methods for retrieving a vertical rain profile from airborne or spaceborne radar data. *J. Atmos. Oceanic Technol.*, **11**, 1507–1516.

Iguchi, T., T. Kozu, J. Kwiatkowski, R. Meneghini, J. Awaka, and K. Okamoto, 2009: Uncertainties in the Rain Profiling Algorithm for the TRMM Precipitation Radar. *J. Meteor. Soc. Japan, Vol.*, **87A**, 1–30.

Iguchi, T., S. Seto, et al., 2012: An overview of the precipitation retrieval algorithm for the Dual-frequency Precipitation Radar (DPR) on the Global Precipitation Measurement (GPM) mission's core satellite. *SPIE*, Kyoto, Japan.

Iguchi, T., N. Kawamoto and R. Oki, 2018: Detection of intense ice precipitation with GPM/DPR. *J. Atmos. Oceanic Technol.*, **35**, 491–502, DOI: 10.1175/JTECH-D-17-0120.1.

Klaassen, W., 1988: Radar observations and simulation of the melting layer of precipitation, *J. Atmospheric Sciences*, **45**, 3741–3753.

Kozu, T., 1995: A generalized surface echo radar equation for down-looking pencil beam radar. *IEICE Trans. Commun.*, **E78-B**, 1245–1248.

Kubota, T., T.Iguchi, M. Kojima, L. Liao, T Masaki, H. Hanado, R. Meneghini, R. Oki, 2016: A statistical method for reducing sidelobe clutter for the Ku-band precipitation radar onboard the GPM Core Observatory, *J. Atmos. Oceanic Technol.*, **33 (7)**, 1413-1428.

Kubota, T., T. Iguchi, T. Masaki, N. Yoshida, and R. Oki, 2018: Development of a statistical method for reducing sidelobe clutter in high sensitivity mode of GPM/KaPR, *Proc. IGARSS2018*, 8347-8348.

Kubota, T., M. Satoh, T. Nasuno, S. Seto, T. Iguchi, R. Oki , 2012: Development of cloud liquid water database using global cloud-system resolving model for GPM/DPR algorithm. *Proc. IGARSS 2012*, 350–353.

Kubota, T., N. Yoshida, S. Urita, T. Iguchi, S. Seto, R. Meneghini, J. Awaka, Member, H. Hanado, S. Kida, and R. Oki, 2014: Evaluation of precipitation estimates by at-launch codes of GPM/DPR algorithms using synthetic data from TRMM/PR observations. *IEEE J. Sel. Topics Appl. Earth Observ. Remote Sens.*, **7**, 3931–3944. (doi.10.1109/JSTARS.2014.2320960.)

Kubota, T., S. Seto, M. Satoh, T. Nasuno, T. Iguchi, T. Masaki, J. M. Kwiatkowski, and R. Oki, 2020: Cloud assumption of Precipitation Retrieval Algorithms for the Dual-frequency Precipitation Radar, J. Atmos. Oceanic Technol.,submitted.

Le, M. and V. Chandrasekar, 2013a: Precipitation Type Classification Method for Dual-Frequency Precipitation Radar (DPR) Onboard the GPM, *IEEE Trans. Geosci. Remote Sens.*, **51(3)**, 1784–1790.

Le, M. and V. Chandrasekar, 2013b: Hydrometeor Profile Characterization Method for Dual-Frequency Precipitation Radar Onboard the GPM, *IEEE Trans. Geosci. Remote Sens.*, **51(6-2)**, 3648–3658.

Li, L., E. Im, L.N. Connor, and P.S. Chang, 2004: Retrieving ocean surface wind speed from the TRMM precipitation radar measurements, *IEEE Trans. Geosci. Remote Sens.*, **42**, 1271–1282.

Marzoug, M. and P. Amayenc, 1994: A class of single- and dual-frequency algorithms for rain rate profiling from a spaceborne radar. Part I: Principle and tests from numerical simulations. *J. Atmos. Oceanic Technol.*, **11**, 1480–1506.

Meneghini, R., and T. Kozu, 1990: *Spaceborne weather radar.* Artech House (Boston/London), Norwood, MA, 197pp.

Meneghini, R. and K. Nakamura, 1990: Range profiling of the rain rate by an airborne weather radar. *Remote Sens. Environ.*, **31**, 193–209.

Meneghini, R., T. Iguchi, T. Kozu, L. Liao, K. Okamoto, J.A. Jones, and J. Kwiatkowski, 2000:

Use of the surface reference technique for path attenuation estimates from the TRMM Radar. *J. Appl. Meteor.*, **39**, 2053–2070.

Meneghini, R., J.A. Jones, T. Iguchi, K. Okamoto, and J. Kwiatkowski, 2004: A hybrid surface reference technique and its application to the TRMM Precipitation Radar, *J. Atmos. Oceanic Technol.*, **21**, 1645–1658.

Meneghini, R. and J.A. Jones, 2011: Standard deviation of spatially-averaged surface cross section data from the TRMM Precipitation Radar, *IEEE Geosc. Remote Sens. Letters*, **8**, 293–297.

Meneghini, R., L. Liao, S. Tanelli, and S. L. Durden, 2012: Assessment of the Performance of a Dual-Frequency Surface Reference Technique Over Ocean. *IEEE Trans. Geosci. Remote Sens.*, **50**, 2968–2977.

Meneghini, R., and L. Liao, 2013: Modified Hitschfeld-Bordan equations for attenuation-corrected rain reflectivity: Application to nonuniform beamfilling at off-nadir incidence. *J. Atmos. Oceanic Technol.*, **30**, 1149–1160.

Meneghini, R. and H. Kim, 2017: Minimizing the Standard Deviation of Spatially Averaged Surface Cross-Sectional Data From the dual-frequency precipitation radar. *IEEE Geosci. Remote Sens.*, **55**, 1709-1716.

Meneghini, R., L. Liao, T. Iguchi, and H. Kim, 2018: Hybrid estimates of path attenuation for the DPR. IGARSS 2018 Proceedings, Valencia, Spain, 23-27 July.

Onogi, K., J. Tsutsui, H. Koide, M. Sakamoto, S. Kobayashi, H. Hatsushika, T. Matsumoto, N. Yamazaki, H. Kamahori, K. Takahashi, S. Kadokura, K. Wada, K. Kato, R. Oyama, T. Ose, N. Mannoji and R. Taira , 2007 : The JRA-25 Reanalysis. *J. Meteor. Soc. Japan*, **85**, 369–432.

Press, W. H., Teukolsky, Flannery, S. B. P., and Vetterling W.T., 1992, "14.8 Savitzky-Golay Smoothing Filters" *Numerical Recipes: The Art of Scientific Computing,* Second Edition, 994 pp. Cambridge University Press.

Rosenkranz, P. W., 1975: Shape of the 5mm oxygen band in the atmosphere. *IEEE Trans. Ant. and Propag.*, AP-23, 498–506.

Savitzky, A., and Golay, M.J.E., 1964: Smoothing and Differentiation of Data by Simplified Least Squares Procedures. *Analytical Chemistry.* **36 (8)**, 1627-1639. doi:10.1021/ac60214a047.

Seto, S. and T. Iguchi, 2007: Rainfall-induced changes in actual surface backscattering cross sections and effects on rain-rate estimates by spaceborne precipitation radar. *J. Atmos. Oceanic Technol.*, **24**, 1693–1709.

Seto, S., and T. Iguchi, 2011: Applicability of the iterative backward retrieval method for the GPM Dual-frequency Precipitation Radar. *IEEE Transactions on Geoscience and Remote Sensing*, **49(6)**, pp.1827–1838.

Seto, S., T. Iguchi, and T. Oki, 2013: The basic performance of a precipitation retrieval algorithm for the Global Precipitation Measurement mission's single/dual-frequency radar measurements. *IEEE Transactions on Geoscience and Remote Sensing*, **51(12)**, 5239–5251.

Seto, S., T. Iguchi, T. Shimozuma, and S. Hayashi, 2015: NUBF correction method for the GPM/DPR level-2 algorithms. *Proc. IGARSS 2015*, 2612–2614, DOI: 10.1109/IGARSS.2015.7326347.

Smyth, T. J., A. J. Illingworth, and A. B. Smith, 1998: Radar estimates of rainfall rates at the ground in bright band and non-bright band events, *Q. J. R. Meteorol. Soc.*, **124(551)**,

2417–2434.

Steiner, M., R.A. Houze, Jr., and S.E. Yuter, 1995: Climatological characterization of three-dimensional storm structure from operational radar and rain gauge data, *J. Appl. Meteor.*, **34**, 1978–2007.

Tagawa, T., 2009: Derivation of sub-footprint scale σ^0 observed by TRMM Precipitation Radar. *IEEE. Trans. Geosci. Remote Sens.,IGARSS 2008*, IV, 137–140.

Takahashi, N., and T. Iguchi, 2004: Estimation and correction of beam mismatch of the Precipitation Radar after an orbit boost of the Tropical Rainfall Measuring Mission Satellite, *IEEE. Trans. Geosci. Remote Sens.*, **42**, 2362–2369.

Takahashi, N., H. Hanado, and T. Iguchi, 2005: Estimation of path-integrated attenuation and its nonuniformity from TRMM/PR range profile data. *IEEE. Trans. Geosci. Remote Sens.*, **44**, 3276–3283.

Tan, J. and J.W.F. Goddard, 1995: The use of dual-polarisation techniques for bright-band detection with PPI-based radars, *Eng.-Colloq. Radar Meteorol.*, 11/1–11/6.

Tanelli, S., S.L. Durden, and E. Im, 2006: Simultaneous measurements of Ku- and Ka-band sea surface cross sections by an airborne radar. *IEEE. Trans. Geosci. Remote Sens. Letters*, **3**, 359–363.

Tanelli, S., G.F. Sacco, S.L. Durden, and Z.S. Haddad, 2012: Impact of non-uniform beam filling on spaceborne cloud and precipitation radar retrieval algorithms. *SPIE*, Kyoto, Japan.

Tilford, K.A., I. D. Cluckie, R. J. Griffith, and A. Lane, 2001: Vertical reflectivity characteristics and bright band correction, Proc. Radar Hydrol. Real Time Flood Forecast., *Proc. Adv. Course*, 47–65, European Communities.

Ulaby, F.T., R. K. Moore, and A. K. Fung, 1981: *Microwave Remote Sensing: Active and Passive.* Vol. I. Artech House, Norwood, MA, 456pp.

Waters, J.W., 1976: Absorption and emission of microwave radiation by atmospheric gases, in Methods of Experimental Physics, M. L. Meeks, ed. 12, Part B, *Radio Astronomy*, Academic Press, Section 2.3.

Yuter, S. E., and R. A. Houze, Jr., 1997: Measurements of Raindrop Size Distributions over the Pacific Warm Pool and Implications for Z-R Relations, *J. Appl. Meteorol.*, **36(7)**, 847–867.

Zrnic, D.S., R. Raghavan, and V. Chandrasekar, 1994: Observations of copolar correlation coefficient through a bright band at vertical incidence, *J. Appl. Meteorol.*, **33(1)**, 45–52.

6. ACRONYMS

BB:	Bright band
CSF module:	Classification module
DB:	dual-beam
DF:	dual-frequency
DFRm:	Measured Dual Frequency Ratio
DPR:	Dual-frequency Precipitation Radar
DSD:	drop size distribution
HS:	high-sensitivity
KuPR:	Ku-band precipitation radar
KaPR:	Ka-band precipitation radar
ML:	Melting layer
MS:	matched scan
NP-attenuation:	Attenuation due to non-precipitation particles
NS:	normal scan
NUBF:	non-uniform beam filling
PIA:	path-integrated attenuation
PRE module:	Preparation module
PSD:	particle size distribution
SB:	single-beam
SF:	single-frequency
SLV module:	Solver module
SRT:	surface reference technique
VER module:	Vertical module

Appendix

1. Level 2 Data Format Structure

Changes in the DPR Level-2 products from V06A to V06X.

· Implementation of a new group "FS" (Full Scan) in V06X and later version as shown in Fig.1-1.

· In V 06A, there are three types of group, which are "NS" (Normal Scan), "MS" (Matched Scan) and "HS" (High-sensitivity Scan).

· In V06X, the FS was implemented instead of the NS and the MS.
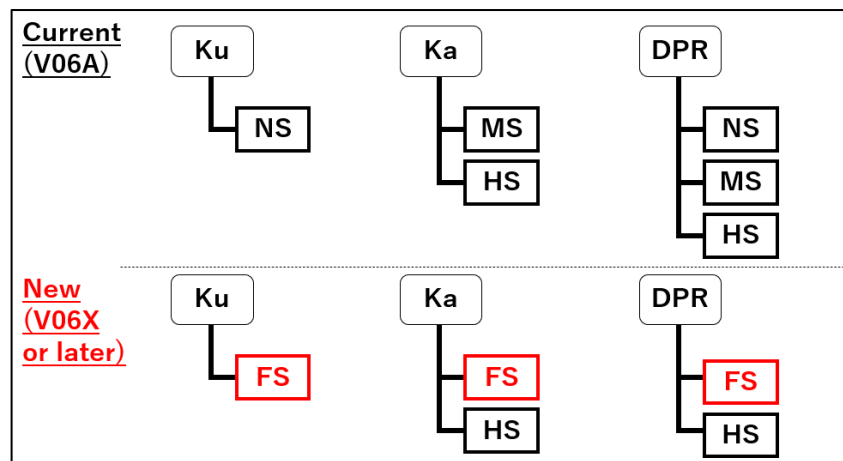
Figure 1-1 Schematic image of changes between current and new format.

1.1. Data Format Structure

The DPR and Level-2 algorithm provide four standard products which are 2AKu, 2AKa, 2ADPR. The 2AKu and 2AKa products are made by single-frequency algorithm and the 2ADPR product is made by dual-frequency algorithm. All products have following data format structure.
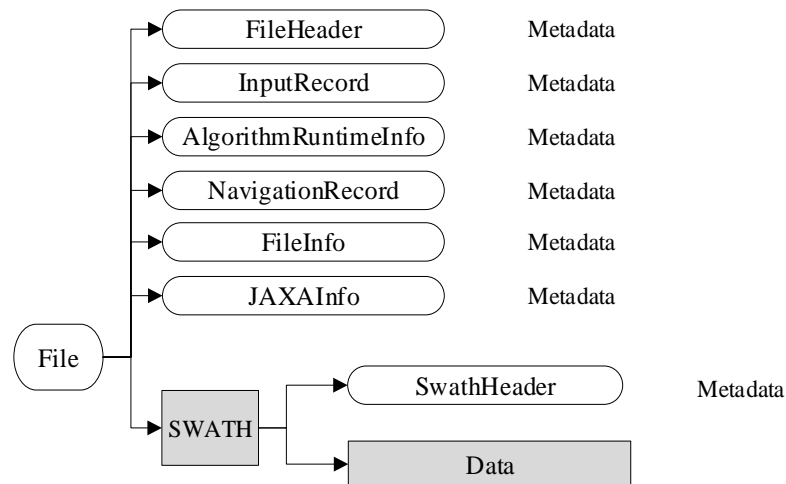
Figure 1.1-1 Data Format Structure

Swath definitions:

- 2AKu has FS swath.
- 2AKa and 2ADPR have FS and HS swath. HS swath is set to missing in V06X.

Dimension definitions:

All bin numbers are specified starting with 1 and ending with nray or nbin (FORTRAN convention), and not from 0 to (nray-1) or 0 to (nbin-1) (C convention).

- nscan

  Number of scans in the granule.

- nray

  Number of angle bins in each scan.

  49 angle bins in each scan in the FS swath (1-49 and not 0-48).

  24 angle bins in each scan in the HS swath (1-24 and not 0-23).

- nbin

  Number of range bins in each ray.

  176 range bins in each ray in the FS swath (1-176 and not 0-175).

  88 range bins in each ray in the HS swath (1-88 and not 0-87).

- Others are described in 1.3 Data Group section.

1.2. Metadata

Metadata has seven elements. Figure 1.2-1 shows metadata structure.
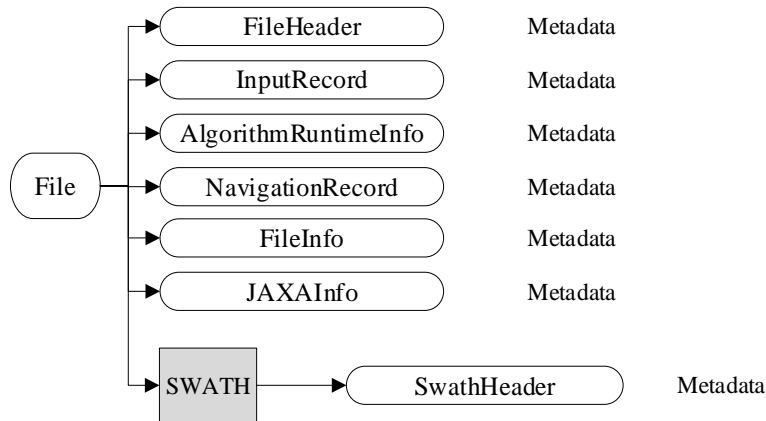
Figure 1.2-1 Metadata

1.2.1. FileHeader

FileHeader contains metadata of general interest. This group appears in all data products. Table 1.2-1 shows each metadata elements in FileHeader.

Table 1.2-1 FileHeader Elements

No	Element	Description	Data size (bytes)
1	DOI	Digital Object Identifier. *Value is blank currently.	256
2	DOIauthority	Digital Object Identifier Authority.	256
3	DOIshortName	Digital Object Identifier Short Name. *Value is blank currently.	256
4	AlgorithmID	The algorithm that generated this product, e.g., 2A12.	50
5	AlgorithmVersion	The version of the algorithm that generated this product.	50
6	FileName	The file name of this granule.	50
7	SatelliteName	Values are: TRMM GPM MULTI F10 ... F18 AQUA GCOMW1 CORIOLIS MT1 NOAA15 ... NOAA19 METOPA NPP. More values will be added as they are known.	10

1.2 Metadata

No	Element	Description	Data size (bytes)
8	InstrumentName	Values are: PR TMI VIRS PRTMI KU KA DPR GMI DPRGMI MERGED SSMI SSMIS AMSRE AMSR2 WINDSAT MADRAS AMSUA AMSUB SAPHIR MHS ATMS. More values will be added as they are known.	10
9	GenerationDateTime	The date and time this granule was generated. The format is YYYY-MM-DDTHH:MM:SS.sssZ, where YYYY is 4-digit year, MM is month number, DD is day of month, T is "T", HH is hour, MM is minute, SS is second, sss is millisecond, and Z is "Z". All fields are zero-filled. The missing value is constructed by replacing all digits with 9, i.e., 9999-99-99T99:99:99.999Z.	50
10	StartGranuleDateTime	The start time defining this granule. The format is the same as GenerationDateTime. DETAILS: An orbital granule starts when the satellite is at the position defined by GranuleStart. Thus the start time is not the first scan time. Some algorithms have overlap scans in the file before the start time as defined in SwathHeader. A monthly granule starts on the first ms of the month, for example March 1998 would be 1998-03-01T00:00:00.000Z.	50
11	StopGranuleDateTime	The stop time defining this granule. The format is the same as GenerationDateTime. DETAILS: An orbital granule stops when the satellite is at the position defined by GranuleStart. Thus the stop time is not the last scan time. Some algorithms have overlap scans in the file after the stop time as defined in SwathHeader. A monthly granule stops on the last ms of the month, for example March 1998 would be 1998-03-31T23:59:59.999Z.	50
12	GranuleNumber	The number of this granule, which starts as in GranuleStart. If the GranuleStart is identical to the orbit start, then the GranuleNumber will be the same as the orbit number. The GranuleNumber will have 6 digits, including leading zeroes, for example 001234.	50
13	NumberOfSwaths	The number of swaths in this granule.	50
14	NumberOfGrids	The number of grid structures in this granule.	50
15	GranuleStart	The starting place in the orbit of this granule. Currently defined values are "SOUTHERNMOST LATITUDE" and "NORTHBOUND EQUATOR CROSSING".	50
16	TimeInterval	The time interval covered by this granule. Values are "ORBIT", "HALF ORBIT", "HALF HOUR", "HOUR", "3 HOUR", "DAY", "DAY ASC", DAY DES", "MONTH", "CONTACT".	50
17	ProcessingSystem	The name of the processing system, e.g.,"PPS", "JAXA".	50
18	ProductVersion	The data version assigned by the processing system.	50
19	EmptyGranule	Whether a granule is empty. Values are "EMPTY" or "NOT EMPTY".	50
20	MissingData	The number of missing scans.	50

1.2.2. InputRecord

InputRecord contains a record of input files for this granule. This group appears in Level1, Level 2, and Level 3 orbital data products. Level 3 times averaged products have the same information separated into 3 groups since they have many inputs. Table 1.2-2 shows each metadata elements in InputRecord.

<u>**Table 1.2-2 InputRecord Elements**</u>

No	Element	Description	Data size (bytes)
1	InputFileNames	A list of input file names for this granule.	1000
2	InputAlgorithmVersions	A list of algorithm versions of the input files for this granule.	1000
3	InputGenerationDateTimes	A list of generation date times of the input files for this granule. The format is the same as GenerationDateTime.	1000

1.2.3. AlgorithmRuntimeInfo

AlgorithmRuntimeInfo contains text runtime information written by the algorithm. This group is a "Long Metadata Group", which has no elements. This group appears in products if the algorithm developer asks for it.

1.2.4. NavigationRecord

NavigationRecord contains navigation metadata for this granule. This group appears in Level 1, Level 2, and Level 3 orbital data products. Table 1.2-3 shows each metadata elements in NavigationRecord.

Table 1.2-3 NavigationRecord Elements

No	Element	Description	Data size (bytes)
1	LongitudeOnEquator	The longitude where the satellite crosses the equator going from south to north.	50
2	UTCDateTimeOnEquator	The UTC time when the satellite crosses the equator going from south to north. The format is the same as GenerationDate Time.	50
3	MeanSolarBetaAngle	The average solar beta angle in this granule.	50
4	EphemerisFileName	Name of the ephemeris file input for processing.	50
5	AttitudeFileName	Name of the attitude file input for processing.	50
6	GeoControlFileName	Name of the GeoTK Control Parameters File input for processing.	50
7	EphemerisSource	Values are "0 CONSTANT INPUT TEST VALUE", "1 GROUND ESTIMATED STATE (GES)", "2 GPS FILTERED SOLUTION (GEONS)", "3 GPS POINT SOLUTION (PVT)", "4 ON BOARD PROPAGATED (OBP)", "5 OEM GROUND EPHEMERIS FILE", "6 GEONS WITH FALLBACK AS FLAGGED", "7 PVT WITH FALLBACK AS FLAGGED", "8 OBP WITH FALLBACK AS FLAGGED", "9 GES WITH FALLBACK AS FLAGGED".	50
8	AttitudeSource	values are "0 CONSTANT INPUTS FOR TESTING", "1 ON BOARD CALCULATED PITCH ROLL YAW"	50
9	GeoToolkitVersion	Version of the GeoToolkit.	50
10	SensorAlignmentFirstRotationAngle	Alignment angle, first rotation, in degrees. Rotation adjustment from sensor coordinates to the Attitude Control System Flight Coordinates.	50
11	SensorAlignmentSecondRotationAngle	Alignment angle, second rotation, in degrees.	50
12	SensorAlignmentThirdRotationAngle	Alignment angle, third rotation, in degrees.	50
13	SensorAlignmentFirstRotationAxis	Euler rotation sequence, first rotation axis. Values are "1","2", "3" (representing X, Y, Z).	50
14	SensorAlignmentSecondRotationAxis	Euler rotation sequence, second rotation axis. Values are "1","2", "3" (representing X, Y, Z).	50
15	SensorAlignmentThirdRotationAxis	Euler rotation sequence, third rotation axis. Values are "1","2", "3" (representing X, Y, Z).	50

1.2.5. FileInfo

FileInfo contains metadata used by the PPS I/O Toolkit. This group appears in all data products. Table 1.2-4 shows each metadata elements in FileInfo.

Table 1.2-4 FileInfo Elements

No	Element	Description	Data size (bytes)
1	DataFormatVersion	The version of the data format used to write this file. This version is separate for each AlgorithmID. The order is: "a" "b" ... "z" "aa" "ab" ... "az" "ba" "bb".	50
2	TKCodeBuildVersion	Usually TK CodeBuildVersion is "1". If the I/O routines built by TKIO change even though the DataFormatVersion is unchanged, then TK CodeBuildVersion increments to "2", "3", ...If subsequently DataFormatVersion changes, TKCodeBuildVersion becomes "1" again.	50
3	MetadataVersion	The version of metadata used to write this file. This version is separate for each AlgorithmID. The order is: "a" "b" ... "z" "aa" "ab" ... "az" "ba" "bb" ...	50
4	FormatPackage	The underlying format of this granule. Values are "HDF4","HDF5", "NETCDF", "TKBINARY".	50
5	BlueprintFilename	The filename of the primary blueprint file that defined the format used to write this file.	50
6	BlueprintVersion	The BlueprintVersion of the format definition.	50
7	TKIOVersion	The version of TKIO used to create I/O routines to write this file. TKIOVersion does not define the format used to write this file.	50
8	MetadataStyle	The style in which the metadata was written, e.g., "PVL"."PVL" means < parameter >=< value >.	50
9	EndianType	The endian type of the system that wrote this file. Values are "BIG ENDIAN" and "LITTLE ENDIAN".	50

1.2.6. JAXAInfo

JAXAInfo contains metadata requested by JAXA. Used by DPR algorithms and GSMaP. Table 1.2-5 shows each metadata elements in JAXAInfo.

Table 1.2-5 JAXAInfo Elements

No	Element	Description	Data size (bytes)
1	GranuleFirstScanUTCDateTime	The date and time of first scan (incl. missing scan). The format is YYYY-MM-DDTHH:MM:SS.sssZ, where YYYY is 4-digit year, MM is month number, DD is day of month, T is "T", HH is hour, MM is minute, SS is second, sss is millisecond, and Z is "Z". All fields are zero-filled. The missing value is constructed by replacing all digits with 9, i.e., 9999-99-99T99:99:99.999Z.	50
2	GranuleLastScanUTCDateTime	Granule Last Scan UTC Date. Date is a 24 character string. The format is YYYY-MM-DDTHH:MM:SS.sssZ, where YYYY is 4-digit year, MM is month number, DD is day of month, T is "T", HH is hour, MM is minute, SS is second, sss is millisecond, and Z is "Z". All fields are zero-filled.	50

3	TotalQualityCode	The total quality of product is defined based on the quality of input data. Quality meaning are
		(a) GPM KuPR/KaPR TRMM PR L2 product
		    Good: The total quality of input data (Ku/Ka/PR L1B) is Good.
		    Fair: The GPM KuPR/KaPR L2 is not JMA's global weather forecast (FCST) or JMA's Global ANALsis model data (GANAL) but weather DB file.
		    EG (Empty Granule): The total quality of input data (Ku/Ka/PR L1B) is EG
		(b) GPM DPR L2 product
		    Good: The total quality of both Ku L2 and Ka L2 is Good.
		    Fair: (i)The total quality of either Ku L2 or Ka L2 is EG
		        (ii)The input data used in GPM DPR L2 is not JMA's global weather forecast (FCST) or JMA's Global ANALysis model data (GANAL) but weather DB file.
		    EG (Empty Granule): The total quality of both Ku L2 and Ka L2 is EG.
		(c) GPM DPR SLH L2 product
		    Good: The total quality of input data (DPR L2) is Good
		    Fair: The total quality of input data is Fair.
		    EG (Empty Granule): The total quality of input data (DPR L2) is EG.
			50

4	FirstScanLat	Latitude of orbit first scan.	50
5	FirstScanLon	Longitude of orbit first scan.	50
6	LastScanLat	Latitude of orbit last scan.	50
7	LastScanLon	Longitude of orbit last scan.	50
8	NumberOfRainPixelsFS	Number of rain pixels in the FS swath, judged at DPR L2 algorithm. At DPR L1, value is "-9999".	50

No	Element	Description	Data size (bytes)
9	NumberOfRainPixelsHS	Number of rain pixels in the HS swath, judged at DPR L2algorithm. At DPR L1, value is "-9999".	50
10	ProcessingSubSystem	The name of the processing sub-system, e.g., "ALGORITHM","PCS".	50
11	ProcessingMode	The name of the processing mode, e.g., "STD","NRT".	50
12	lightspeed	Constant value of light speed.	50
13	dielectricFactorKa	The dielectric factor $|K^2|$ at Ka.	50
14	dielectricFactorKu	The dielectric factor $|K^2|$ at Ku.	50

1.2.7. SwathHeader

SwathHeader contains metadata for swaths. This group appears in Level 1 and Level 2 data products. Table 1.2-6 shows each metadata elements in SwathHeader.

Table 1.2-6 SwathHeader Elements

No	Element	Description	Data size (bytes)
1	NumberScansInSet	The scans read by TKreadScan are a "set". For single swath data, one scan is read so NumberScansInSet=1. For multiple swath data, one TKreadScan may read more than one scan. For example, for SSM/I data one TKreadScan reads one low frequency scan and two high frequency scans. Therefore NumberScansInSet=1 for the low frequency swath and Number-ScansInSet=2 for the high frequency swath.	50
2	MaximumNumberScansTotal	The maximum allowed number of total scans in this swath. Total scans = overlap scans before granule + scans in granule + overlap scans after granule.	50
3	NumberScansBeforeGranule	The number of overlap scans before the first scan of the granule in this swath.	50
4	NumberScansGranule	The number of scans in the granule in this swath.	50
5	NumberScansAfterGranule	The number of overlap scans after the last scan of the granule in this swath.	50

1.2 Metadata

No	Element	Description	Data size (bytes)
6	NumberPixels	The number of IFOV in each scan in this swath.	50
7	ScanType	The type of scan in this swath. Values are: "CROSSTRACK" and "CONICAL".	50

1.3. Data Group

Elements of data group are explained in detail in this section. Each swath has 11 data group (12 data group for FS swath of 2ADPR) and 2 data (Latitude and Longitude) commonly. Figure 1.3-1 shows data group structure.
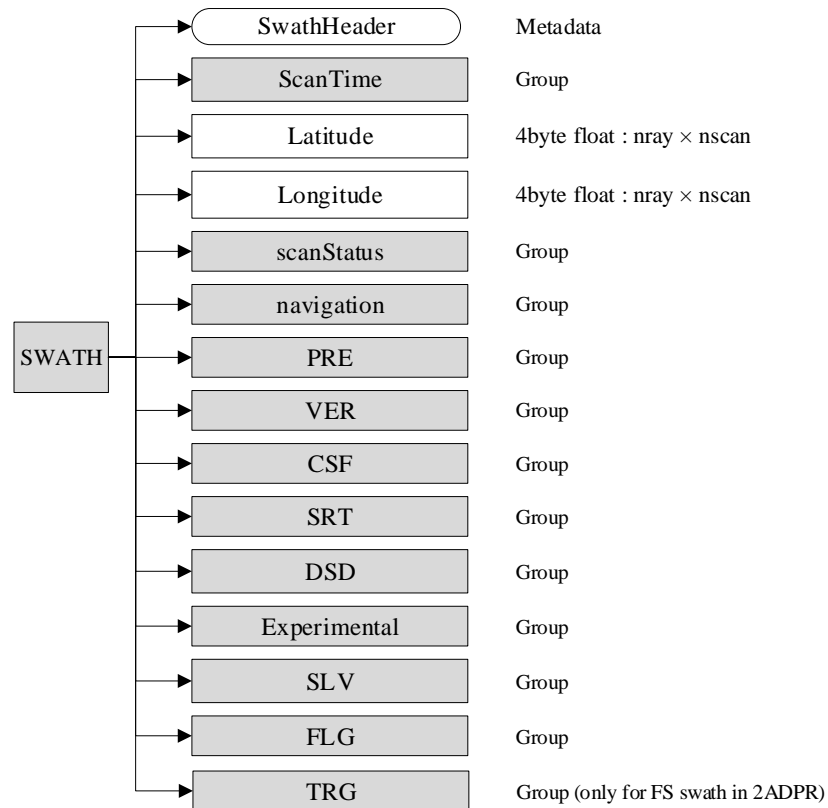
Figure 1.3-1 Data Format Structure for Data Group

1.3.1. ScanTime (Group)

(1) Year

Type	Array	Unit
2-byte integer	nscan	year

4-digit year, e.g., 1998. Values range from 1950 to 2100 years:

Missing Value :

  -9999

(2) Month

Type	Array	Unit
1-byte integer	nscan	month

Month of the year. Values range from 1 to 12 months.

Missing Value：

   -99

(3) DayOfMonth

Type	Array	Unit
1-byte integer	nscan	day

Day of the month. Values range from 1 to 31 days.

Missing Value：

   -99

(4) Hour

Type	Array	Unit
1-byte integer	nscan	hour

UTC hour of the day. Values range from 0 to 23 hours.

Missing Value：

   -99

(5) Minute

Type	Array	Unit
1-byte integer	nscan	minute

Minute of the hour. Values range from 0 to 59 minutes.

Missing Value：

   -99

(6) Second

Type	Array	Unit
1-byte integer	nscan	s

Second of the minute. Values range from 0 to 60 s.

Missing Value：

   -99

(7) MilliSecond

Type	Array	Unit
2-byte integer	nscan	ms

Thousandths of the second. Values range from 0 to 999 ms.

Missing Value：

-9999

(8) DayOfYear

Type	Array	Unit
2-byte integer	nscan	day

Day of the year. Values range from 1 to 366 days.

Missing Value：

-9999

(9) SecondOfDay

Type	Array	Unit
8-byte float	nscan	s

A time associated with the scan. It is expressed as the UTC seconds of the day.

Values range from 0 to 86400 s.

Missing Value：

-9999.9

(10) Latitude

Type	Array	Unit
4-byte float	nray * nscan	degrees

The earth latitude of the center of the IFOV at the altitude of the earth ellipsoid. Latitude is positive north, negative south.

Values range from -90 to 90 degrees.

Missing Value：

-9999.9

(11) Longitude

Type	Array	Unit
4-byte float	nray * nscan	degrees

The earth longitude of the center of the IFOV at the altitude of the earth ellipsoid. Longitude is positive east, negative west. A point on the 180th meridian has the value -180 degrees.

Values range from -180 to 180 degrees.

Missing Value：

-9999.9

1.3.2. scanStatus (Group)

(1) dataQuality

Type	Array	Array (2ADPR)	Unit
1-byte integer	nscan	nfreq * nscan	N/A

A summary of data quality in the scan. Unless this is 0 (normal), the scan data is meaningless to higher precipitation processing. Bit 0 is the least significant bit (i.e., if bit i = 1 and other bits = 0, the unsigned integer value is 2**i).

In the 2ADPR,

nfreq(1) : Estimated by KuPR single-frequency algorithm.

nfreq(2) : Estimated by KaPR single-frequency algorithm.

```
Bit Meaning

0 : missing

5 : geoError is not zero

6 : modeStatus is not zero
```

(2) dataWarning

Type	Array	Array (2ADPR)	Unit
1-byte integer	nscan	nfreq * nscan	N/A

Flag of data warning for each scan. Bit Meaning is below.

In the 2ADPR,

nfreq(1) : Estimated by KuPR single-frequency algorithm.

nfreq(2) : Estimated by KaPR single-frequency algorithm.

```
Bit Meaning

0 : beam Matching is abnormal

1 : VPRF table is abnormal

2 : surface Table is abnormal

3 : geoWarning is not Zero

4 : operational mode is not observation mode.

5 : GPS status is abnormal
```

(3) missing

Type	Array	Array (2ADPR)	Unit
1-byte integer	nscan	nfreq * nscan	N/A

Indicates whether information is contained in the scan data. Bit Meaning is below.

In the 2ADPR,

nfreq(1) : Estimated by KuPR single-frequency algorithm.

nfreq(2) : Estimated by KaPR single-frequency algorithm.

```
Bit Meaning

0 : Scan is missing

1 : Science telemetry packet missing

2 : Science telemetry segment withing packet missing

3 : Science telemetry other missing

4 : Housekeeping (HK) telemetry packet missing

5 : Spare (always 0)

6 : Spare (always 0)

7 : Spare (always 0)
```

(4) modeStatus

Type	Array	Array (2ADPR)	Unit
1-byte integer	nscan	nfreq * nscan	N/A

A summary of status modes. If all status modes are routine, all bits in modeStatus = 0. Routine means that scan data has been measured in the normal operational situation as far as the status modes are concerned. modeStatus does not assess geolocation quality. modeStatus is broken into 8 bit flags. Each bit = 0 if the status is routine but the bit = 1 if the status is not routine. Bit 0 is the least significant bit (i.e., if bit i = 1 and other bits = 0, the unsigned integer value is $2^{**}i$). The non-routine situations follow:

```
Bit Meaning

0 : Spare (always 0)

1 : SCorientation not 0 or 180

2: pointingStatus not 0

3 : Non-routine limitErrorFlag

4 : Non-routine operationalMode (not 1 or 11)

5 : Spare (always 0)

6 : Spare (always 0)

7 : Spare (always 0)
```

In the 2ADPR,

nfreq(1) : Estimated by KuPR single-frequency algorithm.

nfreq(2) : Estimated by KaPR single-frequency algorithm.

(5) geoError

Type	Array	Array (2ADPR)	Unit
2-byte integer	nscan	nfreq * nscan	N/A

A summary of geolocation errors in the scan. geoError is used to set a bit in dataQuality. A zero integer value of geoError indicates 'good' geolocation. A non-zero value broken down into the bit flags below indicates the specified reason, where bit 0 is the least significant bit (i.e., if bit i = 1 and other bits = 0 the unsigned integer value is 2**i). Bits 0, 4, 5, 8 and 9 are per pixel error flags. If the number of bad pixels (for any of the reasons specified by these flags) is greater than the threshold then bit 7 = 1 and each of these flags is set to 1 if any pixel is bad for that reason. At launch this threshold is zero, so data is flagged if any pixel is bad. If the number of bad pixels is less than or equal to the threshold then bit 7 = 0 and all of these flags are also 0. Bit Meaning is below.

In the 2ADPR,

nfreq(1) : Estimated by KuPR single-frequency algorithm.

nfreq(2) : Estimated by KaPR single-frequency algorithm.

```
Bit Meaning

 0 : Latitude limit exceeded for viewed pixel locations

 1 : Negative scan time, invalid input

 2 : Error getting spacecraft attitude at scan mid-time

 3 : Error getting spacecraft ephemeris at scan mid-time

 4 : Invalid input non-unit ray vector for any pixel

 5 : Ray misses Earth for any pixel with normal pointing
```

 6 : Nadir calculation error for subsatellite position

 7 : Pixel count with geolocation error over threshold

 8 : Error in getting spacecraft attitude for any pixel

 9 : Error in getting spacecraft ephemeris for any pixel

10 : Spare (always 0)

11 : Spare (always 0)

12 : Spare (always 0)

13 : Spare (always 0)

14 : Spare (always 0)

15 : Spare (always 0)

(6) geoWarning

Type	Array	Array (2ADPR)	Unit
2-byte integer	nscan	nfreq * nscan	N/A

A summary of geolocation warnings in the scan. geoWarning does not set a bit in dataQuality. Warnings indicate unusual conditions. These conditions do not indicate bad geolocation but are flagged as a warning that further review of the data may be useful. A zero integer value indicates usual geolocation. A non-zero value broken down into the following bit flags indicates the following, where bit 0 is the least significant bit (i.e., if bit i = 1 and other bits = 0 the unsigned integer value is 2**i). Bit Meaning is below.

In the 2ADPR,

nfreq(1) : Estimated by KuPR single-frequency algorithm.

nfreq(2) : Estimated by KaPR single-frequency algorithm.

```
Bit Meaning

  0 : Ephemeris Gap Interpolated

  1 : Attitude Gap Interpolated

  2 : Attitude jump/discontinuity

  3 : Attitude out of range

  4 : Anomalous Time Step

  5 : GHA not calculated due to error

  6 : SunData (Group) not calculated due to error

  7 : Failure to calculate Sun in inertial coordinates

  8 : Fallback to GES ephemeris

  9 : Fallback to GEONS ephemeris

 10 : Fallback to PVT ephemeris

 11 : Fallback to OBP ephemeris

 12 : Spare (always 0)

 13 : Spare (always 0)

 14 : Spare (always 0)

 15 : Spare (always 0)
```

(7) SCorientation

Type	Array	Unit
2-byte integer	nscan	degrees

The positive angle of the spacecraft vector (v) from the satellite forward direction of motion, measured clockwise facing down. We define v in the same direction as the spacecraft axis +X, which is also the center of the GMI scan. If SCorientation is not 0 or 180, a bit is set to 1 in modeStatus.

```
Value Meaning

     0 : +X forward (yaw 0)

   180 : -X forward (yaw 180)

 -8000 : Non-nominal pointing

 -9999 : Missing
```

(8) pointingStatus

Type	Array	Array (2ADPR)	Unit
2-byte integer	nscan	nfreq * nscan	N/A

It is provided by the GeoTK. A value of zero means the pointing is good. Non-zero values indicate non-nominal pointing. If pointingStatus is non-zero, a bit in modeStatus is set to 1. Value Meaning is below.

In the 2ADPR,

nfreq(1) : Estimated by KuPR single-frequency algorithm.

nfreq(2) : Estimated by KaPR single-frequency algorithm.

```
Value Meaning

     0 : Nominal pointing in Mission Science Mode

     1 : GPS point solution stale and PVT ephemeris used

     2 : GEONS solution stale and GEONS ephemeris used

 -8000 : Non-nominal mission science orientation

 -9999 : Missing
```

(9) acsModeMidScan

Type	Array	Unit
1-byte integer	nscan	N/A

It is provided by the GeoTK as taken from Attitude Control System telemetry and is provided in this format for information only.

```
Value Meaning

0 : LAUNCH

1 : RATENULL

2 : SUNPOINT

3 : GSPM (Gyro-less Sun Point)

4 : MSM (Mission Science Mode)

5 : SLEW

6 : DELTAH

7 : DELTAV
```

(10) targetSelectionMidScan

Type	Array	Unit
1-byte integer	nscan	N/A

It is provided by the GeoTK as taken from Attitude Control System telemetry and is provided in this format for information only.

```
Value Meaning

0 : S/C Z axis nadir, +X in flight direction

1 : Flight Z axis nadir, +X in flight direction

2 : S/C Z axis nadir, -X in flight direction

3 : Flight Z axis nadir, -X in flight direction

4 : +90 yaw for DPR antenna pattern calibration

5 : -90 yaw for DPR antenna pattern calibration

-99 : Missing

Other standard target orientations TBD
```

(11) operationalMode

Type	Array	Array (2ADPR)	Unit
1-byte integer	nscan	nfreq * nscan	N/A

The operational mode of KuPR/KaPR/PR stored in science telemetry basically. However, if science telemetry is not made like as stand-by mode, KuPR/KaPR L1B algorithm decides it using HK telemetry. PR L1B algorithm stored missing value. The values range is 1 to 20 for KuPR/KaPR. The values range is 1 to 3, 5, 6, 10, -99. The value meaning is shown below.

In the 2ADPR,

nfreq(1) : Estimated by KuPR single-frequency algorithm.

nfreq(2) : Estimated by KaPR single-frequency algorithm.

```
Value Meaning

1 : Ku/Ka/PR Observation

2 : Ku/Ka/PR External Calibration

3 : Ku/Ka/PR Internal Calibration

4 : Ku/Ka SSPA Analysis

5 : Ku/Ka/PR LNA Analysis

6 : Ku/Ka/PR Health-Check

7 : Ku/Ka Standby VPRF Table OUT

8 : Ku/Ka Standby Phase Out

9 : Ku/Ka Standby Dump Out

10 : Ku/Ka Standby (No Science Data)

11 : Ku/Ka/PR Independent Observation

12 : Ku/Ka Independent External Calibration

13 : Ku/Ka Independent Internal Calibration

14 : Ku/Ka Independent SSPA Analysis

15 : Ku/Ka Independent LNA Analysis

16 : Ku/Ka Independent Health-Check

17 : Ku/Ka Independent Standby VPRF Table OUT

18 : Ku/Ka Independent Standby Phase Out

19 : Ku/Ka Independent Standby Dump Out

20 : Ku/Ka Independent Standby (No Science Data)

-99 : PR missing value (No Science Data)
```

(12) limitErrorFlag

Type	Array	Array (2ADPR)	Unit
1-byte integer	nscan	nfreq * nscan	N/A

It has 2 error information. One is as for noise power limit, another one is as for binEllipsoid limit. The former is defined that if there are more than 2 overlimitted rays in a swath, limitErrorFlag(at 0bit) is adapted. On the other hand, the later is defined that if there is even an overlimitted ray, limitErrorFlag(at 1bit) is adapted. Then, LimitErrorFlag is used in modeStatus, dataQuality in scanStatus Group picks it up consequently. Bit Meaning is below.

In the 2ADPR,

nfreq(1) : Estimated by KuPR single-frequency algorithm.

nfreq(2) : Estimated by KaPR single-frequency algorithm.

Bit Meaning

0 : noise power limit error

1 : binEllipsoid is missing

2 : Spare (always 0)

3 : Spare (always 0)

4 : Spare (always 0)

5 : Spare (always 0)

6 : Spare (always 0)

7 : Spare (always 0)

(13) FractionalGranuleNumber

Type	Array	Unit
8-byte float	nscan	N/A

The floating point granule number. The granule begins at the Southern-most point of the spacecraft's trajectory. For example, FractionalGranuleNumber = 10.5 means the spacecraft is halfway through granule 10 and starting the descending half of the granule. Values range from 0 to 100000. In Near Real Time (NRT) process, granule number is stored only '0', so Fractional Granule Number less than 1.0.

Missing value:

N/A

1.3.3. navigation (Group)

(1) scPos

Type	Array	Unit
4-byte float	XYZ * nscan	m

The position vector(m) of the spacecraft in Earth-Centered Earth Fixed (ECEF) Coordinates at the Scan mid-Time (i.e., time at the middle pixel/IFOV of the active scan period). Values range from -10000000 to 10000000 m.

Missing value:

-9999.9

(2) scVel

Type	Array	Unit
4-byte float	XYZ * nscan	m/s

The velocity vector (m/s) of the spacecraft in ECEF Coordinates at the Scan mid-Time. Values range from -10000000 to 10000000 m/s.

Missing value:

-9999.9

(3) scLat

Type	Array	Unit
4-byte float	nscan	degrees

The geodesic latitude (decimal degrees) of the spacecraft at the Scan mid-Time. Values range from -70 to 70 degrees.

Missing value:

-9999.9

(4) scLon

Type	Array	Unit
4-byte float	nscan	degrees

The geodesic longitude (decimal degrees) of the spacecraft at the Scan mid-Time. Values range from -180 to 180 degrees.

Missing value:

-9999.9

(5) scAlt

Type	Array	Unit
4-byte float	scan	m

The altitude (m) of the spacecraft above the Earth Ellipsiod at the Scan mid-Time. It is computed by GeoTK. Values range from 350000 to 500000 m.

Missing value:

-9999.9

(6) dprAlt

Type	Array	Unit
4-byte float	nscan	m

The altitude (m) of the spacecraft above the Earth Ellipsiod at the Scan mid-Time from DPR science telemetry. This is empty in non-DPR products. It is stored 'GPS Altitude Data' with LSB equal to 10m in DPR science telemetry. Values range from 350000 to 500000 m.

Missing value:

-9999.9 : at missing scan and internal calibration mode.

(7) scAttRollGeoc

Type	Array	Unit
4-byte float	nscan	degrees

The geocentric satellite attitude Euler roll angle (degrees) at the Scan mid-Time. The order of the components in the file is roll, pitch, and yaw. However, the angles are computed using a 3-2-1 Euler rotation sequence representing the rotation order yaw, pitch, and roll for the rotation from Orbital Coordinates to the spacecraft body coordinates. Orbital Coordinates represent an orthogonal triad in Geocentric Inertial Coordinates where the Z-axis is toward the geocentric nadir, the Y-axis is perpendicular to the spacecraft velocity opposite the orbit normal direction, and the X-axis is approximately in the velocity direction for a near circular orbit. Note this is geocentric, not geodetic, referenced, so that pitch and roll will have twice orbital frequency components due to the onboard control system following the oblate geodetic Earth horizon. Note also that the yaw value will show an orbital frequency component relative to the Earth fixed ground track due to the Earth rotation relative to inertial coordinates. Values range from -180 to 180 degrees.

Missing value:

-9999.9

(8) scAttPitchGeoc

Type	Array	Unit
4-byte float	nscan	degrees

The geocentric satellite attitude Euler pitch angle (degrees) at the Scan mid-Time. Values range from -180 to 180 degrees.

Missing value:

-9999.9

(9) scAttYawGeoc

Type	Array	Unit
4-byte float	nscan	degrees

The geocentric satellite attitude Euler yaw angle (degrees) at the Scan mid-Time. Values range from -135 to 225 degrees.

Missing value:

-9999.9

(10) scAttRollGeod

Type	Array	Unit
4-byte float	nscan	degrees

The geodetic satellite attitude Euler roll angle (degrees) at the Scan mid-Time. The order of the components in the file is roll, pitch, and yaw. However, the angles are computed using a 3-2-1 Euler rotation sequence representing the rotation order yaw, pitch, and roll for the rotation from Geodetic Coordinates to the spacecraft body coordinates. Geodetic Coordinates represent an orthogonal triad in Geocentric Inertial Coordinates where the Z-axis is toward the geodetic nadir, the Y-axis is perpendicular to the spacecraft velocity opposite the orbit normal direction, and the X-axis is approximately in the velocity direction for a near circular orbit. Values range from -180 to 180 degrees.

Missing value:

-9999.9

(11) scAttPitchGeod

Type	Array	Unit
4-byte float	nscan	degrees

The geodedic satellite attitude Euler pitch angle (degrees) at the Scan mid-Time. Values range from -180 to 180 degrees.

Missing value:

-9999.9

(12) scAttYawGeod

Type	Array	Unit
4-byte float	nscan	degrees

The geodedic satellite attitude Euler yaw angle (degrees) at the Scan mid-Time. Values range from -135 to 225 degrees.

Missing value:

-9999.9

(13) greenHourAng

Type	Array	Unit
4-byte float	nscan	degrees

The rotation angle (degrees) from Geocentric Inertial Coordinates to Earth Fixed Coordinates. Values range from 0 to 390 degrees.

Missing value:

-9999.9

(14) timeMidScan

Type	Array	Unit
8-byte float	nscan	s

The Scan mid-Time in GPS Atomic time, namely the seconds since 0000 UTC, 6 Jan 1980. timeMidScan is used as the reference time for the scPos and scVel values. Values range from 0 to 10000000000 s.

Missing value:

-9999.9

(15) timeMidScanOffset

Type	Array	Unit
8-byte float	nscan	s

Offset from the secondary header packet time to the timeMidScan. Values range from 0 to 100 s.

Missing value:

-9999.9

1.3.4. PRE (Group)

(1) elevation

Type	Array	Unit
4-byte float	nray * nscan	m

Elevation of the measurement point. It is a copy of DEMHmean of level 1B product.

Missing Value:

-9999.9

In the 2ADPR, it is estimated by dual-frequency algorithm.

(2) landSurfaceType

Type	Array	Unit
4-byte integer	nray * nscan	N/A

Land surface type.

The values are

Value Meaning

0-99 : Ocean

100 - 199 : Land

200 - 299 : Coast

300 - 399 : Inland water

-9999 : Missing

In the 2ADPR, it is estimated by dual-frequency algorithm.

(3) localZenithAngle

Type	Array	Array (2ADPR)	Unit
4-byte float	nray * nscan	nfreq * nray * nscan	degrees

Local zenith angle of each ray. It is a copy of scLocalZenith of level 1B product.

Missing Value:

-9999.9

In the 2ADPR,

nfreq(1) : Estimated by KuPR single-frequency algorithm.

nfreq(2) : Estimated by KaPR single-frequency algorithm.

(4) flagPrecip

Type	Array	Unit
4-byte integer	nray * nscan	N/A

The values are

Value Meaning

0 : No precipitation

1 : Precipitation

-9999 : Missing

In the 2ADPR,

Value Meaning

00: No precipitation estimated by both KuPR and KaPR single-frequency algorithm.

01: Precipitation estimated by KaPR single-frequency algorithm only.

10: Precipitation estimated by KuPR single-frequency algorithm only.

11: Precipitation estimated by both KuPR and KaPR single-frequency algorithm.

(5) binRealSurface

Type	Array	Array (2ADPR)	Unit
2-byte integer	nray * nscan	nfreq * nray * nscan	range bin

Range bin number for real surface.

Missing Value：

-9999

In the 2ADPR,

nfreq(1) : Estimated by KuPR single-frequency algorithm.

nfreq(2) : Estimated by dual-frequency algorithm.

(6) binStormTop

Type	Array	Unit
2-byte integer	nray * nscan	range bin

Range bin number for the storm top.

Missing Value：

-9999

In the 2ADPR, it is estimated by dual-frequency algorithm.

(7) heightStormTop

Type	Array	Unit
4-byte float	nray * nscan	m

Height of storm top.

Missing Value：

-9999.9

In the 2ADPR, it is estimated by dual-frequency algorithm.

(8) height

Type	Array	Unit
4-byte float	nbin * nray * nscan	m

Height of precipitation.

Missing Value：

-9999.9

In the 2ADPR,

Estimated by KuPR single-frequency algorithm

(9) binClutterFreeBottom

Type	Array	Unit
2-byte integer	nray * nscan	range bin

Range bin number for clutter free bottom.

Missing Value：

-9999

In the 2ADPR, it is estimated by KuPR single-frequency algorithm

(10) sigmaZeroMeasured

Type	Array	Array (2ADPR)	Unit
4-byte float	nray * nscan	nfreq * nray * nscan	dB

Surface backscattering cross section without attenuation correction (as measured).

Missing Value：

-9999.9

In the 2ADPR,

nfreq(1) : Estimated by KuPR single-frequency algorithm.

nfreq(2) : Ka-band sigmaZeroMeasured estimated by dual-frequency algorithm.

(11) zFactorMeasured

Type	Array	Array (2ADPR)	Unit
4-byte float	nbin *nray * nscan	nfreq * nbin * nray * nscan	dBZ

Vertical profile of reflectivity factor (Z) without attenuation correction (as measured).

$10\log10(Z)$ where Z is in mm^6/m^3.

Missing Value :

   -9999.9

In the 2ADPR,

nfreq(1) : Estimated by KuPR single-frequency algorithm.

nfreq(2) : Estimated by KaPR single-frequency algorithm.

(12) ellipsoidBinOffset

Type	Array	Array (2ADPR)	Unit
4-byte float	nray * nscan	nfreq * nray * nscan	m

Distance between the ellipsoid and a center range bin of binEllipsoid defined by level 1B algorithm.

ellipsoidBinOffset =scRangeEllipsoid – (startBinRange + (binEllipsoid-1) * rangeBinSize)

scRangeEllipsoid : Distance between a sensor and the ellipsoid [m]

startBinRange : Distance between a sensor and a center of the highest observed range bin [m]

binEllipsoid : Range bin number of the Ellipsoid (1 - 260)

rangeBinSize : Range bin size [m]

Missing Value :

   -9999

In the 2ADPR,

nfreq(1) : Estimated by KuPR single-frequency algorithm.

nfreq(2) : Estimated by KaPR single-frequency algorithm.

(13) snRatioAtRealSurface

Type	Array	Array (2ADPR)	Unit
4-byte float	nray * nscan	nfreq * nray * nscan	N/A

Signal/Noise ratio at real surface range bin.

snRatioAtRealSurface= 10*log10(echoPowertrueV[mW]/noisePowertrueV[mW])

Missing Value :

-9999

In the 2ADPR,

nfreq(1) : Estimated by KuPR single-frequency algorithm.

nfreq(2) : Estimated by KaPR single-frequency algorithm.

(14) adjustFactor

Type	Array	Array (2ADPR)	Unit
4-byte float	nray * nscan	nfreq * nray * nscan	dB

Adjustment factor (dB) for zFactorMeasured (dBZm') and sigmaZeroMeasured (dBs0m'). dBZm' and dBs0m' are used and stored as follows:

dBZm' = dBZm – adjustFactor

dBs0m' = dBs0m – adjustFactor

The adjustment factor is the sum of 3 components:

base adjustment for instrument dependency,

angle-bin adjustment for angle-bin dependency, and

temporal adjustment for orbit number dependency.

Missing Value :

-9999.9

In the 2ADPR,

nfreq(1) : Estimated by KuPR single-frequency algorithm.

nfreq(2) : Estimated by KaPR single-frequency algorithm.

(15) snowIceCover

Type	Array	Unit
1-byte integer	nray * nscan	N/A

Snow and ice cover information. It refers to the multisensor snow/ice cover maps provided by NOAA.

The values are

```
Value Meaning

0 : Open water

1 : Land, no snow

2 : Snow cover on land

3 : Ice on water

-99 : Missing
```

In the 2ADPR, it is estimated by KuPR single-frequency algorithm

(16) flagSigmaZeroSaturation

Type	Array	Array (2ADPR)	Unit
1-byte unsigned integer	nray * nscan	nfreq * nray * nscan	N/A

A flag to show whether echoPower is under a saturated level or not at a range bin with a calculation of sigmaZeroMeasured. The values are below.

Value Meaning

0 : Normal (under saturated level)

1 : Possible saturated level at real surface

2 : Saturated level at real surface

99 : Missing

In the 2ADPR,

nfreq(1) : Estimated by KuPR single-frequency algorithm.

nfreq(2) : Estimated by KaPR single-frequency algorithm.

1.3.5. VER (Group)

(1) binZeroDeg

Type	Array	Unit
2-byte integer	nray * nscan	range bin

Range bin number with 0 degrees C level.

Missing Value :

-9999

(2) attenuationNP

Type	Array	Array (2ADPR)	Unit
4-byte float	nNP *nray * nscan	nfreq * nNP *nray * nscan	dB/km

Vertical profile of attenuation by non-precipitation particles (cloud liquid water, cloud ice water, water vapor, and oxygen molecules).

Missing Value :

-9999.9

nNP (1) : Total (sum of 2, 3, and 4)

nNP (2) : Water Vapor

nNP (3) : Oxygen molecules

nNP (4) : Cloud liquid water

In the 2ADPR,

nfreq(1) : Ku

nfreq(2) : Ka

(3) piaNP

Type	Array	Array (2ADPR)	Unit
4-byte float	nNP * nray * nscan	nfreq * nNP * nray * nscan	dB

Path integrated attenuation caused by non-precipitation particles (cloud liquid water, water vapor, and oxygen molecules).

Missing Value：

　-9999.9

nNP (1) : Total (sum of 2, 3, and 4)

nNP (2) : Water vapor

nNP (3) : Oxygen molecules

nNP (4) : Cloud liquid water

In the 2ADPR,

nfreq(1) : Ku

nfreq(2) : Ka

(4) sigmaZeroNPCorrected

Type	Array	Array (2ADPR)	Unit
4-byte float	nray * nscan	nfreq * nray * nscan	dB

Surface backscattering cross section with attenuation correction only for non-precipitation particles.

Missing Value：

　-9999.9

In the 2ADPR,

nfreq(1) : Ku

nfreq(2) : Ka

(5) heightZeroDeg

Type	Array	Unit
4-byte float	nray * nscan	m

Height of freezing level (0 degrees C level) Values are in m.

Missing Value：

-9999.9

(6) airTemperature

Type	Array	Unit
4-byte float	nbin *nray * nscan	K

Air temperature. Values are in K.

Missing Value:

-9999.9

1.3.6. CSF (Group)

(1) flagBB

Type	Array	Unit
4-byte integer	nray * nscan	N/A

Bright band (BB) exists or not.

In case of 2AKu and 2AKa,

The values are

Value Meaning

0 : BB not detected

1 : BB detected

-1111 : No rain value

-9999 : Missing

In case of 2ADPR,

The values are

Value Meaning

0 : BB not detected

≥ 1: BB detected

 1: BB detected by both single-frequency (Ku-band) and dual-frequency algorithm.

 2: BB detected by single-frequency (Ku-band) algorithm only.

 3: BB detected by dual-frequency algorithm only.

-1111 : No rain value

-9999 : Missing

(2) binBBPeak

Type	Array	Unit
2-byte integer	nray * nscan	range bin

Range bin number for the peak of bright band.

Missing Value：

-9999

(3) binBBTop

Type	Array	Unit
2-byte integer	nray * nscan	range bin

Range bin number for the top of bright band.

Missing Value：

-9999

(4) binBBBottom

Type	Array	Unit
2-byte integer	nray * nscan	range bin

Range bin number for the bottom of bright band.

The values are

Value Meaning

0 : BB not detected

-1111 : No rain value

-9999 : Missing

(5) heightBB

Type	Array	Unit
4-byte float	nray * nscan	m

Height of bright band.

The values are

Value Meaning

0.0 : BB not detected

-1111.1 : No rain value

-9999.9 : Missing

(6) widthBB

Type	Array	Unit
4-byte float	nray * nscan	m

The width of bright band.

The values are

```
Value Meaning

0.0 : BB not detected

-1111.1 : No rain value

-9999.9 : Missing
```

(7) qualityBB

Type	Array	Unit
4-byte integer	nray * nscan	N/A

Quality of the bright band.

The values are

```
Value Meaning

1 : Good

0 : BB not detected in the case of rain

-1111 : No rain value

-9999 : Missing
```

(8) typePrecip

Type	Array	Unit
4-byte integer	nray * nscan	N/A

When positive, typePrecip shows precipitation type by an 8-digit number as shown in the next box. The negative typePrecip means as follows:

-1111: No rain,

-9999: Missing.

Details of 8-digit typePrecip:

$$10^7 \ 10^6 \ 10^5 \ 10^4 \ 10^3 \ 10^2 \ 10^1 \ 10^0$$

```
┌──┬──┬──┬──┬──┬──┬──┬──┐
│  │  │  │  │  │  │  │  │
└──┴──┴──┴──┴──┴──┴──┴──┘
```

Small cell-size rain, +4 when flagHeavyIcePrecip>0.

Shallow rain.

BB (for Ku-only, Ka-only, and outer-swath of dpr).

H rain type (1: stra., 2: conv., 3: other).

V rain type (1: stra., 2: conv., 3: other,
4: stra. reclassified by Slope method).

DFRm BB (=0 for Ku-only and Ka-only).

DFRm rain type (=0 for Ku-only and Ka-only).
Value = 1: stra., 2: conv, 4: transition,
5: convective winter precipitation by extended DFRm method,
8: DFRm skipped by part B$^{(*)}$, 9: DFRm skipped part A$^{(*)}$.
($^{(*)}$ See ATBD for Part A and B.)

Main rain type.
Value = 1: stra., 2: conv., 3: other.

The three major rain categories, stratiform, convective, and other, can be obtained from typePrecip as follows:

When typePrecip is greater than zero,

Major rain type = typePrecip/10000000

1 : stratiform

2 : convective

3 : other

In the DPR product, rain type by the CSU's DFRm (measured dual frequency ratio) method is also included in typePrecip and can be obtained as follows:

DFRm rain type = (typePrecip%10000000)/1000000 in C

DFRm rain type = (MOD(typePrecip,10000000)/1000000 in FORTRAN

DFRm rain type

1 : stratiform

2 : convective

4 : transition

5 : Decided winter precipitation as convective by extended DFRm method.

8 : DFRm method cannot be applicable at Part B (in this case

the conventional method determines the major rain type)

9 : DFRm method cannot be applicable at Part A (in this case

the conventional method determines the major rain type)

-1111 : No rain value

-9999 : Missing value

(9) qualityTypePrecip

Type	Array	Unit
4-byte integer	nray * nscan	N/A

Quality of the precipitation type.

The values are

```
Value Meaning

1 : Good

-1111 : No rain value

-9999 : Missing
```

(10) flagShallowRain

Type	Array	Unit
4-byte integer	nray * nscan	N/A

Type of shallow rain.

The values are

```
Value Meaning

0 : No shallow rain

10 : Shallow isolated (maybe)

11 : Shallow isolated (certain)

20 : Shallow non-isolated (maybe)

21 : Shallow non-isolated (certain)

-1111 : No rain value

-9999 : Missing
```

(11) binDFRmMLBottom (Only for 2ADPR)

Type	Array	Unit
2-byte integer	nray * nscan	range bin

The DFRm method detects melting layer (ML) the meaning of which is wider than that of BB. Since ML and BB are different, new output item binDFRmMLBottom and binDFRmMLTop are added to MS and HS data.

Range bin number for ML bottom detected by the DFRm method.

The values are

```
Value: Meaning

> 0 : Range bin number when ML bottom is detected

  0 : ML bottom is not detected

-1111 : Value for no rain in MS (HS) mode at Ka band

-9999 : Missing value
```

(12) binDFRmMLTop (Only for 2ADPR)

Type	Array	Unit
2-byte integer	nray * nscan	N/A

The DFRm method detects melting layer (ML) the meaning of which is wider than that of BB. Since ML and BB are different, new output item binDFRmMLBottom and binDFRmMLTop are added to MS and HS data.

Range bin number for ML top detected by the DFRm method.

The values are

```
Value: Meaning

> 0 : Range bin number when ML top is detected

  0 : ML top is not detected

-1111 : Value for no rain in MS (HS) mode at Ka band

-9999 : Missing value
```

(13) binHeavyIcePrecipTop (Other than HS in 2ADPR)

Type	Array	Array(2ADPR)	Unit
2-byte integer	nray * nscan	nfreq * nray * nscan	range bin

Range bin corresponding to the top height wher Heavy Ice Precipitation (HIP) is detected.

The values are:

(A) In the single frequency 2AKu,

>0: Range bin corresponding to the Ku-band top height for HIP when it is detected

0: When HIP is not detected

-1111: No rain value

-9999: Missing value

(B) In the single frequency 2AKa,

>0: Range bin corresponding to the Ka-band top height for HIP when it is detected

0: When HIP is not detected

-1111: No rain value

-9999: Missing value

(C) In the 2ADPR,

nfreq(1) : Same to the above (A)

nfreq(2) : Same to the above (B)

nfreq(3) :

>0: Range bin corresponding to the top height for HIP detected by the dual frequency method

0: When HIP is not detected by the dual frequency method

-1111: No rain value

-9999: Missing value

(14) binHeavyIcePrecipBottom (Other than HS in 2ADPR)

Type	Array	Array(2ADPR)	Unit
2-byte integer	nray * nscan	nfreq * nray * nscan	range bin

Range bin corresponding to the bottom height wher Heavy Ice Precipitation (HIP) is detected.

The values are:

(A) In the single frequency 2AKu,

>0: Range bin corresponding to the Ku-band bottom height for HIP when it is detected

0: When HIP is not detected

-1111: No rain value

-9999: Missing value

(B) In the single frequency 2AKa,

>0: Range bin corresponding to the Ka-band bottom height for HIP when it is detected

0: When HIP is not detected

-1111: No rain value

-9999: Missing value

(C) In the 2ADPR,

nfreq(1) : Same to the above (A)

nfreq(2) : Same to the above (B)

nfreq(3) :

>0: Range bin corresponding to the bottom height for HIP detected by the dual frequency method

0: When HIP is not detected by the dual frequency method

-1111: No rain value

-9999: Missing value

(15) nHeavyIcePrecip (Other than HS in 2ADPR)

Type	Array	Array(2ADPR)	Unit
1-byte unsigned integer	nray * nscan	nfreq * nray * nscan	range bin

Number of range bins where HIP is detected.

The values are:

(A) In the single frequency 2AKu,

>0: The total number of bins where Ku-band HIP is detected

0: When Ku-band HIP is not detected or No rain or Missing

(B) In the single frequency 2AKa,

>0: The total number of bins where Ka-band HIP is detected

0: When Ka-band HIP is not detected or No rain or Missing

(C) In the 2ADPR,

nfreq(1) : Same to the above (A)

nfreq(2) : Same to the above (B)

nfreq(3) :

>0: The total number of bins where HIP is detected by the dual frequency method

0: When HIP is not detected by the dual frequency method or No rain or Missing

(16) flagMLquality (Only for 2ADPR)

Type	Array	Unit
1-byte unsigned integer	nray * nscan	None

This flag will indicate the quality of detected ML related quantities.

In V6X, the following tentative values are assigned to the flag.

Value meaning

1: ML is detected.

1: ML top and/or bottomis detected by the standard DFRm method.

2: ML top and/or bottomis detected by an extension, but the result is not used in the V6X rain type decision.

(Missing value is not assigned in V6X)

---

(17) flagHeavyIcePrecip

Type	Array	Unit
1-byte integer	nray * nscan	N/A

This flag denotes detection of solid ice hydrometeors which cause severely strong Z factor or huge DFRm in the sky less than -10 degree C temperature.

Value Meaning

(A) The case of Ka band MS:

  1 (=0x01): 35dBZ >= Zm(Ka) > 30dBZ

  2 (=0x02): 40dBZ >= Zm(Ka) > 35dBZ

  3 (=0x03): Zm(Ka) > 40dBZ

(B) The case of Ku band NS:

  4 (=0x04): 35dBZ >= Zm(Ku) > 30dBZ

  8 (=0x08): 40dBZ >= Zm(Ku) > 35dBZ

  12 (=0x0c): Zm(Ku) > 40dBZ

(C) The case of DPR NS:

  Outer swaths are same as (B).

  Inner swaths are addition of (A) and (B). If Zm(Ku) > 27dBZ and DFRm > 7dB in inner swaths, the following value is added in addition to (A) and (B).

  16(=0x10)

  0 : Missing value

(18) flagAnvil (Other than 2AKa)

Type	Array	Unit
1-byte integer	nray * nscan	N/A

flagAnvil is positive values when anvil precipitation is detected by the Ku-band radar. 0 when anvil precipitation is not detected.

The values are

Value Meaning

1 : Type 1 (without rain downward)

2 : Type 2 (with rain downward)

0 : Missing

1.3.7. SRT (Group)

(1) PIAalt

Type	Array	Array (2ADPR)	Unit
4-byte float	method * nray * nscan	nfreq * method * nray * nscan	dB

The path-integrated attenuation (dB) from the jth estimate, (PIAj in the notation above), where

PIAalt (j=1) = PIA derived from the forward along-track spatial reference data

PIAalt (j=2) = PIA derived from the backward along-track spatial reference data

PIAalt (j=3) = PIA derived from the forward hybrid/cross-track reference data

PIAalt (j=4) = PIA derived from the backward hybrid/cross-track reference data

PIAalt (j=5) = PIA derived from standard temporal reference data

PIAalt (j=6) = PIA derived from the light-rain temporal reference data

Note that for product versions 1 through 3, the standard temporal path-attenuation estimate, PIAalt(5), is set to missing but is defined for versions 4 and higher. For product versions 1 through 6, the light-rain temporal estimate, PIAalt(6), is set to missing. Note also that the forward/backward hybrid/cross-track path attenuations are defined only over ocean and are set to missing over land.

Missing Value：

-9999.9

In the 2ADPR,

nfreq(1) : TBD

nfreq(2) : TBD

(2) PIAdw (Only for 2ADPR)

Type	Array	Unit
4-byte float	nfreq * nray * nscan	dB

PIAdw (dB) is the path attenuation estimate derived from the standard dual-wavelength method.

Missing Value：

TBD

In the 2ADPR,

nfreq(1) : TBD

nfreq(2) : TBD

(3) PIAhb

Type	Array	Array (2ADPR)	Unit
4-byte float	nray * nscan	nfreq * nray * nscan	dB

PIAhb (dB) is the path attenuation estimate derived from the Hitschfeld-Bordan equation.

Missing Value：

-9999.9

In the 2ADPR,

nfreq(1) : TBD

nfreq(2) : TBD

(4) PIAhybrid

Type	Array	Array (2ADPR)	Unit
4-byte float	nray * nscan	nfreq * nray * nscan	dB

For the dual-frequency output, PIAhybrid (dB) is a weighted sum of the path attenuations from the SRT, HB, and DW methods.　For the single-frequency outputs, PIAhybrid is a weighted sum of the SRT and HB methods.

Missing Value：

-9999.9

In the 2ADPR,

nfreq(1) : TBD

nfreq(2) : TBD

(5) PIAweight

Type	Array	Unit
4-byte float	method * nray * nscan	N/A

The weights, w, of the individual PIA estimates used in deriving the effective PIA. The weight for a particular PIA estimate is proportional to the inverse of the error variance associated with the method. The sum of the weights should equal one. As with PIAalt(6), PIAweight(6) is set to missing.

$$w_j = \frac{1}{\sigma_j^2} \frac{1}{\sum \frac{1}{\sigma_j^2}} \equiv u_j / \Sigma u_j$$

where

$$u_j = 1/\sigma_j^2$$

$$\sum w_j = 1$$

Missing Value :

-9999.9

method(1): TBD

method(2): TBD

method(3): TBD

method(4): TBD

method(5): TBD

method(6): TBD

(6) PIAweightHY

Type	Array	Unit
4-byte float	method * nray * nscan	N/A

TBD

Missing Value :

method(1): TBD

method(2): TBD

method(3): TBD (Only for 2ADPR)

(7) pathAtten

Type	Array	Array (2ADPR)	Unit
4-byte float	nray * nscan	nfreq * nray * nscan	dB

The estimated effective 2-way path-attenuation in (dB) where

$$pathAtten = 2 \int_0^r k(s)ds$$

where k(s) is the attenuation coefficient in dB/km where the integral is taken from the storm top to the surface. The path attenuation is often designated as the PIA, the path-integrated attenuation. In the notation used above and in ATBD:

$$pathAtten = PIA_{eff} = (\Sigma u_j)^{-1} \Sigma u_j PIA_j$$

Where u_j is equal to the inverse of the variance associated with the jth reference data point:

$$u_j = 1/\sigma_j^2$$

Missing Value :

-9999.9

In the 2ADPR,

nfreq(1) : TBD

nfreq(2) : TBD

(8) reliabFactor

Type	Array	Unit
4-byte float	nray * nscan	N/A

Reliability Factor for the effective PIA estimate, pathAtten. This is defined as:

$$reliabFactor = \text{Rel}_{eff} = (\Sigma u_j)^{-1/2} \Sigma u_j PIA_j$$

Missing Value :

-9999.9

(9) reliabFactorHY

Type	Array	Unit
4-byte float	nray * nscan	N/A

reliabFactorHY is the reliability factor associated with the PIAhybrid estimate and is defined as the mean over the standard deviation of the estimate.

Missing Value :

-9999.9

(10) reliabFactorAlt

Type	Array	Unit
4-byte float	method * nray * nscan	N/A

The reliability factors associated with the individual PIA estimates in PIAalt. As with PIAalt(6), (10) reliabFactorAlt(6) is set to missing.

$$reliabFactorAlt_j = \text{Rel}_j = PIA_j/\sigma_j; j = 1,\ldots,6$$

Missing Value :

-9999.9

method(1): TBD

method(2): TBD

method(3): TBD

method(4): TBD

method(5): TBD

method(6): TBD

(11) reliabFlag

Type	Array	Unit
2-byte integer	nray * nscan	N/A

The reliability flag for the effective PIA estimate (pathAtten) based on the reliability factor (Rel_eff) in reliabFactor. Reliability Flag is:

= 1 if Rel_eff > 3   ; PIAeff estimate is considered reliable

= 2 if 3 >= Rel eff > 1   ; PIAeff estimate is considered marginally reliable

= 3 if Rel_eff $\leqq$ 1   ; PIAeff is unreliable

= 4 if SNR at surface < 2dB   ; provides a lower bound to the path-attenuation

= 9 (no-rain case)

Missing Value :

-9999.9

(12) reliabFlagHY

Type	Array	Unit
2-byte integer	nray * nscan	N/A

reliabFlagHY is the reliability flag for the PIAhybrid and is defined in the same way as reliabFlag where PIAeff is replaced by PIAhybrid.

Missing Value :

-9999.9

(13) refScanID

Type	Array	Unit
2-byte integer	nearFar * foreBack * nray * nscan	Number

refScanID gives the number of scan lines between the current scan and the beginning   (or end) of the along-track reference data at each angle bin. The values are computed by the equation: Current Scan Number - Reference Scan Number. The values are positive for the Forward estimates and negative for the Backward estimates. The Fortran indices are:

> Bit Meaning
>
> 1,1 : Forward - Near reference
>
> 2,1 : Forward - Far reference
>
> 1,2 : Backward - Near reference
>
> 2,2 : Backward - Far reference
>
> 9999 : Missing

To illustrate, consider the following example. At a certain incidence angle assume that rain is present at scan numbers from 100 to 105 and from 110 to 120. At scan number 112, refScanID(1,1)=3, refScanID(2,1)=16; i.e., the eight rain-free NRCS data points, used to estimate the mean and standard deviation of the rain-free NRCS, begin at scan 112-16 = 96 and end at scan 112-3=109. These numbers provide information on the distance (in terms of the numbers of scans where 1 scan ~5 km) of the rain-free reference data from the rain pixel of interest. See section 6 for further details.

(14) stddevEff

Type	Array	Array (2ADPR)	Unit
4-byte float	nsdew * nray * nscan	nfreq * nsdew * nray * nscan	N/A

stddevEff(1) contains the standard deviation of the PIAeff (i.e., the composite or effective SRT or hybrid path attenuation estimate).   It is given by

$$\sigma_1 = (\sum 1 / \sigma_{e,j}^2)^{-1/2} = (\sum u_j)^{-1/2}$$

It is important to note that in the definition of the reliability factor, it is this standard deviation that is used. In other words, with the notation in ATBD, we have $\sigma 1 = \sigma$ eff .

stddevEff(2) is a weighted root mean square error and provides a measured of the error of the individual PIA estimates from the effective PIA estimate. It is given by

$$\sigma_2 = [\sum w_j (A_{eff} - A_j)^2]^{1/2}$$

stddevEff(3) is given by

$$\sigma_3 = \left[\sigma_1^2 + \sigma_2^2 \right]^{1/2}$$

Missing Value :

  -9999.9

In the 2ADPR,

nfreq(1) : TBD

nfreq(2) : TBD

(15) stddevHY

Type	Array	Array (2ADPR)	Unit
4-byte float	nray * nscan	nfreq * nray * nscan	N/A

stddevHy is the standard deviation (dB) of the hybrid estimate of path attenuation.

Missing Value：

   -9999.9

In the 2ADPR,

nfreq(1) : TBD

nfreq(2) : TBD

(16) zeta

Type	Array	Array (2ADPR)	Unit
4-byte float	nray * nscan	nfreq * nray * nscan	N/A

zeta (unitless) is a parameter in the Hitschfeld-Bordan equation.

Missing Value：

   -9999.9

In the 2ADPR,

nfreq(1) : TBD

nfreq(2) : TBD

1.3.8. DSD (Group)

(1) phase

Type	Array	Unit
1-byte unsigned integer	nbin * nray * nscan	N/A

Phase state of the precipitation. As an unsigned byte value this represents:

phase < 100 Temperature(C)=phase-100

phase > 200 Temperature(C)=phase-200

phase = 100 Top of the bright band

phase = 200 Bottom of the bright band

phase = 125 is used for the range bins between

the top and peak of bright band

phase = 175 is used for the range bins between

the peak and bottom of bright band

Integer values of phase/100 =

0 - solid

1 - mixed phase

2 - liquid

Missing Value：

   225

(2) binNode

Type	Array	Unit
2-byte integer	nNode * nray * nscan	N/A

The bin number of the 5 nodes defined as:

1 - Bin number of storm top.

2 - Stratiform: 500m above center of bright band.

   Convective: 750m above 0deg C level.

3 - Stratiform: center of bright band.

   Convective: 0deg C level.

4 - Stratiform: 500m below center of bright band.

   Convective: 750m below 0deg C level.

5 - Bin number of real surface equal to binRealSurface in PRE group.

   For NS and MS swaths, bin numbers are 1-based ranging from 1 at the top of the data window with 176 at the Ellipsoid. For HS swaths, bin numbers are 1-based ranging from 1 at the top of the data window with 88 at the Ellipsoid.

Missing Value：

   -9999

1.3.9. Experimental (Group)

(1) precipRateESurface2

Type	Array	Unit
4-byte float	nray * nscan	mm/hr

Estimates Surface Precipitation using alternate method.

Missing Value：

-9999.9

(2) precipRateESurface2Status

Type	Array	Unit
1-byte unsigned integer	nray * nscan	N/A

Status of the estimated surface precipitation using alternate method.

Missing Value:

225

(3) sigmaZeroProfile

Type	Array	Array (2ADPR)	Unit
4-byte float	nbinSZP * nray * nscan	nfreq * nbinSZP * nray * nscan	dB

Surface backscattering cross section profile around the current IFOV.

Missing Value:

-9999.9

nbinSZP(1): TBD

nbinSZP(2): TBD

nbinSZP(3): TBD

nbinSZP(4): TBD

nbinSZP(5): TBD

nbinSZP(6): TBD

nbinSZP(7): TBD

In the 2ADPR,

nfreq(1) : TBD

nfreq(2) : TBD

(4) seaIceConcentration

Type	Array	Unit
4-byte float	nray * nscan	%

Sea ice concentration (30.0 – 100.0%) estimated by Ku.

Missing Value:

-9999.9

(5) flagSurfaceSnowfall (Only for 2ADPR)

Type	Array	Unit
1-byte unsigned integer	nray * nscan	N/A

This flag takes the following value:

1: when surface snowfall exists (on surface, not aloft).

0: when surface snowfall doesn't exist.Missing Value：

-9999.9

(6) surfaceSnowfallIndex (Only for 2ADPR)

Type	Array	Unit
4-byte float	nray * nscan	N/A

flagSurfaceSnowfall is 1 when this index exceed the defined threshold.

When no rain or skipped, the value is 0.0.

Missing Value：

-9999.9

(7) flagGraupelHail (Only for 2ADPR)

Type	Array	Unit
1-byte unsigned integer	nray * nscan	N/A

This flag takes the following value:

1: Flag = 1 indicates graupel or hail exists along vertical profile.

0: Flag = 0 indicates no graupel or hail exists along profile.

Missing Value：

0

(8) binMixedPhaseTop (Only for 2ADPR)

Type	Array	Unit
2-byte integer	nray * nscan	range bin

Range bin number of MixedPhaseTop when it is detected.

Missing Value：

-9999

1.3.10. SLV (Group)

(1) flagSLV

Type	Array	Unit
1-byte integer	nbin * nray * nscan	N/A

A flag for each range bin data. At rain range bins, flagSLV is positive. At no-rain range bins, flagSLV is 0. If a range bin is located below ESurface, flagSLV is negative (-64). When the retrieval is abnormally terminated or data quality is bad, flagSLV is negative (-128).

The values are

> flagSLV%2
>> 0:no rain
>> 1:rain
>
> flagSLV%4
>> 3:Zm is used for the retrieval
>> (1:extrapolated Ze is used for the retrieval)
>> (0:no rain)
>
> flagSLV%16
>> (0-3:no rain)
>> 4-7:only KuPR is used for the retrieval
>> 8-11:only KaPR is used for the retrieval
>> 12-15:Both KuPR and KaPR's Zm are used for the retrieval
>
> flagSLV%64
>> 0-15:Dm takes normal value (or no-rain)
>> 16-31:Dm takes the minimum value
>> 32-47:Dm takes the maximum value
>> 48-63:Dm takes an abnormal value
>
> flagSLV% 256
>> 0-63:R takes an normal value (or no-rain)
>> 64-127:R takes the maximum value
>> (128:bad data quality)
>> (192:below ESurface)

Missing Value：
    -99

(2) binEchoBottom

Type	Array	Unit
2-byte integer	nray * nscan	N/A

The bin number of bottom of echo. For NS and MS swaths, bin numbers are 1-based ranging from 1 at the top of the data window with 176 at the Ellipsoid. For HS swaths, bin numbers are 1-based ranging from 1 at the top of the data window with 88 at the Ellipsoid.

Missing Value :

-9999

(3) piaFinal

Type	Array	Array (2ADPR)	Unit
4-byte float	nray * nscan	nfreq * nray * nscan	dB

The final estimates of path integrated attenuation caused by precipitation particles. It is calculated from the retrieved DSD profiles. It includes the attenuation only by precipitation.

Missing Value :

-9999.9

In the 2ADPR,

nfreq(1) : TBD

nfreq(2) : TBD

(4) sigmaZeroCorrected

Type	Array	Array (2ADPR)	Unit
4-byte float	nray * nscan	nfreq * nray * nscan	dB

Surface backscatter cross section with attenuation correction.

Missing Value :

-9999.9

In the 2ADPR,

nfreq(1) : TBD

nfreq(2) : TBD

(5) zFactorCorrected

Type	Array	Array (2ADPR)	Unit
4-byte float	nbin * nray * nscan	nfreq * nbin * nray * nscan	dBZ

Vertical profile of reflectivity factor with attenuation correction.

$10 \log 10(Z)$ where Z is in mm^6/m^3.

Missing Value：

-9999.9

In the 2ADPR,

nfreq(1) : TBD

nfreq(2) : TBD

(6) zFactorCorrectedESurface

Type	Array	Array (2ADPR)	Unit
4-byte float	nray * nscan	nfreq * nray * nscan	dBZ

Reflectivity factor with attenuation correction at estimated surface.

$10 \log_{10}(Z)$ where Z is in mm^6/m^3.

Missing Value：

-9999.9

In the 2ADPR,

nfreq(1) : TBD

nfreq(2) : TBD

(7) zFactorCorrectedNearSurface

Type	Array	Array (2ADPR)	Unit
4-byte float	nray * nscan	nfreq * nray * nscan	dBZ

Reflectivity factor with attenuation correction at near surface.

$10 \log_{10}(Z)$ where Z is in mm^6/m^3.

Missing Value：

-9999.9

In the 2ADPR,

nfreq(1) : TBD

nfreq(2) : TBD

(8) paramDSD

Type	Array	Unit
4-byte float	nDSD * nbin * nray * nscan	$10 \log_{10}(Nw)$ mm

Parameters of DSD functions, Nw and Dm. Nw in $1/m^3$ mm

nDSD(1) : TBD

nDSD(2) : TBD

Missing Value :

-9999.9

(9) precipRate

Type	Array	Unit
4-byte float	nbin * nray * nscan	mm/hr

Precipitation rate.

Missing Value :

-9999.9

(10) precipWaterIntegrated

Type	Array	Unit
4-byte float	LS * nray * nscan	g/m^2

Precipitation water vertically integrated.

For LS=1, sum of liquid water (phase >= 200)

For LS=2, sum of non-liquid water (phase < 200)

Missing Value :

-9999.9

(11) precipRateNearSurface

Type	Array	Unit
4-byte float	nray * nscan	mm/hr

Precipitation rate for the nearSurface bin, i.e., at binClutterFreeBottom.

Missing Value :

-9999.9

(12) precipRateESurface

Type	Array	Unit
4-byte float	nray * nscan	mm/hr

Precipitation rate for the estimated surface, i.e., at binRealSurface.

Missing Value :

-9999.9

(13) precipRateAve24

Type	Array	Unit
4-byte float	nray * nscan	mm/hr

Average of precipitation rate for 2 to 4km height.

Missing Value:

-9999.9

(14) phaseNearSurface

Type	Array	Unit
1-byte unsigned integer	nray * nscan	N/A

Value of the Phase parameter in the DSD module at binClutterFreeBottom (nearSurface bin).

Missing Value:

255

(15) epsilon

Type	Array	Unit
4-byte float	nbin * nray * nscan	N/A

Epsilon is the indication of the adjustment away from the initial drop size distribution, epsilon = 1 is no adjustment.

Missing Value:

-9999.9

(16) paramNUBF

Type	Array	Unit
4-byte float	nNUBF * nray * nscan	N/A

The parameter to adjustment of None Uniform Beam Filling (NUBF).

paramNUBF(1) is σ_T^2 where $\sigma_T = \sqrt{\frac{\sigma^2+1}{p}} - 1$.

paramNUBF(2) is σ^2 where σ is the coefficient of variation of Nw.

paramNUBF(3) is p where p is the ratio of the raining area to the total area in FOV. (Currently p is set to 1.)

Missing Value:

-9999.9

(17) qualitySLV

Type	Array	Unit
4-byte integer	nscan	N/A

T.B.D

The values are

T.B.D

Missing Value :

-9999

1.3.11. FLG (Group)

(1) flagEcho

Type	Array	Unit
1-byte integer	nbin * nray * nscan	N/A

The values are

Bit Meaning
0 : For L2 Ku/PR: Precipitation judged by L2 Ku algorithm (copy of bit 2)
0 : For L2 Ka: Precipitation judged by L2 Ka algorithm (copy of bit 3)
0 : For L2 DPR: Precipitation judged by L2 DPR algorithm (copy of bit 1)
1 : Precipitation judged by L2 DPR algorithm
2 : Precipitation judged by L2 Ku algorithm
3 : Precipitation judged by L2 Ka algorithm
4 : Main lobe clutter judged by L2 Ku algorithm
5 : Main lobe clutter judged by L2 Ka algorithm
6 : Side lobe clutter judged by L2 Ku algorithm
7 : Side lobe clutter judged by L2 Ka algorithm

(2) qualityData

Type	Array	Unit
4-byte integer	nray * nscan	N/A

Normal data gives "0". Non-zero values mean the kinds of errors

The values are

The 2 bit flag for each module has values:
[higher bit lower bit]
[0 0] : Good
[0 1] : Warning but usable
[1 0] : NG or error
The bits of qualityData are assigned as follows:
0 - 7 : Copy of dataQuality in level 1B product

8 - 9 : Flag by input module

10 - 11 : Flag by preparation module

12 - 13 : Flag by vertical module

14 - 15 : Flag by classification module

16 - 17 : Flag by SRT module

18 - 19 : Flag by DSD module

20 - 21 : Flag by solver module

22 - 23 : Flag by output module

24 - 31 : Spare

-9999 : Missing

(3) flagSensor

Type	Array	Array (2ADPR)	Unit
1-byte integer	nscan	nfreq * nscan	N/A

Flag of input Ku/Ka data condition.

In the 2ADPR,

nfreq(1) : TBD

nfreq(2) : TBD

The values are

1 : Valid

-99 : Invalid (judged by dataQuality)

(4) qualityFlag

Type	Array	Array (2ADPR)	Unit
1-byte integer	nray*nscan	nfreq * nscan	N/A

qualityFlag is a sample flag gererated by qualityData.

In the 2ADPR,

nfreq(1) : TBD

nfreq(2) : TBD

The values are

0: High quality. No issues.

1 : Low quality. (DPR modules had warnings but still made a retrieval)

2: Bad. (DPR modules had errors or dataQuality is bad and retrieval is missing)

-99: Missing value

(5) flagScanPattern

Type	Array	Array (2ADPR)	Unit
2-byte integer	nscan	nfreq * nscan	N/A

Flag of scan pattern information. Ku and PR are always "0".

In the 2ADPR,

nfreq(1) : Ku

nfreq(2) : Ka

The values are

> 0 : Original scan pattern. (from the beginning of the mission until May 21, 2018)
>
> 1 : KaHS outer swath scan pattern(After May 21, 2018)
>
> -99: Others or Missing

1.3.12. TRG (Group)

(1) NUBFindex

Type	Array	Unit
4-byte float	nray * nscan	N/A

The value is 0.

(2) MSindex

Type	Array	Unit
1-byte unsigned integer	nray * nscan	N/A

The value is 0.

(3) MSindexKu

Type	Array	Unit
1-byte integer	nray * nscan	N/A

The value is 0.

(4) MSindexKa

Type	Array	Unit
1-byte integer	nray * nscan	N/A

The value is 0.

(5) precipFrac

Type	Array	Unit
1-byte unsigned integer	3*nray * nscan	N/A

The value is 0.

(6) RNUBFcond

Type	Array	Unit
4-byte float	nray * nscan	N/A

The value is 0.

(7) MSsurfPeakIndexKu

Type	Array	Unit
1-byte unsigned integer	nray * nscan	N/A

The value is 0.

(8) MSsurfPeakIndexKa

Type	Array	Unit
1-byte unsigned integer	nray * nscan	N/A

The value is 0.

(9) MSthroughsurfIndexKu

Type	Array	Unit
1-byte unsigned integer	nray * nscan	N/A

The value is 0.

(10) MSthroughsurfIndexKa

Type	Array	Unit
1-byte unsigned integer	nray * nscan	N/A

The value is 0.

(11) MSkneeDFRindex

Type	Array	Unit
1-byte unsigned integer	nray * nscan	N/A

The value is 0.

(12) MSthrZindex

Type	Array	Unit
1-byte unsigned integer	nray * nscan	N/A

The value is 0.

(13) NUBFratioPIAindex

Type	Array	Unit
1-byte unsigned integer	nray * nscan	N/A

The value is 0.

(14) NUBFnZmVarIndex

Type	Array	Unit
1-byte unsigned integer	3 * nray * nscan	N/A

The value is 0.

(15) NUBFnZkVarIndex

Type	Array	Unit
1-byte unsigned integer	3 * nray * nscan	N/A

The value is 0.

(16) NUBFnZmVarScaling

Type	Array	Unit
2-byte integer	nray * nscan	N/A

The value is 0.

(17) NUBFnZkVarScaling

Type	Array	Unit
2-byte integer	nray * nscan	N/A

The value is 0.

(18) NUBFsurfSliceIndex

Type	Array	Unit
4-byte float	30 * nray * nscan	N/A

The value is 0.

(19) NUBFprofZPC

Type	Array	Unit
4-byte float	30 * nray * nscan	N/A

The value is 0.

(20) MSbreakpoints

Type	Array	Unit
2-byte integer	13 * nray * nscan	N/A

The value is 0.

(21) MSslopes

Type	Array	Unit
4-byte float	10 * nray * nscan	N/A

The value is 0.

(22) MSslopePoints

Type	Array	Unit
4-byte float	13 * nray * nscan	N/A

The value is 0.

(23) MSslopeFits

Type	Array	Unit
4-byte float	6 * nray * nscan	N/A

The value is 0.

(24) MSlowSNRrangeFilter

Type	Array	Unit
1-byte unsigned integer	4 * nray * nscan	N/A

The value is 0.

(25) NUBFcorrPIA

Type	Array	Unit
4-byte float	2 * nray * nscan	N/A

The value is 0.

(26) triggerParameters

Type	Array	Unit
4-byte float	8 * nray * nscan	N/A

The value is 0.